

Institut für Photovoltaik

Microcrystalline Silicon Solar Cells Prepared by 13.56 MHz PECVD

Prerequisites for High Quality Material at High Growth Rates

Tobias Roschek

Microcrystalline Silicon Solar Cells Prepared by 13.56 MHz PECVD

Prerequisites for High Quality Material at High Growth Rates

Tobias Roschek

Berichte des Forschungszentrums Jülich ; 4083 ISSN 0944-2952 Institut für Photovoltaik Jül-4083 D 61 (Diss., Düsseldorf, Univ., 2003)

Zu beziehen durch: Forschungszentrum Jülich GmbH · Zentralbibliothek D-52425 Jülich · Bundesrepublik Deutschland

□ 02461/61-5220 · Telefax: 02461/61-6103 · e-mail: zb-publikation@fz-juelich.de

Mikrokristalline Silizium-Solarzellen mittels 13.56 MHz PECVD

Kurzfassung: Thema dieser Arbeit war die Entwicklung von Dünnschichtsolarzellen auf der Basis von mikrokristallinem Silizium mittels PECVD (plasma-enhanced chemical vapor deposition) bei 13.56 MHz Anregungsfrequenz und hohen Depositionsraten. Mittels umfassender Solarzellenstudien, die von Materialcharakterisierungen begleitet wurden, konnten wir die wichtigsten Bedingungen, die zu hoher Materialqualität bei hohen Depositionsraten notwendig sind, herausarbeiten. Bei der Entwicklung von Solarzellen in verschiedenen Druckbereichen stellte sich heraus, dass ein hoher Depositionsdruck entscheidend für hohe Materialqualität bei hohen Depositionsraten ist. Plasmen bei hohem Druck (>10 Torr) ließen sich nur bei kleinen Elektrodenabständen zünden. Weitere wichtige Faktoren für gute Solarzellen waren ein hoher Gesamtgasfluss und eine Substrattemperatur, die einen Wert von $\sim 200\,^{\circ}$ C nicht überschreitet. Alternativ wurden Zellen mittels gepulster Plasmaanregung abgeschieden. Bis zu Depositionsraten von ~ 5 Å/s wurden ähnlich gute Ergebnisse wie mittels konventioneller Abscheidung erreicht, bei höheren Raten nahm der Wirkungsgrad der Solarzellen stark ab. Zusammenfassend ist zu sagen, dass wir das Ziel hochwertige mikrokristalline Solarzellen bei hohen Depositionsraten herzustellen erreichten. Die größten technologischen Erfolge waren Solarzellen mit Wirkungsgraden von 9.1 %, 9.0 % und 8.9 % bei Depositionsraten von 1, 3 und 4 Å/s. Bei Depositionsraten von 9 Å/s konnten immer noch Wirkungsgrade von 7.9 % erreicht werden. Weiterhin erarbeiteten wir ein Verständnis dafür, welche Plasmabedingungen zu hoher Materialqualität bei hohen Depositionsraten führen.

Microcrystalline Silicon Solar Cells Prepared by 13.56 MHz PECVD

Abstract: Topic of this thesis was the development of thin film solar cells based on microcrystalline silicon prepared by 13.56 MHz PECVD (plasma-enhanced chemical vapor deposition) at high deposition rates. Comprehensive solar cell studies, which were accompanied by material studies, resulted in the identification of the most important prerequisites for high quality solar cells at high growth rates. During the development of solar cells in various pressure regimes, a high deposition pressure emerged as key parameter for good solar cell performance at high deposition rates. Plasma ignition at high deposition pressures (>10 Torr) was only possible at low electrode distances. Other important factors were a high total gas flow and a substrate temperature, which should not exceed ~200 °C. As alternative approach deposition by pulsed plasma excitation was investigated. At deposition rates up to ~ 5 Å/s efficiencies comparable to continuous excitation were achieved, at higher rates the efficiency significantly decreased. In summary we succeeded in developing high quality solar cells at high deposition rates. Highlights were solar cells with 9.1, 9.0 and 8.9 % efficiency for deposition rates of 1, 3 and 4 Å/s, respectively. At 9 Å/s still a high efficiency of 7.9 % was achieved. Furthermore we gained an understanding of the prerequisites regarding the plasma properties to achieve high growth rates and high quality material.

Contents

Li	st of	Figures	vi
Li	st of	Tables	vii
1	Intro	oduction	1
2	Fund 2.1 2.2 2.3	damentals Microcrystalline and Amorphous Silicon	
3	Cha 3.1	Solar Cell Characterization	15 15 15 18 20
4	Sola 4.1 4.2 4.3 4.4 4.5 4.6	Substrates and Back Reflectors Plasma-Enhanced Chemical Vapor Deposition (PECVD) PECVD System Electrode Design Deposition Procedure (PECVD) Powder Formation	35
5	Mic 5.1 5.2 5.3	Influence of Pressure	41
6	μ c-S 6.1	Si:H Solar Cells: Growth Regime and Key Deposition Parameters Silane Concentration, Deposition Pressure and Plasma Power	47 47

		6.1.2	Solar Cell Properties at the Transition between Microcrystalline and	
			Amorphous Growth	50
		6.1.3	Solar Cells Prepared under Optimized Conditions	53
		6.1.4	Solar Cell Performance versus Deposition Rate	57
	6.2	Role o	f the Substrate Temperature	57
	6.3	Summ	ary	62
7	μ c -\$	Si:H Sol	lar Cells: Role of Electrode Distance, Gas Flow and Pulsed Plasma	a
	Exc	itation		65
	7.1	Electro	ode Distance	65
	7.2	Total (Gas Flow	68
	7.3	Pulsed	Plasma Excitation	71
	7.4	Summ	ary	75
8	Disc	cussion		77
	8.1	Correla	ation with Plasma Properties	77
	8.2		lines for the Development of μ c-Si:H Solar Cells	
9	Sun	nmary a	and Conclusions	81
Α	Deg	gradatio	n	85
В	Up-	Scaling		87
Bi	bliog	raphy		89

List of Figures

1.1	From process parameters to solar cell characteristics	3
2.1 2.2	Schematic diagram of microstructure of μ c-Si:H	9
2.3 2.4	Band diagram of a p-n and a p-i-n solar cell	11 14
3.1 3.2 3.3 3.4 3.5	Equivalent circuit of a solar cell	16 17 18 19 23
4.1 4.2 4.3 4.4 4.5 4.6 4.7 4.8 4.9 4.10 4.11 4.12	p-i-n structure of μ c-Si:H solar cell Sputtering and etching of ZnO Cell geometry of p-i-n cells J_{SC} with Ag and ZnO/Ag back reflector Definition of pulse parameters Layout of deposition system Layout of gas supply and pumping scheme Layout of a single deposition chamber Electrode designs Sketch of structural inhomogeneity J-V parameters for two electrode configurations Powder stream	26 27 28 30 31 32 33 34 35 36 37
5.1 5.2 5.3 5.4 5.5	Conductivity and deposition rate of μ c-Si:H p-layers vs. deposition pressure Conductivity and deposition rate of μ c-Si:H p-layers vs. dopant gas flow . QE of a μ c-Si:H solar cell	41 42 43 44 45
6.1 6.2	Transition regime between a-Si:H and μ c-Si:H growth	

6.3	Light J-V parameters vs. deposition pressure
6.4	Quantum efficiencies of solar cells prepared close to the amorphous-
	microcrystalline transition
6.5	Raman spectra of pressure series
6.6	Light J-V parameters vs. silane concentration
6.7	Deposition rate vs. P_{RF} , p_{dep} and $[SiH_4]/[H_2]$
6.8	FF and V_{OC} , achieved at various deposition pressures
6.9	Raman spectra of optimized solar cells
6.10	TEM images of optimized solar cells
6.11	FF and V_{OC} vs. deposition rate
6.12	Light J-V-parameters vs. heater temperature
6.13	Raman spectra of solar cells prepared at various T_H and $[SiH_4]/[H_2]$ 6
6.14	Raman crystallinity vs. T_H for various $[SiH_4]/[H_2]$ 6
6.15	Hydrogen effusion curves vs. T for various T_H and $[SiH_4]/[H_2]$ 6
7.1	Deposition rate vs. $[SiH_4]/[H_2]$ for two electrode distances 6
7.2	$V_{\rm OC}$ and FF of optimized solar cells vs. deposition rate for various electrode
	distances
7.3	SiH_4 flow and concentration, deposition rate and gas utilization for optimized cells vs. H_2 flow
7.4	FF and V_{OC} of optimized cells vs. H_2 flow
7.5	Deposition rate vs. pulse frequency
7.6	V_{OC} and FF vs. pulse frequency
7.7	Deposition rate of μ c-Si:H i-layers of optimized solar cells for CW and
	pulsed excitation vs. plasma power
7.8	V_{OC} and FF of optimized solar cells vs. deposition rate for CW and pulsed
	excitation
A.1	Degradation of μ c-Si:H solar cells prepared at various p_{dep} 80
B.1	Light J-V curves of μ c-Si:H and a-Si:H/ μ c-Si:H solar cell prepared in
	$30\times30~\mathrm{cm^2~reactor}$
B.2	Light I-V curve of a-Si:H/ μ c-Si:H 30×30 cm ² module 8

List of Tables

5.1	Comparison of RF and VHF deposition regime for μ c-Si:H-p-layers	40
	Deposition parameters applied for material study	55
6.2	Deposition parameters and efficiencies of solar cells with Ag back contact	
	prepared at various heater temperatures	60

1 Introduction

Solar cells transform the energy of the sunlight directly into electric energy. This direct form of solar electricity generation is called photovoltaics. Compared to the combustion of fossil fuels and nuclear fission, which are today the most commonly applied methods of energy generation, solar energy has the advantages of no environmental hazards (no greenhouse effect or nuclear waste) and almost infinite supply (as long as the sun shines). Therefore photovoltaics fulfills all criteria of a sustainable energy source.

Today the world market is dominated by wafer-based mono- or polycrystalline silicon solar cells. Thin film solar cells promise a price reduction for solar modules [1]. The reasons are:

- The material consumption is significantly lower due to the thin film approach (required silicon thickness is $\sim 1~\mu m$ instead of 200–300 μm).
- The lower material consumption together with low process temperatures lead to a lower consumption of energy during manufacturing. Therefore the energy payback time (the time the solar module needs to produce the energy that is used during its production) is reduced [2].
- The thin film deposition techniques allow a large area production. However, it is a challenging task to achieve homogeneous deposition on areas of the order of 1 m².
- Low process temperatures allow the use of a variety of low-cost substrate materials like float-glass, metal- or plastic foils [3–5].

Compared to other thin film materials silicon has the advantage of its almost infinite availability [6] and its harmlessness for the environment. Thin film solar cells based on hydrogenated amorphous silicon (a-Si:H) are already produced in several production plants with multi-megawatt capacity and have a market share of $\sim 10 \%$ [7]. While the prospected production costs for large scale manufacturing ($\geq 10 \text{ MW}$) in terms of costs per Watt of module power are lower than for the crystalline silicon (c-Si) wafer technology [1], the efficiencies achieved in production (5–7 %) are still significantly lower than for solar modules based on mono- or polycrystalline silicon wafers (10–14 %). One reason for this is the fact that a-Si:H shows light induced degradation (Staebler-Wronski-Effekt

[8]), an increase of the defect density under illumination. In solar cells this leads to a reduction of efficiency until after typically ~ 1000 h a stabilized efficiency is reached. In the past years, microcrystalline silicon (μ c-Si:H) emerged as a promising new material for photovoltaics. Advantages of μ c-Si:H compared to a-Si:H are the stability against lightinduced degradation and the extension of the wavelength range of absorption to red and IR light (up to 1100 nm). However, due to the indirect bandgap of μ c-Si:H the absorption coefficient for light of $\lambda > 800$ nm is rather low and i-layer thicknesses of more than one μm and an efficient light trapping are required for sufficient absorption. The growth of microcrystalline silicon has been reported first by Vepřek and Mareček using chemical transport by a hydrogen plasma [9]. Usui and Kikuchi showed that, like in the case of a-Si:H, the preparation was possible by plasma-enhanced chemical vapor deposition (PECVD) [10], providing full compatibility with a-Si:H technology. First μ c-Si:H single junction solar cells were realized by Wang and Lucovsky [11], Faraji et al. [12] and Flückiger et al. [13]. Pioneering work at the University of Neuchâtel raised the efficiency level of μ c-Si:H solar cells and proved the potential of this new cell-type as bottom cell in a-Si:H/ μ c-Si:H tandem cells (e. g. [14–16]). Microcrystalline silicon solar cells consist of two thin doped layers and a thick intrinsic layer ($\sim 1 \ \mu m$) in between. Today the best μ c-Si:H solar cells show efficiencies between 8.5 and 9.5 % [17–21]. The highest conversion efficiency for a single junction thin film silicon solar cell (10.7 %) was reported by Kaneka Corp. [22]. Since details of the process are not reported, it is unknown if the process and the material are comparable to those of the other works mentioned above. Even higher efficiencies are achieved using stacked cells consisting of a-Si:H top cells and μ c-Si:H bottom cells [19, 23–25].

A general problem of photovoltaic devices is the high cost of the generated energy. This is mostly due to the production costs of the solar cells. The cost-effectiveness of solar cells can be improved in two ways: The production costs per module can be reduced at a fixed solar cell efficiency or at fixed costs the efficiency can be increased. For μ c-Si:H the deposition time and thus the prospected throughput in industrial production is limited by the deposition time for the μ c-Si:H i-layer. One way to reduce the costs of solar cell production is therefore to increase the deposition rate of the i-layer and hence increase the throughput. Then the deposition systems, whose high capital cost makes up a major part of the production costs, can be used more effectively. Therefore high deposition rates are an essential prerequisite for an industrial mass production.

Different deposition techniques and parameters have been studied to provide both high quality material and high growth rate (e.g. [17, 26, 27]). Among them the very high frequency (VHF: \sim 100 MHz) PECVD technique has been widely used [24, 28]. However, at these high frequencies problems arise due to the lower plasma impedance and therefore higher currents in combination with enhanced Ohmic losses in the electrical parts (cables, wires, joints, etc.) due to the reduced skin depth [29]. Further problems come up when the wavelength of the plasma excitation (e. g. \sim 3 m for an excitation frequency of 100 MHz) becomes comparable to reactor and substrate dimensions ($\sim m^2$ for an industrial production). Interelectrode voltage inhomogeneities increase with increasing

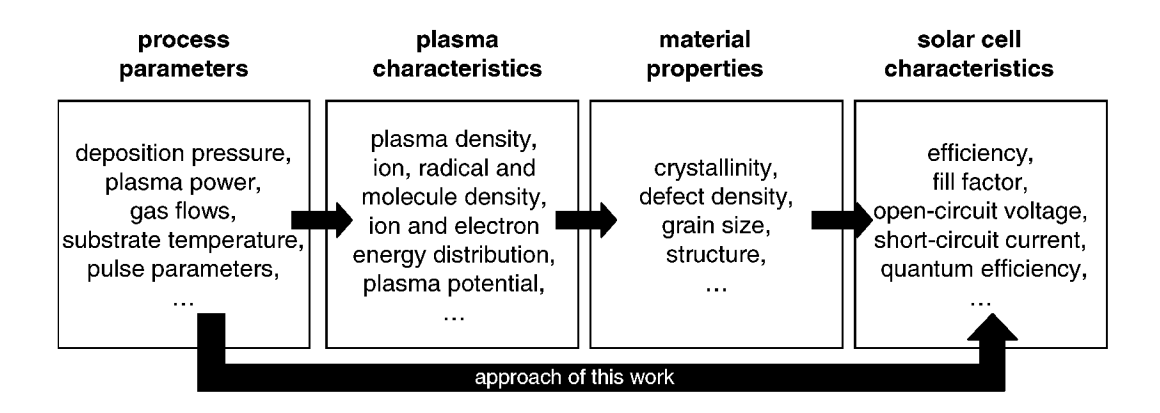


Figure 1.1: The correlation of process parameters, plasma characteristics, material properties and solar cell characteristics.

excitation frequency and cause inhomogeneities in the deposition rate [30]. Even though novel reactor and deposition concepts (e. g. "U" shaped [31] or ladder-shaped antennas [32, 33]) might solve these problems, lower excitation frequencies still facilitate deposition on larger substrates [30, 34]. For this reason one favors conventional RF (13.56 MHz) excitation frequency which is also compatible with existing deposition equipment.

The aim of this work was the development of high efficiency microcrystalline solar cells under the constraint of using 13.56 MHz excitation frequency. The solar cells were prepared in the deposition regime of high RF power P_{RF} and high deposition pressure p_{dep} (1 - 40 Torr) which guarantees high deposition rates. High rate deposition of μ c-Si:H films in a high pressure regime has been reported by Guo et al. [35]. The first efficient μ c-Si:H solar cells prepared in a similar regime at high deposition rates were prepared in our group [36, 37].

The PECVD process, which is used in this work, is based on a glow discharge of silane and hydrogen (for intrinsic layers) which are decomposed in an alternating electric field. As a result, film precursors (e. g. SiH₃) are produced which contribute to the film growth onto the substrate. The correlation of process parameters and the resulting solar cell properties is quite complex. The process parameters (e. g. deposition pressure, ...) determine the plasma characteristics (e. g. plasma density, ...). The film growth and the resulting material properties are critically dependent on these plasma characteristics. A

change of the plasma properties can for example induce a transition between amorphous and microcrystalline growth. But even for μ c-Si:H layers different plasma conditions lead to quite different materials regarding properties like defect density, grain size and other structural features. The solar cell characteristics are to a major part determined by the i-layer properties (ignoring substrates, interfaces, doped layers). This chain of effects is illustrated in figure 1.1. Each of the described steps is complex and is topic of long term investigations partly done elsewhere. We used here mainly an empirical approach of studying all deposition parameter variations in solar cells resulting in a direct correlation between process parameters and solar cell properties. This approach is based on the long-term experience that an advanced and reproducible solar cell process is the most reliable probe for i-layer quality. Another reason for this approach was that the growth of μc-Si:H strongly depends on the underlying substrate [38–41]. In our case the substrate for i-layer growth was always the microcrystalline p-layer grown on a ZnO-coated glass substrate¹. The effects of the process parameters on solar cells are interpreted based on material characterization performed within a joint German-Israeli research project (project number 01647 E01073) and comparison with literature data.

This work is structured as follows:

- Chapter 2 describes the fundamental background of this work. The material properties of microcrystalline silicon are described. Next the operation principle of solar cells in general and the difference between the p-i-n structure used for Si thin film solar cells and the p-n structure used in the wafer technology are explained. Finally, the basic properties of RF discharges are described.
- In chapter 3 the characterization methods used for the examination of solar cells and material are explained.
- Chapter 4 describes the deposition of solar cells. The preparation of substrates and back reflectors is shortly explained. In more detail, the PECVD process for the deposition of the silicon layers is described with special emphasis on the electrode design for homogeneous μ c-Si:H deposition.
- Chapter 5 describes the development of microcrystalline p-layers at 13.56 MHz.
- In chapter 6 the development of μ c-Si:H in solar cells is shown. The influence of varying one or more of the process parameters like deposition pressure, plasma power, process gas flow ratio and substrate temperature is described in detail. We will learn that these parameters can be used to adjust and optimize the material. The solar cell results are accompanied by results on material characterization.
- In chapter 7 the influence of the parameters total gas flow and electrode distance is examined. The focus is on the comparison of optimized solar cells which are prepared

¹Al-doped ZnO is a so-called transparent conductive oxide (TCO). High transparency and conductivity are essential requirements for the front contact of a solar cell.

at various gas flows and electrode distances, respectively. The optimization is based on the results described in chapter 6. Furthermore, pulsed plasma deposition is examined as an alternative approach.

• In chapter 8 the relationship between process parameters, plasma characteristics, material properties and solar cell characteristics is discussed. General guidelines for the development of μ c-Si:H solar cells are proposed, followed by a summary of this work and a brief outlook in chapter 9.

2 Fundamentals

2.1 Microcrystalline and Amorphous Silicon

For this work two different silicon-based materials are of interest: amorphous (a-Si) and microcrystalline silicon (μ c-Si). In this work we will develop solar cells based on microcrystalline silicon. However, since both materials are prepared under similar conditions and the microcrystalline material prepared close to the transition to amorphous growth will turn out especially interesting for solar cell application, it is necessary to know the basic material properties of amorphous silicon, as well.

Throughout this work, microcrystalline silicon will be used as a general term for a material which is a composition of crystalline grains, amorphous phase and voids, where the grain size is in the μ m range or smaller. Hydrogen saturates dangling bonds which occur at the grain boundaries and in the amorphous phase. Correspondingly, the material is called hydrogenated microcrystalline silicon (μ c-Si:H). The actual structure of the material depends strongly on the deposition conditions and has a strong impact on the device performance. More details on the material properties of μ c-Si:H can be found in the works of Luysberg et al. [42], Tzolov et al. [38], Houben [43] and Vetterl [44].

A structural model of μ c-Si:H material according to [43] is schematically shown in figure 2.1. From the left to the right hand side of this figure the deposition conditions change from a highly crystalline to a predominantly amorphous growth regime. As will be discussed later in this work, this transition can be achieved by almost every deposition parameter (see sections 6.1.1, 7.1 and 7.2).

In the highly crystalline growth regime the crystalline growth originates from nucleation centers near the substrate. At increasing distance to the substrate the diameter of the crystallites increases resulting in a conical shape. The space between the crystalline grains can be filled with amorphous silicon and/or voids, dependent on the deposition conditions and the substrate (see [38, 42–44] and references therein). This growth region is called the incubation zone.

At a certain stage, equally fast growing crystalline columns with stable grain boundaries are formed. In this steady-state of growth, characteristic properties like grain sizes and phase composition are independent of the film thickness, and disordered network is

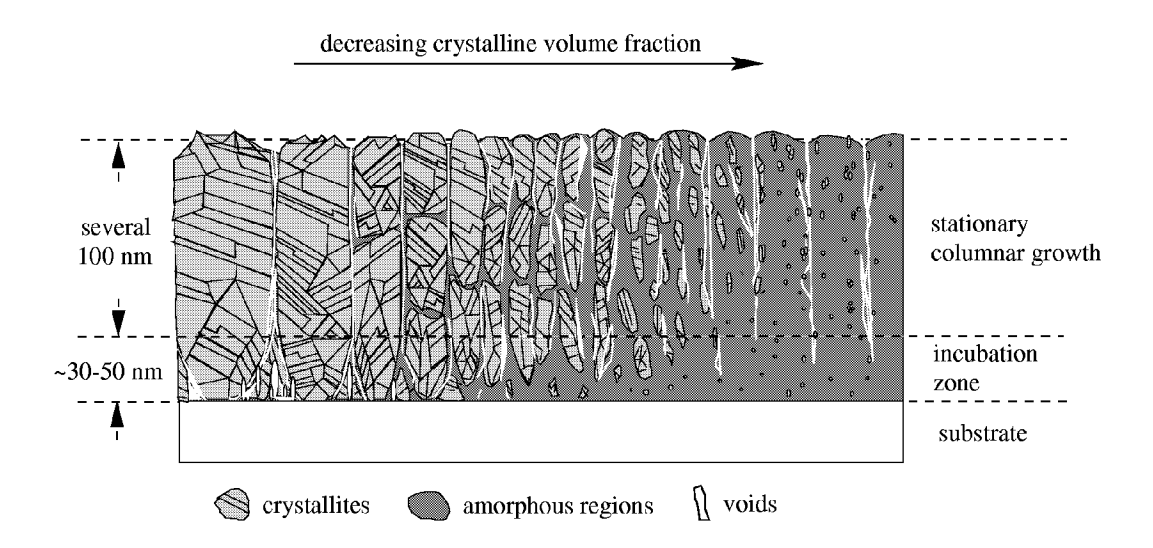


Figure 2.1: Schematic diagram illustrating the microstructural characteristics of μ c-Si:H obtained for growth on foreign substrates. From the left to the right, the film composition changes from highly crystalline to predominantly amorphous. (From [43])

only present at grain boundaries between the crystalline columns. The diameter of the crystalline grains depends thereby on the deposition regime (i. e. combination of silane concentration, deposition pressure, plasma power, etc., see section 4.2). The structure of the silicon inside these columns is not monocrystalline. It exhibits a high density of twin defects and stacking faults [43, 45, 46].

Under highly crystalline growth conditions the presence of voids is especially emphasized. For this reason, the material obtained in this regime can be considered as porous [38, 43]. These voids occur especially in the nucleation zone near the substrate and along the boundaries of the large diameter grains. Approaching the transition to amorphous growth, the most significant effect is a reduction of the column diameter, while extended disordered phase is only incorporated in the nucleation layer. Further adjustment of the deposition conditions in direction of amorphous growth leads to the occurrence of films with predominantly amorphous structure. Interruptions of the columns in growth direction occur, which reduces the crystallites to small embeddings within the amorphous matrix. Such material does not represent standard a-Si:H used e. g. for solar cells, but is a transition material between amorphous and microcrystalline silicon.

At the transition between microcrystalline and amorphous growth the material properties change significantly. Microcrystalline silicon is in many aspects comparable to

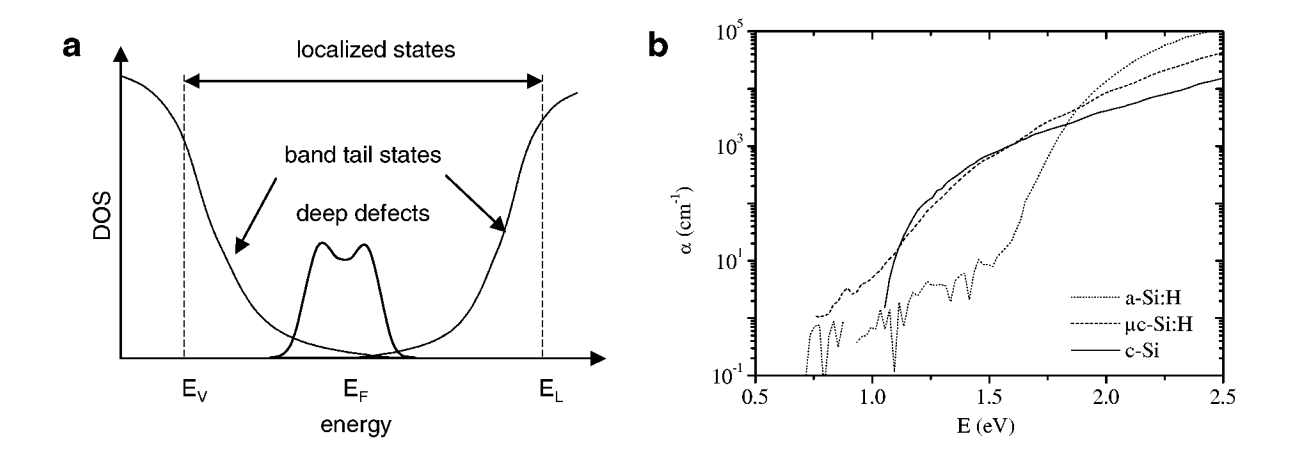


Figure 2.2: (a) Density of states (DOS) as a function of energy for amorphous silicon (sketch according to [47]). (b) Absorption coefficient α vs. energy for a-Si:H, μ c-Si:H and crystalline silicon (c-Si)

monocrystalline silicon (c-Si). The optical band gap and absorption coefficient α are very similar. Only at high photon energies α is significantly higher than for c-Si. This can partly be attributed to the high α of the amorphous phase contained in μ c-Si:H (see figure 2.2b).

In amorphous silicon the bonding angles and distances show slight variations. While the short range order is very similar to crystalline silicon, no long range order exists. This leads to charge carrier scattering, broadening of the density of states and to an uncertainty in the wave vector \vec{k} of the electrons. This leads to massive changes in the electrical and optical properties of the material. Unsaturated valences (dangling bonds) cause energy states within the band gap leading to material with bad semiconducting properties. Saturation of the dangling bonds with hydrogen reduces this defect density and makes the material suitable for semiconductor devices. This material is then called hydrogenated amorphous silicon (a-Si:H).

A sketch of the density of states in amorphous silicon is shown in figure 2.2a. The structural disorder leads to the formation of localized "band tail" states. However, the rough classification in valence- and conduction band still holds in a-Si:H. But one can observe a smooth merging between extended states of the valence- and the conduction band, respectively, and the localized tail states, whose density decreases exponentially with energy towards the mid gap. Since these states are localized between the valence and the conduction band it is difficult to define the optical band gap in a-Si:H. Instead the concept of a mobility gap is used: due to the localized nature of the tail states, the mobility of charge carriers sharply drops several orders of magnitude. This mobility gap is significantly higher ($\sim 1.8 \text{ eV}$) than the band gap of crystalline silicon ($\sim 1.1 \text{ eV}$).

In a-Si:H there is a large uncertainty in the wave vector \overrightarrow{k} . Therefore \overrightarrow{k} is not conserved in electronic transitions; the material acts as a direct semiconductor which increases the absorption probability of photons drastically. Figure 2.2b shows the absorption spectra of a-Si:H, μ c-Si:H and crystalline silicon (c-Si). The absorption coefficient of a-Si:H for photon energies above 1.8 eV is much higher than in crystalline and microcrystalline silicon. The incident light is absorbed almost completely in film thicknesses below 1 μ m (c-Si: \sim 50 μ m). More details on the properties of amorphous silicon can be found e. g. in [48].

2.2 Solar Cells

This section briefly describes the basic operation principle of solar cells. Furthermore, it addresses the differences between a classical wafer based p-n solar cell and a thin film silicon based p-i-n solar cell. Details about solar cell theory are described in a number of textbooks (e. g. [49–56]).

A photon of sufficient energy entering a semiconductor can, by interaction with valence band electrons, produce an electron-hole pair in the semiconductor. If an electric field is present, the electrons and holes are separated. The separated charge carriers lead to a voltage across the semiconductor. This voltage is known as the photovoltage. If the separated charge carriers are allowed to flow through an external load before recombining, they constitute a photocurrent. The product of the photovoltage and the photocurrent represents a net flow of energy from the solar cell to the external load. This way the energy originating from the sun is converted into electrical energy.

In all silicon based solar cells the electric field is generated by varying the type of impurity doping within the semiconductor (p-n or p-i-n junction). Other possibilities are altering the composition (heterotransition) or varying both composition and doping (heterojunction). Here we will only treat the p-n (and p-i-n) homojunctions.

Figure 2.3a shows the sketch of a p-n junction and the corresponding band diagram. This is a typical structure of a monocrystalline silicon solar cell. The space charge region of a p-n junction depends on the doping level and is typically less than 0.5 μ m thick for a wafer based crystalline silicon solar cell. Since the absorption depth¹ of crystalline silicon is typically higher (e. g. 10 μ m at \sim 1.5 eV) the main part of the sunlight is absorbed outside the space charge region. The charge carriers rely on diffusion to get to the electric field where they can be separated. Therefore this type of solar cell is called a diffusion cell.

In case of a-Si:H the diffusion length is too low (especially in degraded material) to allow this cell concept. Therefore a different approach is used. The diffusion length of μ c-Si:H is significantly higher, but nevertheless the same approach has turned out to be

¹absorption depth: depth were the intensity of the light decreased to 1/e of the initial value

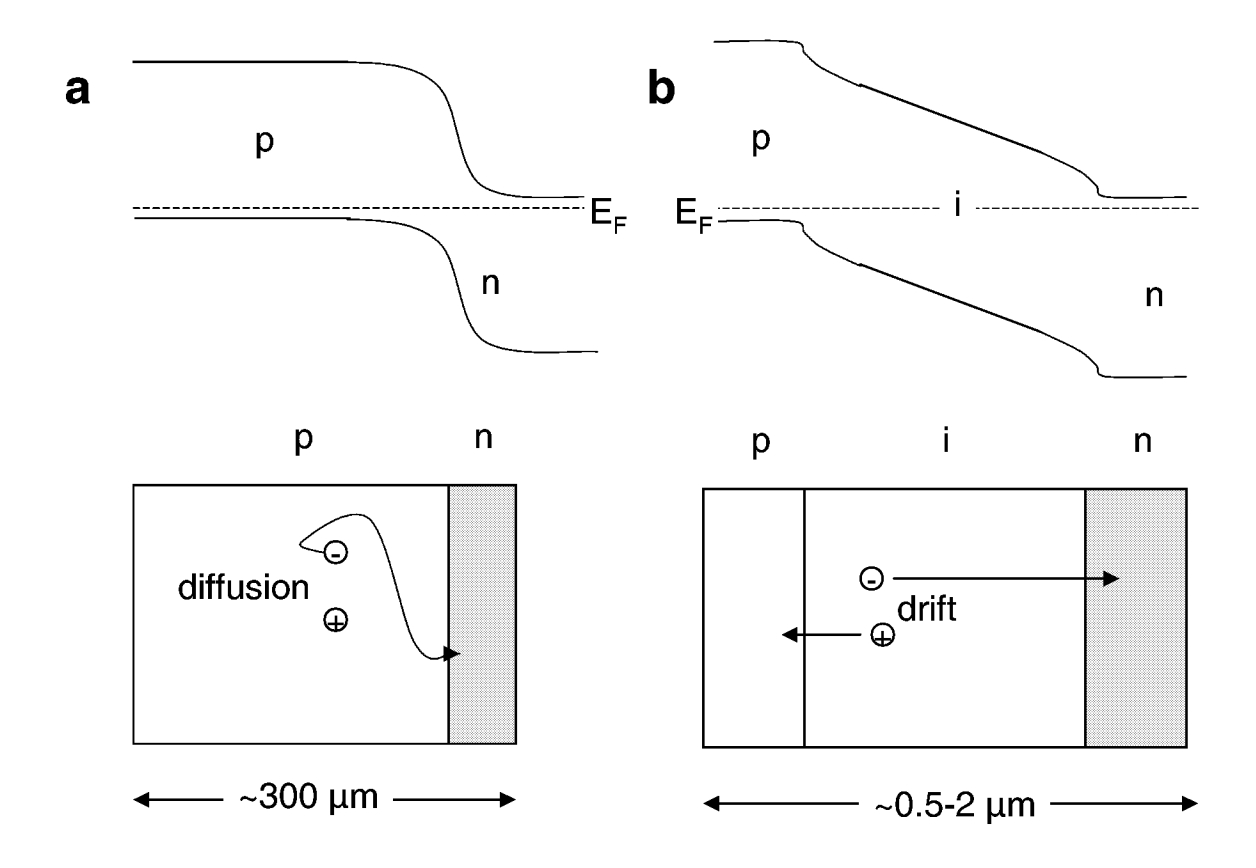


Figure 2.3: Band diagram and sketch of a) a p-n and b) a p-i-n solar cell.

favorable for μ c-Si:H as well. Figure 2.3b shows a sketch of a so-called p-i-n junction and its band diagram. This is the cell type usually applied for a-Si:H and μ c-Si:H solar cells. In the μ c-Si:H p-i-n junction there is an intrinsic layer with a thickness of usually more than 1 μ m between the thin doped layers. The electric field of an ordinary p-n junction is effectively stretched across the i-layer. The extended electric field throughout the i-layer, which is where most of the light is absorbed (supported by light trapping, see section 4.1), leads to the direct separation of photogenerated carriers due to drift (migration in an electric field). Therefore this cell is also called a drift cell. An a-Si:H solar cell is usually illuminated through the p-layer. This has the following reasons: The main part of the light is absorbed close to the illuminated side of the cell (Lambert's Law: $I(d) = I_0 \times e^{-\alpha d}$ and the mobility of the holes, which follow the electric field towards the p-layer, is lower than that of the electrons. Therefore, it is favorable for the holes to have the shorter way through the i-layer. As was recently found out there are indications that this is not necessary for μ c-Si:H solar cells [57], because the mobility of holes is high enough to travel the longer distance. However, for compatibility reasons in a-Si:H/ μ c-Si:H tandem solar cells μ c-Si:H solar cells are usually illuminated from the p-side, as well. Due

to the p-side illumination the p-layer is of crucial importance for the solar cell. It has not only to build up the electric field together with the n-layer, also the absorbance has to be low because the light absorbed in the p-layer is mostly lost for the solar cell.

2.3 Plasma Properties

This section treats general characteristics of a plasma and especially the properties which are needed for discussion in this work. Details on deposition plasmas can be found in [58–62]. The PECVD technique will be treated extensively in section 4.2.

A plasma is defined as a partially ionized gas, where electromagnetic interactions of the charged particles with each other or with external fields define the properties. Since there is a balance between negative and positive charges in the bulk of the plasma it is called quasineutral. To achieve the high ionization of the plasma, sufficient energy has to be supplied, which can be done by several means (e. g. heating, radiation,...). Among them the electrical RF discharge used in this work is one of the simplest and most widespread ways to sustain a plasma. There, electrons and ions are accelerated in an electric field. The energy that a singly charged particle gains in an electrical field is $\frac{(Eet)^2}{2m}$, where E is the electrical field strength, e the elementary charge, t the time during which the field is applied and m the mass of the particle. Therefore, free electrons are accelerated to high energies of about $1-10\ eV$. Due to their large mass and the weak energy transfer between light and heavy particles, neutrals and ions have low energy ($\sim 1/100\ eV$). The energy difference results in a high temperature for the electrons and a low, or "cold" temperature of the neutrals and ions. Under these non-equilibrium conditions, the initiation of chemical reactions occurs by collisions with the "hot" electrons. This way the processing temperature is much lower than in conventional thermal processes.

The shape of the electron energy distribution function (EEDF) is the result of two opposite processes: the first is their energy loss by collisions and the second is their energy gain from the electric field of the discharge. In general, this EEDF is not Maxwellian due to non-equilibrium conditions. In an electrical discharge, electrons tend to dominate the plasma characteristics as they are responsible for inelastic collisions leading to rotational, vibrational and electronic excitations, dissociations and ionizations, and elastic collisions. Further reactions are induced by collision of heavy particles leading to radicals, ions and larger molecules (e. g. higher silanes).

When there is a separation of a large number of electrons from positive ions in a plasma reactor, the neutrality is violated and an electric field, as in a parallel plate capacitor, arises between the positive- and negative-charge layers. In fact, because of their high energy and small mass, electrons usually diffuse toward all the surfaces in contact with the plasma (walls and electrodes), leaving the plasma bulk positively charged. Thus, all the surfaces in contact with the plasma carry a negative charge and the relative electric field between surfaces and the plasma bulk creates a thin sheath. The grounded electrode is typically

larger than the RF electrode, especially for small area reactors as used in research (e. g. in this work). That is because, apart from the "real" electrodes all other surfaces (chamber wall, shield, ...) exposed to the plasma are grounded. In an asymmetrical reactor, like the one used for this work, the potential distribution is asymmetrical, as well (see figure 2.4). On the other hand large area parallel plate reactors are quite symmetric. At the powered electrode a self-bias voltage V_b is established. The sheath voltage (potential difference across the sheath) at this electrode is given by $V_b + V_{Pl}$ (plasma potential). At the grounded electrode the sheath voltage equals V_{Pl} . The plasma potential is given by $V_{Pl} = V_{RF}[1 + (A_a/A_c)]^{-1}$ [58], where V_{RF} is the peak RF voltage and A_a and A_c are the areas of anode (larger electrode) and cathode (smaller electrode), respectively. The energy of ions impinging on the electrodes (and the substrate) is given by the sheath voltage and is significantly higher (up to ~100 eV) than the ion energies in the plasma bulk. Such a high energy bombardment can lead to deteriorated material.

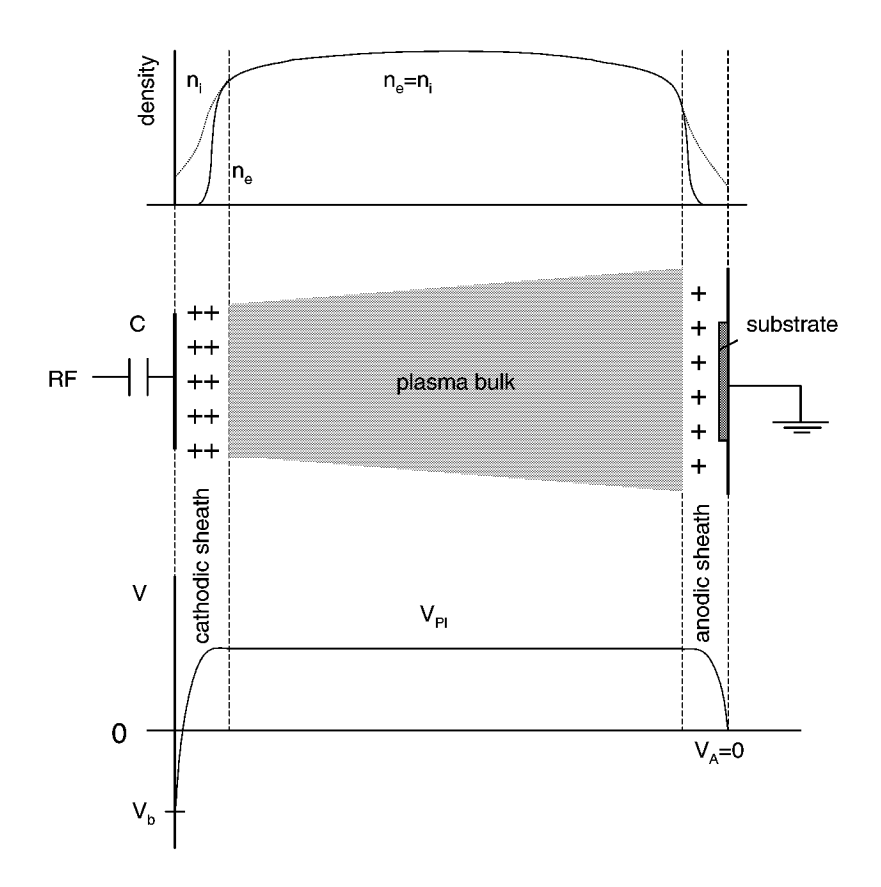


Figure 2.4: Scheme of an RF discharge in a parallel-plate reactor with capacitive coupling of the RF generator; also included are the spatial distributions of potential V (plasma potential V_{pl} , bias voltage V_b , and anode voltage V_A) and electron and ion densities (n_e, n_i) . Draft adapted from [58].

3 Characterization

In this chapter, the different applied characterization methods are explained. For solar cell characterization we used current-voltage (J-V) measurements under illumination and quantum efficiency (QE) measurements. Material characterization methods were Raman spectroscopy, transmission electron microscopy (TEM), hydrogen effusion and X-ray diffraction (XRD). This measurement was performed in a joint German-Israeli research project (project number 01647 E01073) with the Technion Haifa.

3.1 Solar Cell Characterization

A good introduction to solar cell characterization is given by Heidler [63]. An equivalent circuit of a solar cell is shown in figure 3.1, which consists of a diode and a current source in parallel, the latter represents the light generated current. The parallel resistance (shunt resistance) R_{sh} and the series resistance R_s describe Ohmic losses in the solar cell.

3.1.1 Current-Voltage Characteristics

The measurement of the current-voltage characteristics (J-V characteristics) is the primary method to evaluate solar cells. In this work all light J-V measurements were performed at 25 °C using a class A double source solar simulator (WACOM-WXS-140S-Super), which provides an AM1.5 spectrum with 100 mW/cm² light intensity. The solar simulator is calibrated before each measurement with a Hamamatsu photodiode S1336-8BQ (spectral range: 190-1100 nm). The run-to-run reproducibility is better than 2 %. For simple spectral evaluation, a variety of band-pass and cut-on filters is available.

For the p-i-n solar cells examined in this work, the 36 individual cells per substrate (see figure 4.3 for cell area and contact configuration) could be contacted simultaneously and the measurement was carried out by a software program controlling a source-measure unit (Keithly Instruments Inc., type SMU238). The applied voltage was standardly varied between -0.1 and +0.6 V in 10 mV steps.

According to an equivalent circuit as described in figure 3.1 the J-V characteristic of a p-i-n junction without illumination $(J_{Ph}=0)$ $J_d(V)$ can be described by

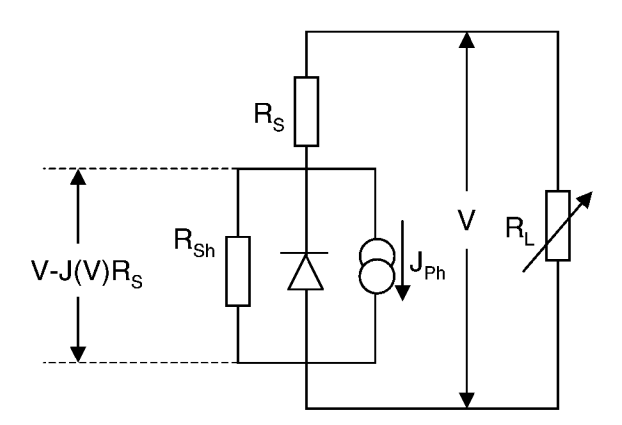


Figure 3.1: Equivalent circuit of a solar cell with shunt (R_{Sh}) , series (R_S) , and load resistance (R_L)

$$J_d(V) = J_0 \cdot \left(exp\left(\frac{e \cdot (V - J(V) \cdot R_S)}{n \cdot k \cdot T}\right) - 1\right) + \frac{V - J(V) \cdot R_S}{R_{Sh}}$$
(3.1)

J(V) is the current density, V is the applied voltage, J_0 is the saturation current density, e is the elementary charge, n the diode quality factor, k is the Boltzmann constant and T is the temperature. The shunt (R_{Sh}) and series resistance (R_S) are defined from the equivalent circuit in figure 3.1. Figure 3.2a shows a typical dark J-V curve of a μ c-Si:H solar cell. In region A the J-V curve is determined by the shunt resistance. In region B the current increases exponentially with the applied voltage (diode behavior), series and shunt resistance can be neglected here. In region C the curve is dominated by the series resistance.

In case of monocrystalline p-n solar cells the superposition principle is valid and in the illuminated case the dark current density $J_d(V)$ and the voltage-independent photo current J_{Ph} add up to the total current. In drift controlled devices, like amorphous and microcrystalline p-i-n junctions, an applied voltage affects the electric field strength inside the i-layer and therefore the charge carrier extraction. The photo current is therefore voltage dependent and the current density under illumination is given by

$$J_l(V) = J_d(V) + J_{Ph}(V) (3.2)$$

From the light J-V characteristic (see figure 3.2b), one can determine several photovoltaic parameters:

• The efficiency η is defined as the ratio of the maximum power generated by the

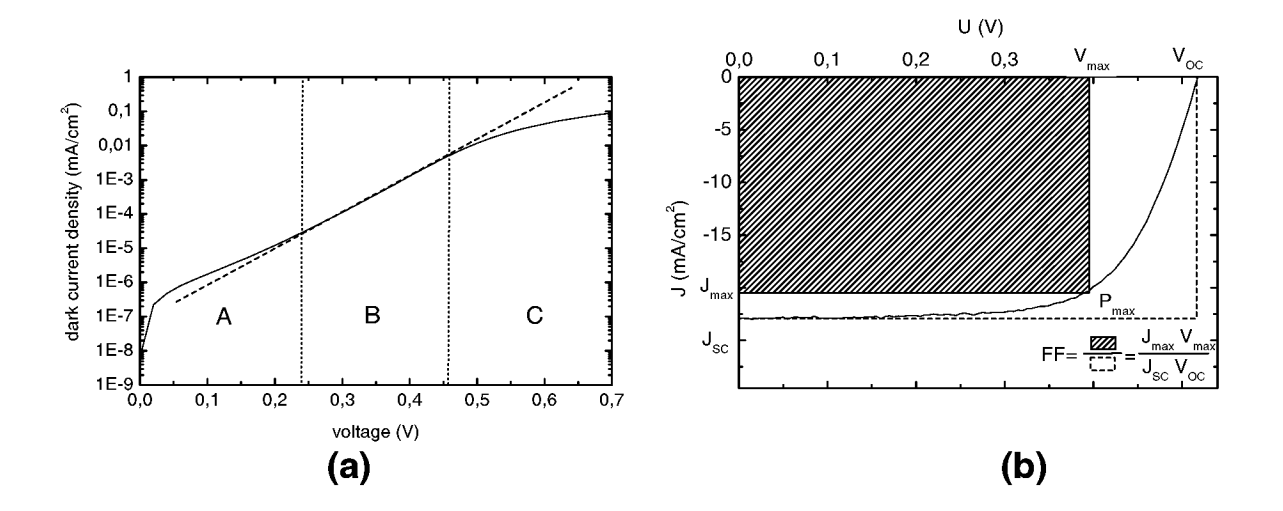


Figure 3.2: a) Dark J-V characteristics of a μ c-Si:H solar cell, b) Light J-V characteristics with important J-V parameters (see text)

device (given by $P_{max} = J_{max} \cdot V_{max}$) and the radiation power incident on the area of the device.

- \bullet The short-circuit current density J_{SC} is the maximum current density generated by the device.
- The open-circuit voltage V_{OC} is the maximum voltage generated by the solar cell under illumination.
- The fill factor FF is defined as

$$FF = \frac{J_{max} \cdot V_{max}}{J_{SC} \cdot V_{OC}} \tag{3.3}$$

and gives a description of the "rectangularness" of the light J-V characteristics and is an integral measure of the collection efficiency at the maximum power point. In this work V_{OC} and FF are used as a measure for the material quality.

Differences in the J-V characteristics of μ c-Si:H and a-Si:H solar cells

As was described in section 2.1 the material properties of a-Si:H and μ c-Si:H are quite different. The property leading to the most obvious difference in the light J-V characteristics of solar cells based on amorphous and microcrystalline silicon is the band gap (mobility gap) of the absorber material. The mobility gap in a-Si:H is significantly higher

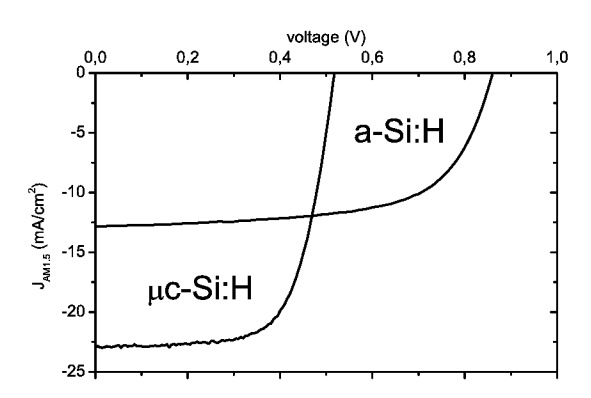


Figure 3.3: Light J-V characteristics of an amorphous (after light-induced degradation) and a microcrystalline solar cell.

than the band gap in μ c-Si:H. This leads on the one hand to a higher V_{OC} (up to ~1 V instead of ~0.5 V) and on the other hand to a lower J_{SC}. Typical J-V characteristics of an amorphous and an microcrystalline solar cells are shown in figure 3.3. The recombination losses in the carrier extraction process are determined by the mobility-life time ($\mu\tau$) products for electrons and holes, respectively, which is significantly lower in a-Si:H than in μ c-Si:H. This, in combination with the higher absorption coefficient for energies above the band gap, leads to a significantly lower optimum i-layer thickness of a-Si:H cells (~300 nm) compared to μ c-Si:H cells > 1 μ m. An amorphous solar cell with the thickness of a typical μ c-Si:H cell exhibits a significantly reduced FF.

3.1.2 Quantum Efficiency

Spectral response measurements give additional insight into the working principle of solar cells. Conclusions about the optical losses and the field distribution in the solar cell can be drawn. The quantum efficiency $QE(\lambda)$ of a solar cell is defined by

$$QE(\lambda) = \frac{J_{Ph}(\lambda)}{e \cdot \Phi(\lambda)} \tag{3.4}$$

with Φ as the number of photons per time, area, and wavelength interval, e as the elementary charge and J_{Ph} as generated photo current density per wavelength interval. Therefore the quantum efficiency describes the probability that an incident photon generates a charge carrier pair which contributes to the photo current.

Figure 3.4 shows as examples the quantum efficiencies of an amorphous and a microcrystalline solar cell. The main difference between these cells is the higher quantum efficiency

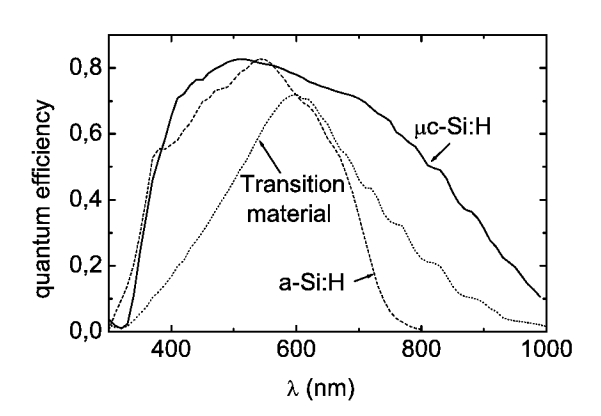


Figure 3.4: Quantum efficiencies of solar cells with different i-layers: microcrystalline (i-layer thickness: $\sim 1.6 \ \mu \text{m}$), amorphous ($\sim 0.4 \ \mu \text{m}$) and microcrystalline with a high amorphous volume content (transition material, $\sim 1.3 \ \mu \text{m}$).

for the μ c-Si:H solar cell in the red and infra-red spectral range ($\lambda > 800$ nm) due to the lower band gap. For solar cells with similar i-layer material the quantum efficiency in the long wavelength range is determined by the i-layer thickness and the light-trapping properties. Because of the high absorption coefficient for low wavelengths the quantum efficiency for $\lambda < 400$ nm is to a large extend determined by the absorption in the p-layer. For both the a-Si:H and the μ c-Si:H solar cell the high quantum efficiency in this spectral range indicates low absorption losses in the p-layer. Additionally a μ c-Si:H solar cell with a high amorphous volume content is shown which exhibits not only a reduced quantum efficiency for wavelengths >800 nm due to the reduced crystalline volume fraction but also a reduced quantum efficiency below 600 nm due to carrier extraction problems. More details on the origins of quantum efficiency losses can be found in [64]. Additional insights can be obtained e. g. by voltage-dependent measurements [65].

For the measurement of the quantum efficiency, the differential spectral response method was used: a chopped monochromatic sample beam is used to generate a small photo current. The wavelength can be varied in the desired wavelength region. All measurements were carried out at 25 °C. Setup and method are described in [66] and [67], respectively.

Using the flux density $\Phi(\lambda)$ of the AM1.5 solar spectrum, $QE(\lambda)$ is connected to the voltage dependent photo-generated current $J_{Ph}(V)$ by integrating over all wavelengths:

$$J_{Ph}(V) = e \cdot \int QE(\lambda; V)\Phi(\lambda)d\lambda \tag{3.5}$$

3.2 Material Characterization

Film Thickness and Gas Utilization

All film thicknesses were measured using a surface profiler from Veeco Instruments Inc., type DEKTAK 3030. For the measurement, an abrupt step has to be created first. In case of solar cells this was done by scratching the Si layer through to the ZnO substrate with a scalpel and then etching the ZnO away with HCl. Then the thickness of ZnO and the doped layers had to be subtracted to get the i-layer thickness. On other substrates it was done either by scratching the film and jerky removing an applied tape, thereby tearing off part of the film from the substrate or by applying a drop of KOH lye on the film while gently heating the substrate.

From the film thickness the deposition rate r can be calculated by dividing it by the deposition time. From the ratio of deposition rate to silane gas flow a gas utilization η_{gas} can be determined:

$$\eta_{gas} = \frac{silicon\ atoms\ deposited}{silicon\ atoms\ entering\ by\ gas\ flow} = \frac{r\ A\ \rho\ /\ m_{Si}}{f\ p_0\ /\ k\ T_0} \approx 11.1\ \% \times \frac{r[in\ \mathring{A}/s]}{f[in\ sccm]} \ (3.6)$$

where A is the substrate area ($10\times10~{\rm cm^2}$), ρ the density of crystalline silicon, k the Boltzmann constant, T_0 the standard temperature ($273~{\rm K}$), m_{Si} the atomic mass of silicon ($28{\rm u}$), p_0 the standard pressure ($1013~{\rm hPa}$), r is the deposition rate and f is the silane gas flow (in sccm¹). Note that according to this definition η_{gas} is the fraction of atoms entering the chamber which end up on the substrate. Since there is always deposition on the powered electrode and on the substrate holder we estimate $\eta_{gas} = 40~\%$ to be about the limit we can achieve. This estimation is based on the one hand on the ratio of the substrate area to other areas exposed to the plasma and on the other hand on our experience concerning the highest achieved gas utilizations. Note that the deposition rate on the cathode (i. e. the smaller electrode, here: the powered electrode) is often higher than on the substrate [68]. However, this was not checked for the process parameters applied in this work.

Transmission Electron Microscopy (TEM)

Transmission electron microscopy (TEM) provides information on the microstructure of μ c-Si:H. It is based on the diffraction contrast generated by electrons, which have passed through a very thin sample. The method in general is comprehensively discussed in

¹standard cubic centimeters per minute, standard referring to standard temperature (0 °C) and pressure (1 atmosphere)

literature (e. g. [69]). Also the special application of TEM to μ c-Si:H films is subject of several works (see [43] and references therein).

We used a transmission electron microscope JEM-1000 (1 MeV acceleration voltage) with in-situ heating facilities. TEM cross-sectional samples $\sim 0.05-0.1~\mu m$ thick were prepared by standard techniques including mechanical polishing, dimpling and low-angle Ar⁺ etching (2 kV beam).

Hydrogen Effusion

For hydrogen effusion, the films were inserted into an evacuated quartz tube and were heated at a constant heating rate of 20 °Cmin⁻¹ to about 1000 °C. During the evolution experiment, the partial pressure of H_2 detected with a quadrupole mass analyzer were used as a measure of the effusion rate. An overview about hydrogen phenomena in thin film silicon is given in [70]. The experimental set-up is described in detail in [71]. Hydrogen effusion reveals details on the structural film properties by studying at which temperatures hydrogen is released from the film. Hydrogen effusion peaks at characteristic temperatures allow conclusions about the void structure of μ c-Si:H and the binding configuration of the hydrogen in the material.

X-Ray Diffraction (XRD)

X-Ray diffraction is a method to gain information about crystal structure, phases and crystal defects [72] based on Bragg's equation. XRD analysis was carried out by Philips PW3020 diffractometer with Θ -2 Θ scan (Bragg-Brentano geometry) with an angle step of 0.01 ° and a signal collection time of 10 to 20 s. CuK $_{\alpha}$ -radiation characterized with a wavelength of λ =1.542 Å (\sim 8 keV) was initiated by a voltage of 30 kV and a current of 40 mA.

Raman Spectroscopy

Raman spectroscopy is a powerful tool to investigate the structural properties of μ c-Si:H. The theory of this method in general can be obtained from literature [73, 74]. An overview of the application to μ c-Si:H is e. g. given in the works of Hapke [75], Houben [43, 46] and Vetterl [44].

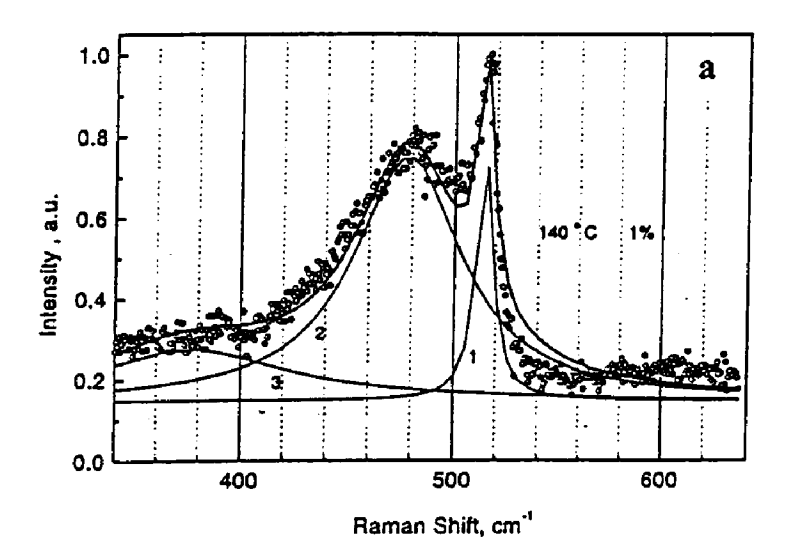
Raman measurements were performed using a DILOR micro-Raman monochromator. The 514.5 nm green line from an argon laser with an output power of 0.2–1.2 mW was used. This power was found to be low enough to prevent any artefacts due to crystallization in the illuminated area. At the used wavelength a depth of approximately 200-300 nm is probed. Since the samples are illuminated from the backside (i. e. not the substrate side)

in case of solar cells the amorphous n-layer is responsible for a part of the amorphous signal. More details on the experimental set-up can be found in [76].

Figure 3.5 shows two Raman spectra as examples. Sample (a) has a high amorphous volume content, sample (b) is a typical microcrystalline sample with a high crystalline volume content. The highly crystalline sample is dominated by the prominent peak at 520 cm⁻¹, related to the excitation of the Γ'_{25} phonon, which is also observed for crystalline silicon. Due to the absence of long-range translation symmetry in a-Si:H, the quantum number k is no longer well-defined and phonon excitation is possible without the restriction of k conservation. For this reason, the Raman spectrum of sample (a) exhibits a broad intensity distribution around 480 cm⁻¹ (corresponding to a transverse optical phonon) indicating amorphous phase. Additionally, it shows a peak with a lower amplitude around 380 cm⁻¹ (corresponding to a longitudinal optical phonon [77]). Since μ c-Si:H is a mixed phase material, generally all peaks are observed in a Raman spectrum. We used the deconvoluted Raman peak intensities to estimate the crystalline volume fraction of the films. For this purpose we introduce the quantity called Raman crystallinity P defined as

$$P = (I_{520})/(I_{480} + I_{380} + I_{520}) (3.7)$$

where I_{520} is the intensity of the crystalline peak and I_{380} and I_{480} are the intensities of the amorphous peaks. However, P is only a estimation for the true crystalline volume content, for differentiation we will call it Raman crystallinity. Especially close to the onset of amorphous growth the crystallinity of microcrystalline silicon is underestimated by Raman crystallinity. For a more detailed discussion on this topic see e. g. [44]. Note that, while the quantity Raman crystallinity is widely used, the employed peaks vary. Sometimes an additional crystalline peak at 500 cm⁻¹ is used, while the peak at 380 cm⁻¹ is sometimes not used. However since the Raman crystallinity is only a qualitative measure for the real crystallinity the results obtained by these methods are similar.



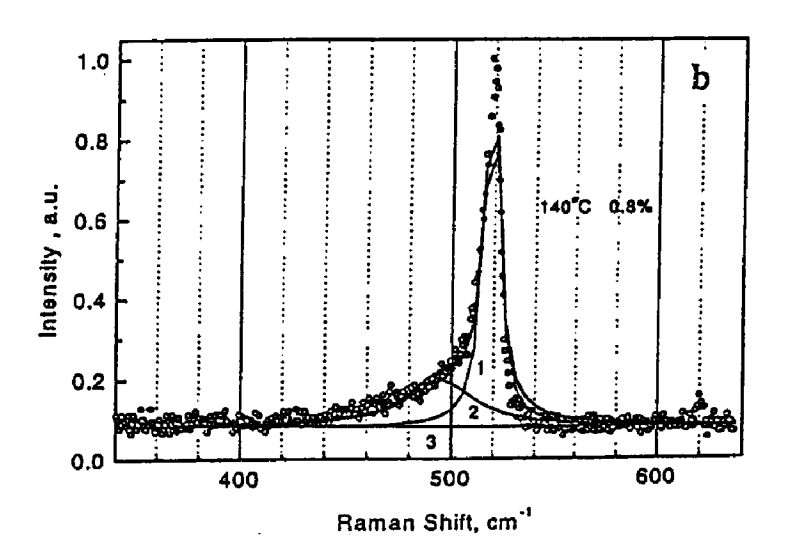


Figure 3.5: Typical examples of Raman spectra of μ c-Si:H and their deconvolution. Sample (a) has a high amorphous volume content, sample (b) is a typical microcrystalline sample with a high crystalline volume content.

4 Solar Cell Preparation

All solar cells prepared in this work are deposited on ZnO coated glass (Corning 1737) substrates. Onto the substrate the silicon layers are deposited in the sequence p-doped, intrinsic and n-doped layer (p-i-n structure or superstrate configuration, figure 4.1). After that a back reflector is deposited. The preparation of these layers is described in detail in the following sections.

4.1 Substrates and Back Reflectors

During this work ZnO: Al was used as a TCO material. This material is highly transparent and conductive (sheet resistance $< 15 \Omega_{\square}$ at ~ 500 nm thickness). Its properties are less affected by the hydrogen rich plasmas which are applied in this work than the SnO₂:F which is mainly used in the industrial production of thin film silicon modules [78, 79]. The ZnO:Al is prepared by magnetron-sputtering. In figure 4.2a a sketch of an rf sputtering process from a ceramic ZnO:Al₂O₃ target (2 wt. % Al) is shown. An electric field is applied between two electrodes in a vacuum chamber filled with argon. This leads to an Ar plasma. Ar ions are accelerated towards a ZnO target mounted on the cathode. By the impact of the ion bombardment target material is removed and may condense on a substrate. In case of magnetron-sputtering magnets are applied at the back of the electrode, forcing the electrons to follow circular trajectories because of the Lorentz force. This increases the residence time of the electrons in the plasma region and thereby the ionization rate significantly. However, the variation of magnetic field strength above the target surface leads to non-uniform erosion of the target. In our case 6" round targets were used leading to a ring-like erosion profile. This influences the homogeneity of the deposited films. In case of the substrates used during this work the region of homogeneous ZnO film thickness was usually confined to a circular area with about 8 cm diameter on the 10×10 cm² substrate. In addition to argon, oxygen can be used as a source gas. This allows the control of the stoichiometric composition of the growing film within certain limits. More details on ZnO substrates and the sputtering process are described in [80].

Due to the low absorption coefficient of μ c-Si:H we need light trapping: The incoming light is scattered by a rough surface. Then a significant fraction of the long wavelength light is trapped within the device due to multiple reflections between back reflector and

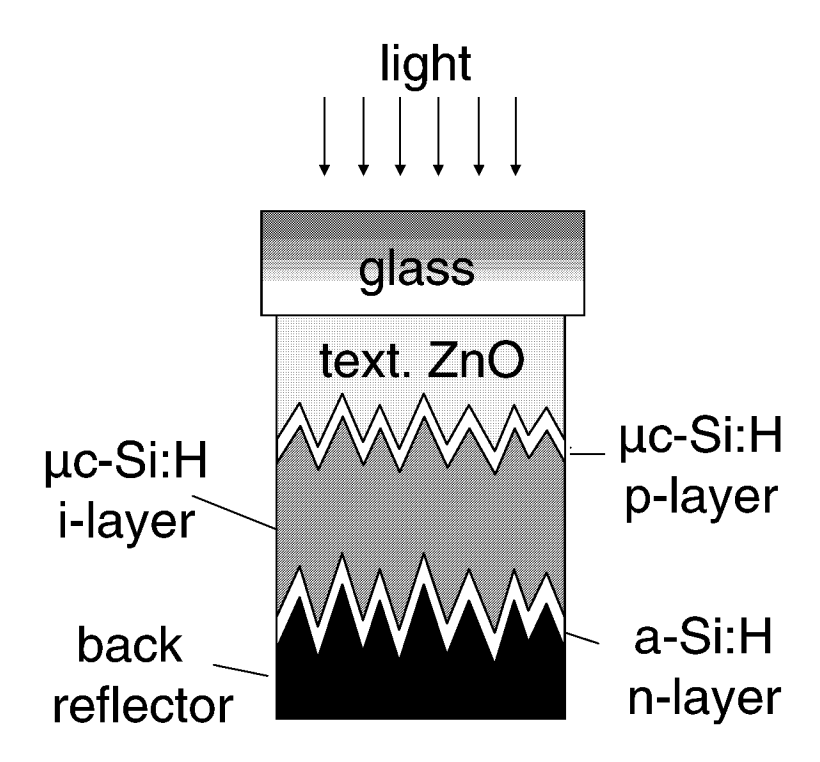


Figure 4.1: p-i-n structure (superstrate configuration) of a μ c-Si:H solar cell. The back reflector is either Ag or ZnO/Ag.

front contact (ignoring reflections at other interfaces) and therefore more efficiently absorbed in the intrinsic layer. For this light trapping the initially smooth ZnO:Al substrate is textured by wet-chemical etching in diluted HCl (see figure 4.2b). This texture can be adjusted to give optimal light scattering over a wide wavelength range [80–83]. Furthermore, due to an index grading effect these textured ZnO layers act as an anti-reflex coating and therefore increase the absorbed light in the short wavelength region, as well.

The back contact of the cells was either thermally evaporated silver (Ag) or a combination of magnetron-sputtered ZnO and Ag. Back reflectors are deposited as pads with a size of 1×1 cm² and smaller defining the solar cell areas (see figure 4.3). Only the values of the best 1×1 cm² cells were considered for the evaluation of solar cells to avoid measurement uncertainties due to errors in the cell area. The smaller cells were used for means of diagnosis only (e. g. contact problems, current collection, etc...). Definition of the solar cell area by this technique relies on low lateral conductivity of the n-layer. To avoid current collection an amorphous n-layer, which has a significantly lower conductivity than a microcrystalline one, was applied.

The J_{SC} depends on the quality of the applied TCO substrate and back reflector. E. g. a ZnO/Ag back reflector improves J_{SC} typically by 2–3 mA/cm² for an i-layer thickness

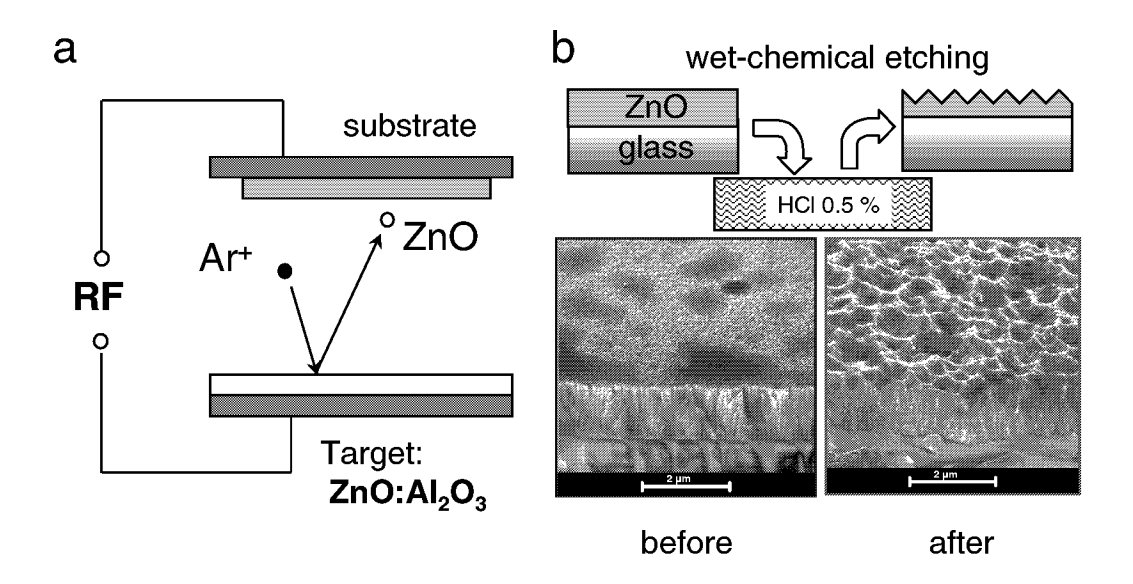
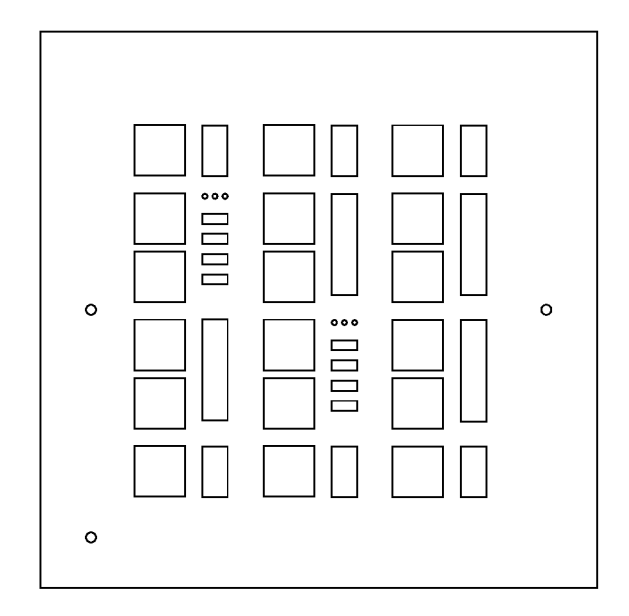


Figure 4.2: (a) Sketch of the rf-sputtering process from a ceramic target, (b) Scanning electron microscope picture of a magnetron-sputtered ZnO:Al film before and after wet-chemical etching in 0.5 % HCl solution (from [80])

of $\sim 1.5~\mu m$ compared to an Ag back contact. This is illustrated in figure 4.4. The J_{SC} is shown as a function of the deposition pressure p_{dep} during i-layer growth for an Ag and a ZnO/Ag back contact, respectively. One can see that for a given p_{dep} the J_{SC} -values for the ZnO/Ag back contact are 2-3 mA/cm² higher. The development of optimized ZnO substrates is one of the research topics in our institute: Light scattering properties and transparency of the texture etched ZnO substrates was significantly improved parallel to this work. Throughout this thesis different TCO qualities were available and often simply Ag back reflectors were applied for fast evaluation. As regularly cross-checked, the different optical properties of different substrates and the use of Ag- or ZnO/Ag back contacts did not or only slightly influence FF and V_{OC} . Therefore FF and V_{OC} were applied for the comparison of solar cells with different light trapping properties. Since these parameters are to a major part determined by the bulk properties of the i-layer, they serve as a measure for the material quality throughout this work.

4.2 Plasma-Enhanced Chemical Vapor Deposition (PECVD)

Plasma enhanced chemical vapor deposition (PECVD, also: glow discharge deposition) is a standard deposition method to prepare a-Si:H and μ c-Si:H films. To date, the technique



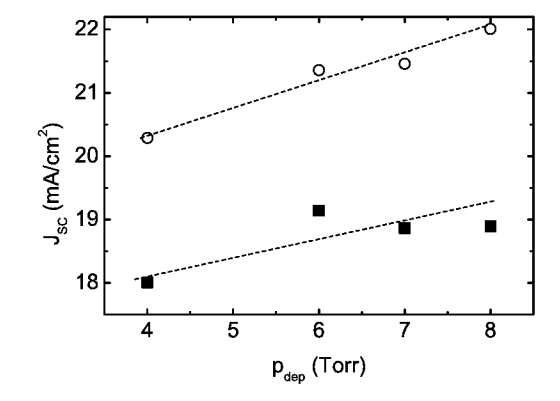


Figure 4.3: Cell geometry of p-i-n cells on a $10\times10~\text{cm}^2$ substrate. The square cells have an area of $1~\text{cm}^2$, the three types of rectangular cells have areas of 1, 0.5 and 0.1 cm². The small dots serve as positioning mark only.

Figure 4.4: Short-circuit current density J_{SC} vs. the deposition pressure p_{dep} applied during deposition of the i-layer with Ag- and ZnO/Ag back reflector (1 % silane concentration, 0.4 W/cm² power density)

is applied by all industrial a-Si:H solar module producers. Detailed information about the PECVD method is given in the books by Chapman [59], Haefer [84], Frey and Kienel [62], Luft and Tsuo [60], or Bruno, Capezzuto and Madan [58].

PECVD is a deposition method where reactive species are produced by an electrical discharge leading to a plasma (see section 2.3). The gas-phase reactions in glow discharges reduce the substrate temperature required for film deposition compared to thermal CVD, which depends completely on thermally-induced gas-surface interaction. Externally applied electrical energy is used to provide the activation energy for gas decomposition in the glow discharge deposition process. This allows to choose a substrate temperature which is independent from the plasma. In this work the electrical energy was capacitively coupled in with 13.56 MHz excitation frequency.

Major steps of the plasma-enhanced CVD process include source gas diffusion, electron impact dissociation, gas-phase chemical reaction, radical diffusion, and deposition. When silane (SiH₄) is used as a source gas in a glow discharge deposition process, the electron-impact processes lead to reactive neutral species, such as SiH, SiH₂, SiH₃, Si₂H₆, H, and H₂ and ionized species, such as SiH⁺, SiH₂⁺, SiH₃⁺, and so on. An overview about the possible reactions in silane plasmas is given in [85]. Some of these ions and free radicals diffuse to the surface of the substrate, and a multiplicity of secondary reactions occurs. The reaction of ions and free radicals with each other or their adsorption onto the substrate surface is followed by the process by which these species or their reaction products are

incorporated into the growing film or are re-emitted from the surface into the gas phase.

The properties of the deposited silicon film and especially whether its structure is amorphous or microcrystalline strongly depend on the combination of the deposition parameters used. The main parameters and their major effects in case of silicon deposition from SiH_4 and H_2 are:

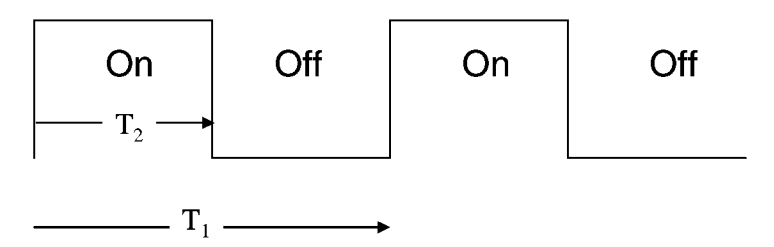
- The power density increases the electron temperature of a plasma leading to a higher dissociation rate. Therefore, sufficiently high power is required to realize high growth rates. It also has a strong impact on the plasma potential.
- The total gas flow controls the residence time in the plasma, influencing the gas utilization and the extent of gas phase polymerization. The silane flow determines the supply of silicon atoms for film growth. Therefore the SiH₄ gas flow defines an upper limit for the deposition rate (when all silicon atoms are built into the film formed on substrate and electrodes).
- The silane concentration (i. e. the ratio of silane to hydrogen flow, [SiH₄]/[H₂]) has a direct impact on the ratio of growth precursors to hydrogen atoms in the plasma. Thereby it is an easy tool to control the transition between amorphous and microcrystalline growth.
- The deposition pressure determines the mean free path length of the gas molecules and thereby the collision probability. It also controls the silane partial pressure and the residence time of gas particles in the plasma. A high deposition pressure also reduces the plasma potential and therefore lowers the energy of the ions impinging on the substrate.
- The excitation frequency has a strong impact on the plasma potential and electron energy distribution. In this work the excitation frequency is fixed at 13.56 MHz.
- By introducing boron- or phosphorous-containing source gases into the reaction, doped films can be achieved.

Pulsed Excitation

During the last few years, modulation of the RF signal of PECVD systems has been investigated as an attempt to improve the material properties of a-Si:H and μ c-Si:H and to improve the deposition process by increasing the growth rate and reducing powder formation. The discharge is modulated by a square-wave frequency variable in the range from 10^{-1} to 10^4 Hz. This, in practice, results in periodically switching on and off the plasma at the mentioned frequency. The modulation parameters are the pulse period (the time between two successive discharge ignitions) or the corresponding pulse frequency, respectively, and the duty cycle, indicating the percentage of the period in which the discharge is switched on (see also figure 4.5).

Pulsed Plasma:

Superposition of RF with square wave signal



Pulse parameters:

Pulse frequency v_p : 1/T₁, Duty Cycle DC: T₂/T₁=60%

Figure 4.5: Definition of pulse parameters

4.3 PECVD System

All depositions made in this work were carried out in a commercial PECVD system which was originally manufactured by Glasstech Solar Inc., USA, and supplied by Materials Research Group Inc., USA. The system consists of four deposition chambers which are interconnected by two transfer chambers; the latter serve also as load locks (see figure 4.6).

Via the loading chambers, a substrate holder containing the substrate was transferred into the desired deposition chamber. In the p- and n-chamber, the boron and phosphorous doped films were deposited, respectively. Both i-chambers (I_1 and I_2) served only for the deposition of the intrinsic layers to minimize cross contamination.

The gas supply and pumping scheme is sketched in figure 4.7. Each chamber is equipped with a needle valve in the Argon purge line. All other gas lines are equipped with automatic mass-flow-controllers. The gas line leading to the i-chamber is furthermore equipped with a gas purifier. Its purpose is to reduce oxygen contamination [86,87]. During deposition, each chamber is pumped by a wide-range turbo pump via a pressure-controlled butterfly-valve. The pumps are running with nitrogen seal gas to prevent contamination of the pump bearings by the toxic waste gases. In addition, each turbo pump has a rotary-pump providing a pre-vacuum which is running with nitrogen gas ballast, which furthermore dilutes the dangerous gases in the exhaust lines.

The layout of a single chamber is shown in figure 4.8. The substrate holder is heated indirectly via the heater system; according to calibration measurements, the substrate temperature T_S is about two thirds of the heater temperature T_H without a plasma. At the

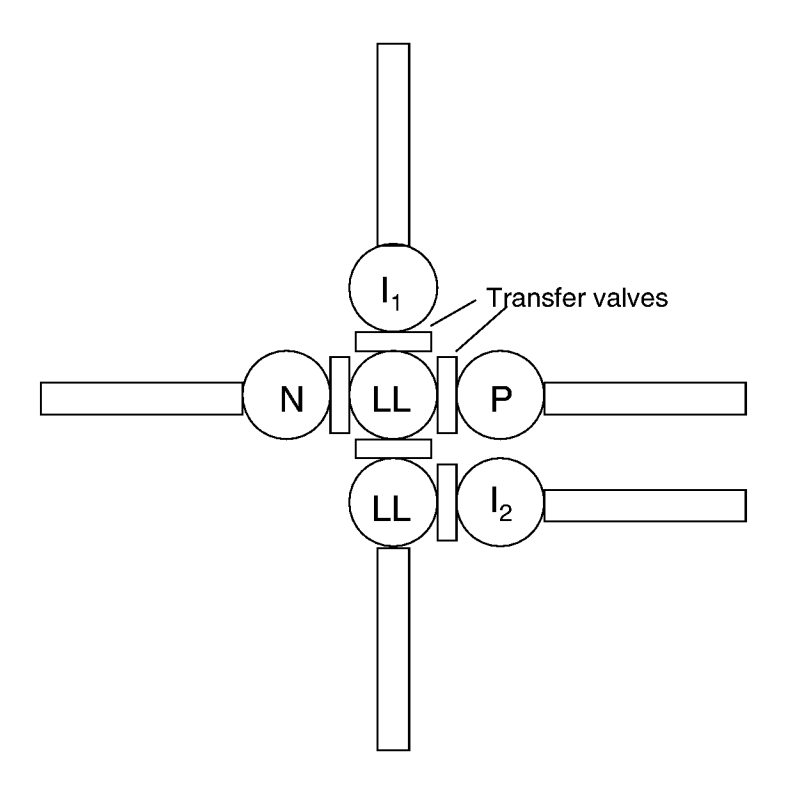


Figure 4.6: Layout of deposition system (top view) showing the four individual chambers to prepare p-, i-, and n-layers as well as the transfer- and loading chambers (load lock, LL), respectively.

high plasma powers and deposition pressures applied for the i-layers in this work additional heating is introduced by the plasma. The measuring of $T_{\rm S}$ under these conditions is difficult and would involve opening the chamber to mount a cable. This would be necessary for every new combination of power and pressure. To avoid this $T_{\rm H}$ instead of $T_{\rm S}$ is used as a parameter. The substrate holder consists of a frame holding the substrate and a heavy metal plate fixing the position of this substrate by its weight. Riding on a grounded track system, the substrate holder serves as a counter electrode during deposition. The circular electrode has a diameter of 13.5 cm and is surrounded by a shield confining the plasma. The high frequency is provided by a HF generator (Dressler Cesar 1310D) and coupled into the system via an impedance matching network ("matchbox").

All chambers are designed identically except for different electrode distances; these are 1.2 cm in the p-, 1 cm in the i- and 2 cm in the n-chamber if not otherwise stated.

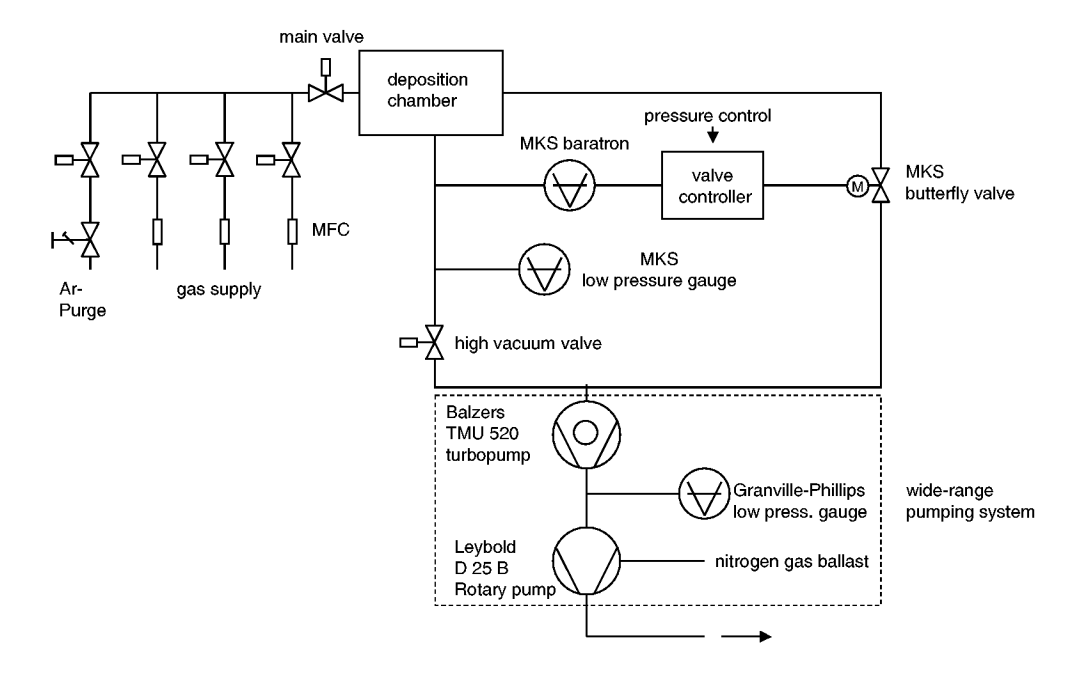


Figure 4.7: Layout of the gas supply and pumping scheme of the 4-chamber deposition system.

4.4 Electrode Design

Two different electrode designs were used during this work. Early results were obtained using an electrode with more or less longitudinal gas flow (figure 4.9a). There the process gas is fed in at one side of the electrode and the pumping is done at the opposite side below the electrode. Later a so-called showerhead electrode was used. A showerhead electrode is a perforated electrode so that the process gas is fed into the plasma space via a multiplicity of holes distributed over the substrate area (figure 4.9b). In this section the influence of both configurations on the homogeneity of the deposition process is described and discussed.

Using an electrode configuration with longitudinal gas flow at high deposition pressures (>5 Torr) and high plasma powers the intrinsic films showed a structural inhomogeneity over the substrate area of 10×10 cm². As sketched in figure 4.10 only a part of the film was μ c-Si:H. The μ c-Si:H region was usually close to the gas exhaust. The structural change could be derived from the J-V parameters of the solar cell or even by eye. In the

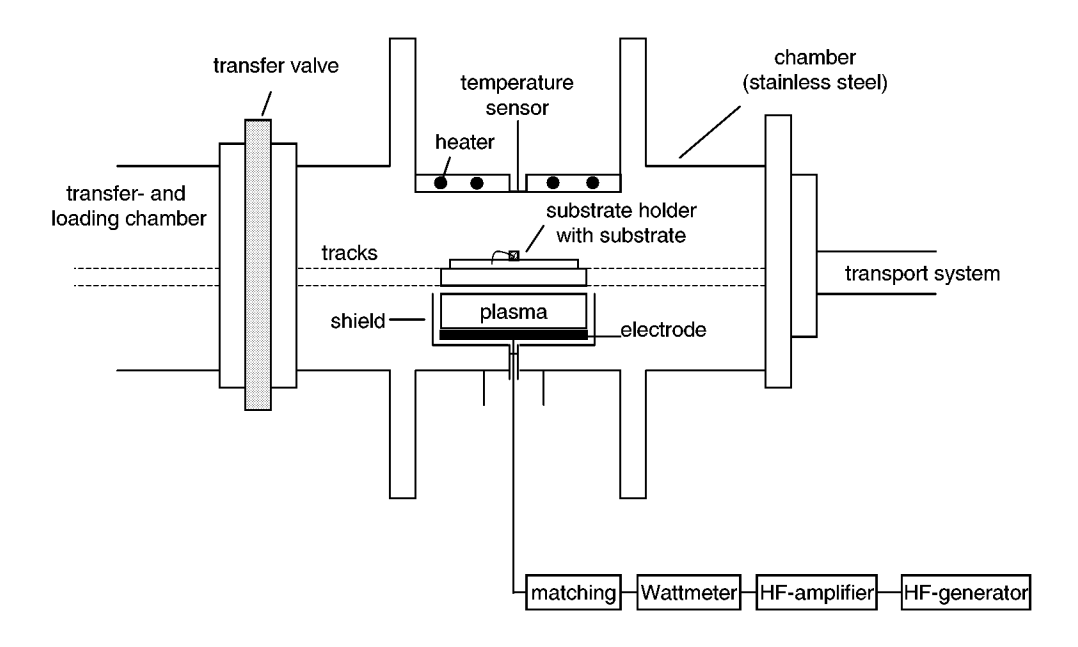


Figure 4.8: Layout of a single deposition chamber.

a-Si:H region the silicon film appears dark red and the μ c-Si:H shows a lighter orange color for i-layer thicknesses in the range between 0.5 and 2 μm . Between both regions a sharp transition line can be seen. The position of this transition line shifted as a function of the deposition parameters, resulting in a smaller microcrystalline area for deposition parameters closer to the amorphous growth regime. Moreover, also within the μ c-Si:H region a characteristic variation of the solar cell parameters on the substrate could be observed. As a typical example figure 4.11 shows the J-V parameters of solar cells with 1 cm^2 area for different positions on the $10 \times 10 \text{ cm}^2$ substrate (see figure 4.10 for the position). In the μ c-Si:H region the efficiency increases steadily until it suddenly drops from 8% to about 4-5%. This is caused by the transition to amorphous growth as can be seen by the high $V_{\rm OC}$ (\sim 700 mV) in combination with the low short-circuit current density $J_{\rm SC}$ $(\sim 10 \text{ mA/cm}^2)$. Fill factor FF and V_{OC} increase until a sudden drop in FF and a strong increase in V_{OC} occur close to the transition. The material close to the transition is the one best suited for microcrystalline solar cell applications. In this work the best 1 cm² cell on the 10×10 cm² substrate was chosen for the interpretation of results obtained in the small area reactor, which is generally in the substrate region close to the transition line.

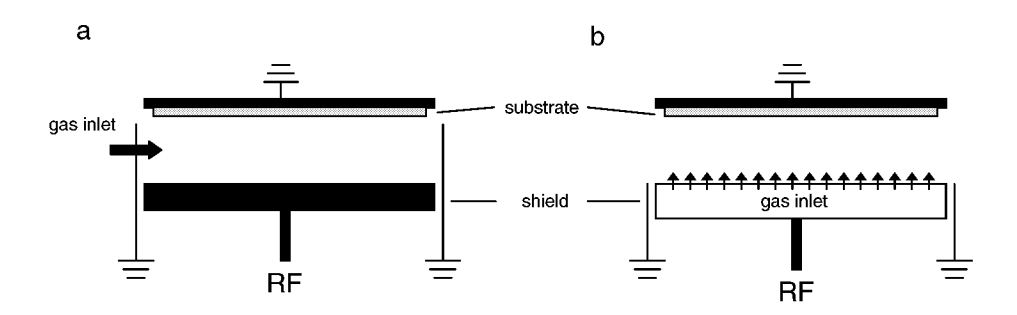


Figure 4.9: Design of (a) longitudinal flow electrode and (b) showerhead electrode.

The trends of the J-V parameters along the substrate are very similar to the ones reported for a variation of the silane concentration for a VHF regime [20, 24] or in our own work (see figure 6.6). We conclude that these inhomogeneous structural material properties are induced by a variation of the effective silane concentration along the substrate due to increasing silane depletion caused by high rate deposition of silicon. Layeillon et al. [88–90] have compared a longitudinal flow reactor and a showerhead reactor by modelling and numerical simulation. They describe a decrease of silane fraction and an increase of hydrogen molecules in the gas phase along the gas flow in a longitudinal flow reactor. The profiles of SiH₂, SiH₃ and H atoms were almost not affected and the deposition was still quite homogeneous. However, they studied a plasma with low pressure and low power conditions and expected a more pronounced inhomogeneity under conditions leading to higher silane consumption rates. Since this is the case in our process there are expected strong variations in the concentration of precursors and hence in the growth process of the material. Caquineau et al. [91,92] described the deposition of silicon nitride. They observed not only a change in the gas composition along the gas flow, but also an effect on the film composition. This effect was pronounced at high plasma powers. Using a showerhead electrode led in both cases to a homogeneous gas composition and therefore uniform film growth [90, 92]. Nienhuis and Goedheer [93] described a homogeneous distribution of silane partial pressure even at high depletion conditions for this type of reactor. Beneficial effects by a showerhead electrode were also reported by Perrin et al. [94] and Sansonnens et al [95].

The up-scaling of microcrystalline silicon layers and solar cells to a substrate size of $30\times30~\rm cm^2$ was subject of the thesis of T. Repmann [96] performed parallel to this work. There a new type of showerhead electrode was developed which was adapted to the require-

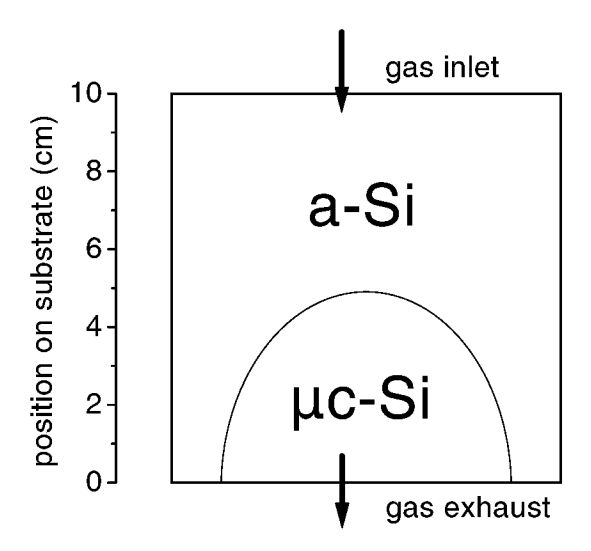


Figure 4.10: Sketch of structural inhomogeneity on the $10 \times 10 \text{ cm}^2$ substrate.

ments of μ c-Si:H prepared at high P_{RF} and high p_{dep} . Based on this design, a showerhead electrode for $10\times10~{\rm cm^2}$ substrate size was developed and implemented in the i-chamber of the PECVD system used in this work. This new electrode strongly improved the homogeneity as can be seen in figure 4.11 by comparing the photovoltaic parameters of similar solar cells prepared using the longitudinal flow and the new showerhead electrode. For solar cells deposited with the latter one, J_{SC} stays constant around $22~{\rm mA/cm^2}$ and V_{OC} varies only from 510 mV at the edges to 525 mV in the center. The variation in FF which decreases from 71 % in the center to 67 % at one edge can, to a large extent, be attributed to an increasing sheet resistance of the ZnO towards the edge of the substrate (due to reduced film thickness, see section 4.1).

4.5 Deposition Procedure (PECVD)

The substrate was heated in one of the chambers under vacuum conditions for at least 45--60 minutes to reach the desired deposition temperature. To prevent any influence of residual gas, the chambers are pumped down to about 10^{-8} Torr before each deposition process. Starting with this high vacuum condition the chamber was flushed with argon for 5 minutes at 5 Torr to achieve a temperature equalization between chamber walls, heater, and substrate before each deposition. For intrinsic film deposition this pre-heating step was done with process gases (H_2 and SiH_4), because the applied gas purifier (preventing a contamination of the process gases with oxygen) needs time to adapt to the process gases and reach an equilibrium state. In the next step, the desired process gases were fed in and the pressure was set. Before plasma ignition, the substrate was removed from the actual

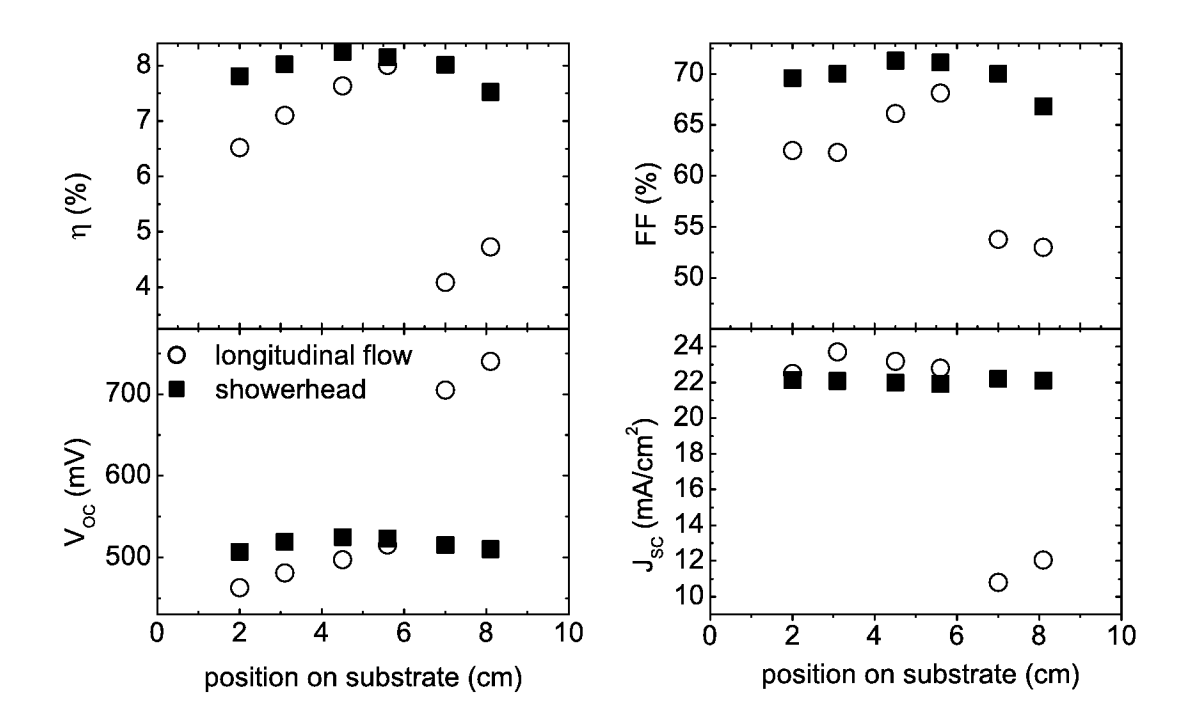


Figure 4.11: Efficiency η , fill factor FF, open-circuit voltage V_{OC} and short-circuit current density J_{SC} vs. the position on the substrate for a showerhead electrode and a longitudinal flow reactor, respectively. See figure 4.10 for position on substrate.

plasma area and the heater served as a counter electrode during the plasma ignition. Then the substrate holder was placed into the plasma region again and the film deposition was carried out. After deposition, the chamber was flushed again with argon at 150 mTorr to remove reactive gases from the chamber, thereby preventing the contamination of the load lock during the transfer. The finished film or device cooled down for about 30 min before taking it out to prevent oxidation.

4.6 Powder Formation

For silane plasmas at high deposition pressures and plasma powers powder formation is often described [97–100]. This powder formation starts with the formation of primary clusters of negatively charged particles which are trapped in the positively charged plasma bulk. Further growth takes place by agglomeration of clusters and addition of neutral and ionic monomers. This can lead to particles up to micrometer-size deteriorating the

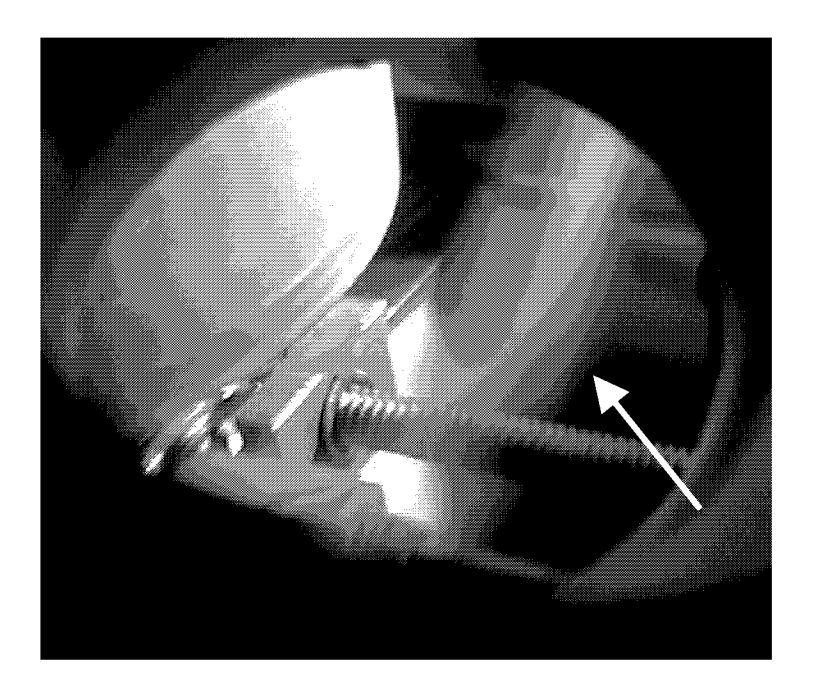


Figure 4.12: Photo of powder stream (marked by arrow) from plasma to gas outlet.

material properties of the growing film [100–102]. Since we worked at extremely high pressure and power this topic is of special interest for this work. A general overview about the so-called dusty plasmas can be found in [103]. This section is a short report about our experiences with powder although we had not the means of studying it quantitatively and systematically.

When we opened the reactor for cleaning, powder deposit was found on the chamber walls already after only a few deposition runs. However, the electrode was usually powder free. Furthermore, the achieved high cell efficiencies made it seem unlikely that there is significant material deterioration due to powder. By a repositioning of the gas outlet to a position next to the deposition area a powder stream outside the plasma zone could be observed through a window (figure 4.12). However, on closer view the powder did not seem to be generated in the plasma area but only at the edge between electrode and plasma shield. This would explain the lack of powder on the electrode and the good material quality. Why is there no severe powder problem in spite of high pressure and power? Reasons could be the high hydrogen dilution and the high gas flows usually applied. In spite of the deposition pressure of typically 10-20 Torr the high hydrogen dilution leads

to corresponding silane partial pressures which are about two orders of magnitude lower. The number of collisions and possible reactions between silicon species in the plasma are strongly reduced. The high gas flows in combination with a low electrode gap lead to low residence times and therefore there would not be the time for powder formation. When we worked at low gas flows (section 7.2) a deterioration of the solar cell efficiency was observed which could be attributed to more porous material due to gas phase polymerization or even powder formation. Since in our configuration the substrate is mounted above the electrode facing downwards, powder – if generated – would settle on the electrode and not onto the growing film.

In summary, powder formation did not seem to be a problem for the material quality. However, the powder deposit in the deposition chamber can lead to laborious cleaning procedures in an industrial production and could therefore be a problem. In that case approaches like pulsed plasma deposition (section 7.3) could be used to reduce this effect.

5 Microcrystalline p-layers

The development of an adapted p-layer is crucial for microcrystalline solar cells. The p-layer has to fulfil many requirements: Together with the n-layer it has to build up the electric field. The absorbance has to be low because the cell is illuminated from the p-side and because due to the low diffusion length in doped μ c-Si:H the light absorbed in the p-layer is mostly lost for the solar cell. Furthermore, since the p-layer is the substrate for the i-layer it influences the structure of the i-layer. As an extreme example it is very difficult to grow a μ c-Si:H i-layer on an a-Si:H p-layer. Also a low-ohmic contact to the ZnO has to be provided.

Usually microcrystalline p-layers are prepared by VHF (very high frequency) deposition [104, 105] which is known to favor μ c-Si:H growth. A VHF deposition process for μ c-Si:H p-layers was already available at the PECVD system applied in this work [106]. Here we wanted to develop μ c-Si:H solar cells completely with 13.56 MHz excitation frequency. Therefore also the p-layer had to be developed at this frequency. This chapter focuses on the development of microcrystalline p-layers in a high pressure and high power regime similar to the one used for i-layers later on (see chapters 6 and 7). Other approaches for μ c-Si:H p-layers prepared at 13.56 MHz are described in [107–109].

Most methods usually applied for the characterization of μ c-Si:H films fail when the films become very thin. Furthermore, the properties of such thin films can vary significantly compared to bulk properties of a thick film prepared under the same conditions. For these reasons an optimization of thick layers deposited on glass substrates for maximum conductivity σ (and, as secondary aspect, a reasonably high deposition rate), was performed only as a first step, while the fine optimization of the p-layers was left for doing inside a solar cell structure. Conductivity measurements were performed at normal room light, i. e. without defined illumination. That was possible, since for doped μ c-Si:H layers light and dark conductivity are virtually identical.

The deposition conditions for μ c-Si:H p-layers prepared at VHF (100 MHz) and RF (13.56 MHz) are shown in table 5.1. If the excitation frequency is lowered to 13.56 MHz the ion bombardment increases [58]. In our experiments we tried to compensate this by an increase of deposition pressure. An increase of the deposition pressure was necessary anyway to ignite the plasma at 13.56 MHz. To achieve microcrystalline growth a quite low [SiH₄]/[H₂]-value of 0.375 % was necessary. In the first experiments we wanted to rule out the influence of carbon on the growth, therefore diborane (B₂H₆) instead of TMB

	power	pressure	gas flows (sccm)			
	(W)	(Torr)	SiH_4	H_2	TMB	B_2H_6
VHF	10	0,2	2,1	200	0,7	_
RF	25	1,5-4,5	0,75	200	_	0,08

Table 5.1: Comparison of RF and VHF (110 MHz) deposition regime for microcrystalline p-layers

(trimethylboron, $B(CH_3)_3$) was used as doping gas for the RF experiments. Since B_2H_6 decomposes thermally at the heater, boron accumulates in the p-chamber. To prevent this the chamber was cleaned after each deposition with a CO_2 plasma [78].

5.1 Influence of Pressure

As a first parameter the deposition pressure p_{dep} was varied under otherwise constant conditions. A too low p_{dep} leads to high ion bombardment whereas high p_{dep} leads to amorphous p-layers (see chapter 8). The latter effect could be counterbalanced by a decrease in silane concentration. Figure 5.1a shows the conductivity of p-doped microcrystalline films deposited at 25 W plasma power and various deposition pressures between 1.5 and 4.5 Torr. The exact deposition parameters are shown in table 5.1. Three different data points for one deposition pressure correspond to different places along the diagonal of the substrate. All layers showed a conductivity above 0.1 S/cm and are therefore microcrystalline (typical for a-Si:H: $< 10^{-3}$ S/cm). A broad maximum around $\sigma \sim 5$ S/cm can be seen. Figure 5.1b displays the deposition rate of these p-layers vs. the deposition pressure. The deposition rate increases with increasing deposition pressure from 0.2 to about 1.1 Å/s. Because the deposition time was held constant, only the layers prepared at $p_{dep}>2$ Torr achieved thicknesses ~ 100 nm. Therefore the reduced conductivities at p_{dep} below 2.5 Torr are not necessarily correlated to a deteriorated structure but can be explained by the low film thicknesses. These depositions were not repeated to achieve thicker layers since the deposition rates are to low for a high deposition rate cell process anyway. The best homogeneity in σ and film thickness (expressed by the deposition rate) was achieved for deposition pressures of 3.0 and 3.5 Torr. For comparison, an older series performed at a plasma power of 5 W [106] is included in both graphs. For this series the conductivity shows a much sharper maximum at 3 Torr, reaching only ~ 0.1 S/cm. Even for thicker layers this value did not improve. The corresponding deposition rates are all below 0.3 Å/s. As a compromise between high σ , homogeneity and deposition rate further optimization was carried out at a p_{dep} of 3 Torr.

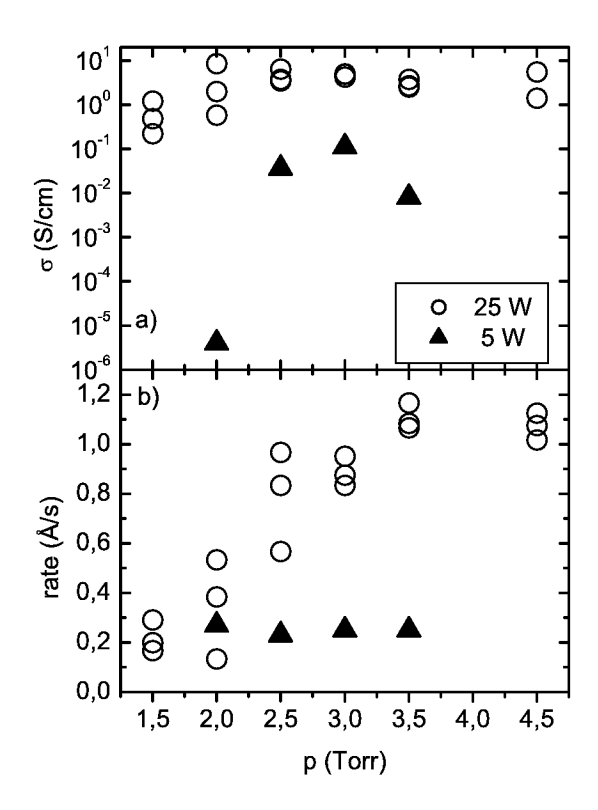


Figure 5.1: a) Conductivity and b) deposition rate of microcrystalline p-layers vs. deposition pressure p_{dep} . Other parameters: ν_{ex} : 13.56 MHz, SiH₄ flow: 0.75 sccm, H₂ flow: 200 sccm, B₂H₆ flow (5 % in He): 0.8 sccm, plasma power: 25 W. For comparison, an older series [106] at low plasma power (5 W) is added.

5.2 Influence of Doping

In the last section we found out that this deposition regime is suited for the deposition of highly conductive p-doped μ c-Si:H layers. In this section we further optimized the B₂H₆-doped layers. Furthermore we examined the influence of TMB-doping. The use of TMB as doping gas is desirable, because then no cleaning step (CO₂ plasma) after the deposition is required. However since TMB contains carbon a disturbance of the growth of the μ c-Si:H p-layer is possible. The optimization of the doping ratio (using TMB and B₂H₆) was carried out at a deposition pressure of 3 Torr and a power of 25 W. These parameters provided a high conductivity, a good homogeneity and a high deposition rate. Figure 5.2a displays the conductivities of the microcrystalline p-layers vs. the used dopant gas flows. The σ -values for B₂H₆ (5 % in He) and TMB (2 % in He), exhibit a broad maximum around 0.1 and 0.2 sccm, respectively. In case of B₂H₆ only dopant gas flows up to 0.2 sccm were applied because of the already achieved high conductivities and the

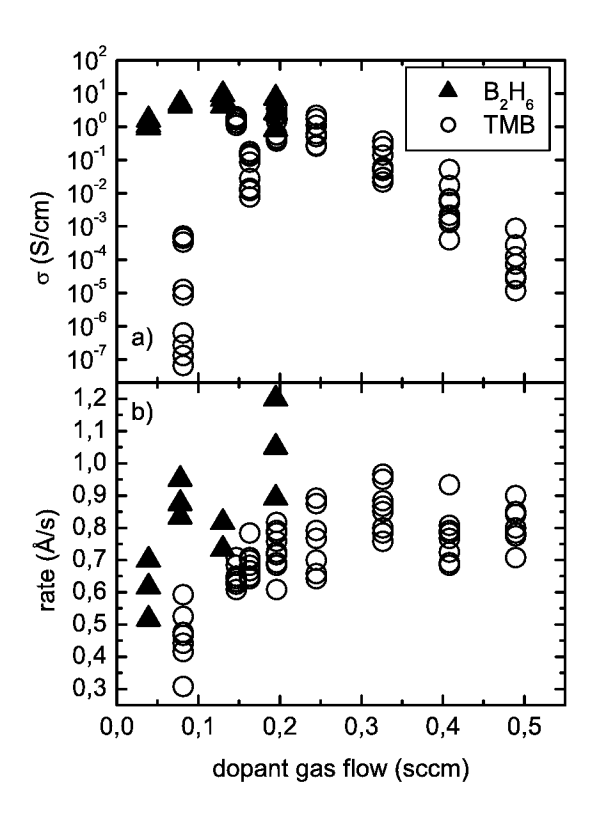


Figure 5.2: a) Conductivity σ and b) deposition rate of microcrystalline p-layers vs. dopant gas flow. Either B_2H_6 (5 % in He) or TMB (2 % in He) are used as dopant gas. Other parameters: SiH₄ flow: 0.75 sccm, H₂ flow: 200 sccm, plasma power: 25 W, deposition pressure: 3 Torr.

increasing inhomogeneity at 0.2 sccm. The conductivities achieved with B_2H_6 (10 S/cm) were higher compared to the values achieved with TMB (~2 S/cm). Nevertheless, both conductivities indicate microcrystalline material. Figure 5.2b shows the corresponding deposition rates for the various dopant gas flows. With both dopant gases there is an increase with increasing flows up to 0.2 sccm. For the TMB-doped layers for dopant gas flows above 0.2 sccm there is a saturation at about 0.8 Å/s. The highest rate achieved with B_2H_6 was above 1 Å/s at 0.2 sccm. The increase in deposition rate with higher dopant gas flows can be explained by the fact that the growth of μ c-Si:H from SiH₄ is a cationic chemisorption [110]. That means that during the adsorption of silicon precursors an electron transfer from the adsorbed molecule to the acceptor level of the surface occurs. Therefore this process is facilitated by p-doped surfaces. In case of B_2H_6 an additional explanation is the catalytic effect of B_2H_6 on the silicon film growth [111]. Boronhydride radicals like BH₃ lead via the generation of e. g. BH₅ to a desorption of hydrogen from the surface. The higher number of dangling bonds on the surface leads to a higher sticking coefficient for SiH₃ radicals.

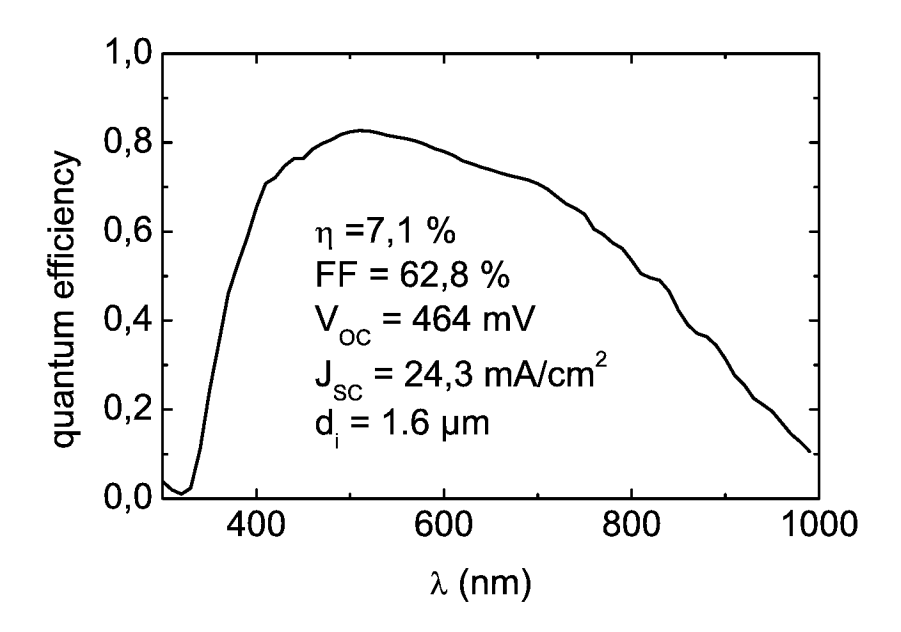


Figure 5.3: Quantum efficiency of a microcrystalline p-i-n-type cell vs. wavelength.

High conductivities were achieved both for TMB and B_2H_6 as doping gases. Both p-layers are promising for solar cell application. For process reproducibility reasons we prefer the use of TMB, which is thermally more stable, for our p-layers. Therefore we use TMB doped layers as p-layers in the next section and during the rest of this work.

5.3 Solar Cells

The boron-doped μ c-Si:H layers most promising for solar cell application in terms of conductivity and deposition rate were thick layers (~ 100 nm). In solar cells the p-layer is significantly thinner (~ 20 nm). When we optimized the conductivity of the p-layer we could only measure the conductivity parallel to the substrate; in a solar cell the properties perpendicular to the substrate are decisive. The conductivity is a good measure to achieve highly doped, highly crystalline p-layers. However it is not clear that the highest conductivity determines which p-layer is best-suited for solar cells. For these reasons it was important to check the impact on solar cell performance. During the course of this work it soon turned out that these p-layers already allow high performance solar cells.

Figure 5.3 shows the quantum efficiency QE of a μ c-Si:H solar cell with 0.2 sccm TMB for the p-layer. The QE is generally quite high yielding a J_{SC} of 24.3 mA/cm² at an

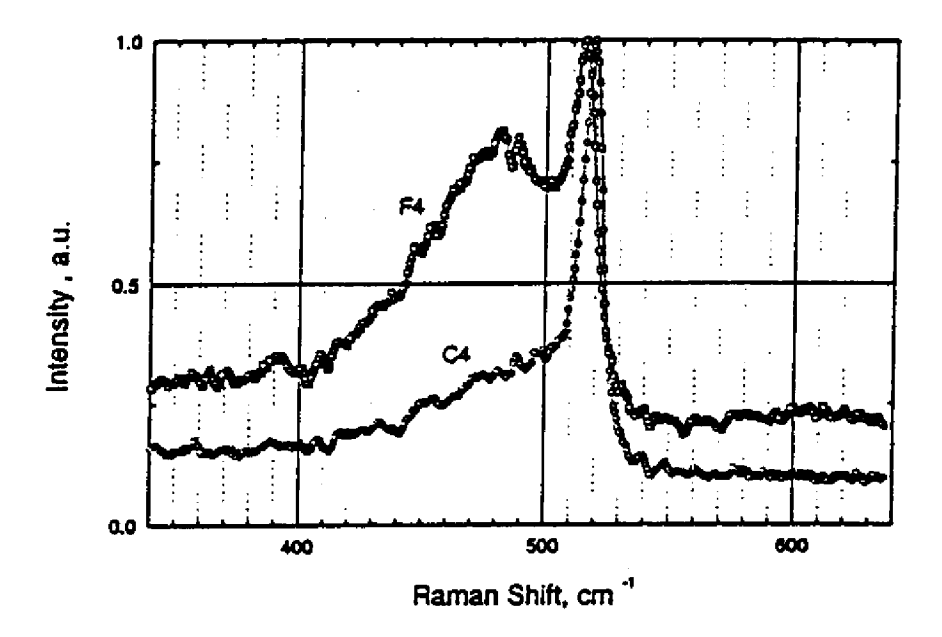


Figure 5.4: Comparison of the Raman spectra of an optimized solar cell (C4) and an identical i-layer deposited on SiO₂/Si (F4). See table 6.2 for deposition conditions.

i-layer thickness of 1.6 μm . Note especially the high quantum efficiency of 65 % at 400 nm indicating low absorption losses in the p-layer.

In figure 5.4 the Raman spectrum of this solar cell is shown. The small size of the shoulder of the peak around 480 cm^{-1} indicates a high crystalline volume fraction. In comparison to that, a Raman spectrum of an i-layer prepared under the same conditions as the one for the solar cell but on a Si/SiO_2 substrate is shown. Here a significant shoulder shows an increased amorphous volume fraction compared to the solar cell.

Figure 5.5 shows the TEM cross-sectional view of this solar cell. The i-layer is highly crystalline throughout the thickness: Due to the underlying μ c-Si:H p-layer no amorphous incubation layer can be seen. These results together with the achieved high V_{OC} and FF in this work (see chapters 6 and 7) show the good suitability of the p-layers optimized for high conductivity. Hence no further optimization of the p-layer for the use in μ c-Si:H solar cells was performed.

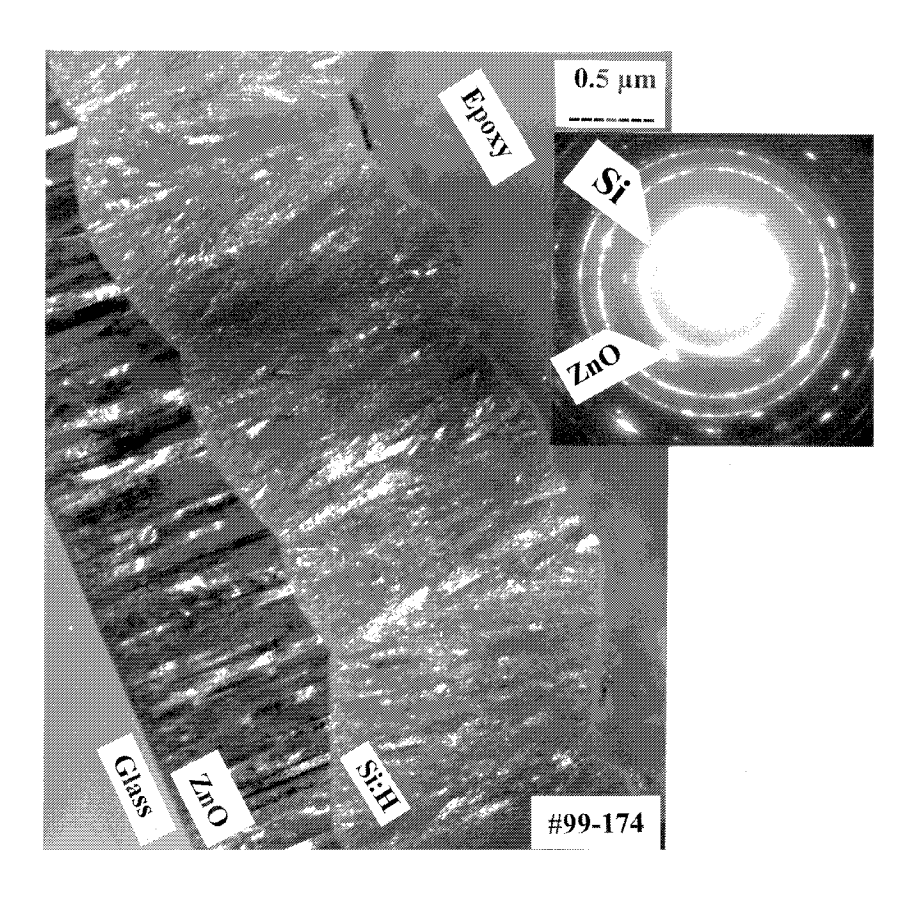


Figure 5.5: Cross-sectional TEM and selected area diffraction pattern (SAD) of a μ c-Si:H solar cell deposited on textured ZnO.

6 μ c-Si:H Solar Cells: Growth Regime and Key Deposition Parameters

In this chapter, the development of microcrystalline silicon solar cells prepared at high deposition rates is described. Focus is on the relationship between the deposition parameters silane concentration [SiH₄]/[H₂], deposition pressure $p_{\rm dep}$ and plasma power $P_{\rm RF}$ applied during i-layer growth and the resulting solar cell performance. First it is discussed which combination of these parameters is necessary to achieve microcrystalline growth. Next the influence of a single parameter variation on the solar cell characteristics is studied. At last the way to optimize a process for high efficiency solar cells at a high deposition rate by adjusting these three parameters is demonstrated. Furthermore the influence of the substrate temperature $T_{\rm S}$ is studied.

Mainly the electrical parameters V_{OC} and FF are used for the discussion of solar cell results. This is due to the strong influence of substrate variations on J_{SC} and therefore η (see section 4).

6.1 Silane Concentration, Deposition Pressure and Plasma Power

6.1.1 Growth Regime

First the deposition parameters plasma power, deposition pressure and silane concentration were varied over a wide range (P_{RF} : 0.25 - 0.7 W/cm², p_{dep} : 1 – 11 Torr, [SiH₄]/[H₂]: 0.6 - 4 %) to characterize the growth regime. Since our goal is to achieve high rate growth, only deposition conditions which allow rates of ~5 Å/s are taken into account for this study. In this deposition regime described above the i-layers of the solar cells can be amorphous or microcrystalline depending on the deposition parameters. The classification whether an i-layer is microcrystalline or not was deduced from solar cell characterization. A significant response in the infrared wavelength regime was taken as evidence for a significant amount of crystalline silicon phase – the i-layer is microcrystalline. On the other hand, a low infrared response combined with an open-circuit voltage

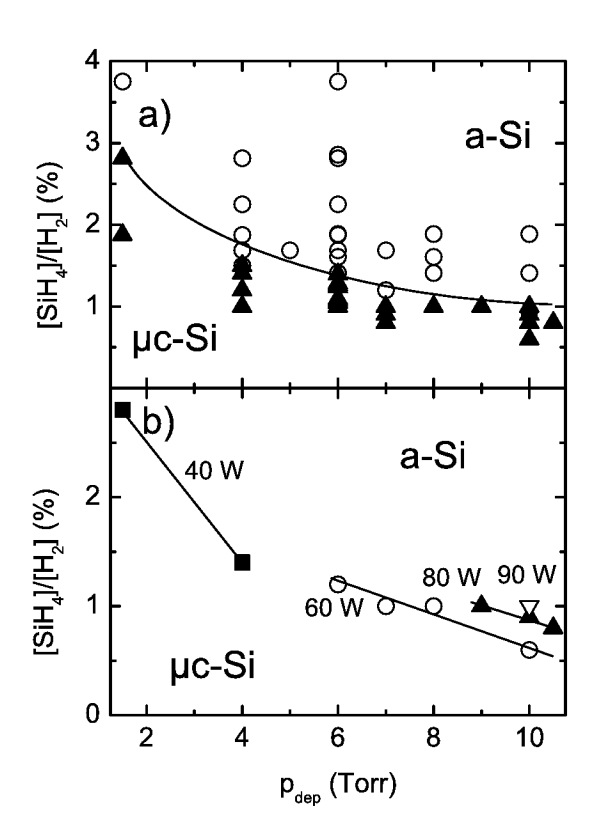


Figure 6.1: a) Silane concentration $[SiH_4]/[H_2]$ vs. deposition pressure p_{dep} during i-layer growth of amorphous (open circles) and microcrystalline (closed triangles) solar cells, respectively. The solid line indicates the transition regime. b) Same plot as a) for different plasma powers of i-layers in the transition regime (indicated by lines) between amorphous and microcrystalline growth.

 V_{OC} above 600 mV gives a clear hint that the i-layer is dominated by a-Si:H material. In Figure 6.1a the silane concentration is plotted vs. deposition pressure for solar cells in the parameter range shown above. Amorphous and microcrystalline growth are indicated by open circles and closed triangles, respectively. The transition regime is sketched by a solid line. At 1.5 Torr microcrystalline i-layers can be deposited at silane concentrations as high as 3 %. With increasing p_{dep} the transition from μ c-Si:H to a-Si:H occurs at lower $[SiH_4]/[H_2]$ -values (~ 1 % for $p_{dep} > 7$ Torr). Note that these cells were deposited using various plasmas powers to maintain similar deposition rates. For those microcrystalline cells which are close to the amorphous growth regime the data are replotted in Figure 6.1b where additionally the respective plasma powers are indicated. For a fixed plasma power a lower silane concentration is needed at high pressures to achieve microcrystalline growth. An increase of plasma power shifts the transition regime to higher pressures or higher silane concentrations, respectively. Improved crystalline growth at high plasma

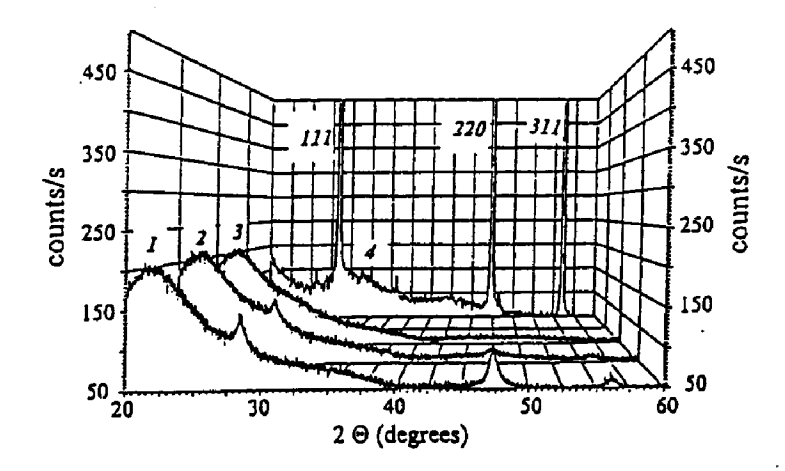


Figure 6.2: XRD spectra of Si:H films grown on SiO_2/Si substrate with minimum, intermediate, and maximum $[SiH_4]/[H_2]$ (1: 0.6 %, 2: 0.9 %, 3: 1.5 %). Deposition pressure, heater temperature and plasma power were fixed at 7 Torr, 210 °C and 60 W, respectively. Curve 4 is a reference spectrum of a thick polycrystalline Si sample. These measurements were performed in a joint German-Israeli research project (project number 01647 E01073) with the Technion Haifa [113].

power was described before by Hapke et al. for material deposited by VHF PECVD [112].

The transition between microcrystalline and amorphous growth on glass or SiO₂ substrates does not take place abruptly, but between these regimes the material shows both amorphous and microcrystalline characteristics. To illustrate this, XRD spectra of Si:H films deposited with different [SiH₄]/[H₂]-values on SiO₂ are shown in figure 6.2. The sample corresponding to lower concentration (curve 1, 0.6 %) exhibits an XRD spectrum typical for microcrystalline material. Spectrum 3 (high concentration, 1.5 %) is characteristic for an amorphous layer. The intermediate concentration (spectrum 2, 0.9 %) produced a mixed phase Si:H film giving low intensity but distinct XRD peaks. Note that this slow transition is typical for silicon grown on glass or SiO₂. In a solar cell this transition occurs within a much smaller range of [SiH₄]/[H₂] due to the μ c-Si:H p-layer serving as nucleation layer. In the next section it will be shown that in the solar cell this transition between microcrystalline and amorphous growth results in an abrupt drop in the short-circuit current density J_{SC} (figures 6.3 and 6.6). During this work in general we will call i-layers microcrystalline if the crystalline volume content is high enough to produce a high J_{SC} in a solar cell. This means that the crystalline phase dominates the

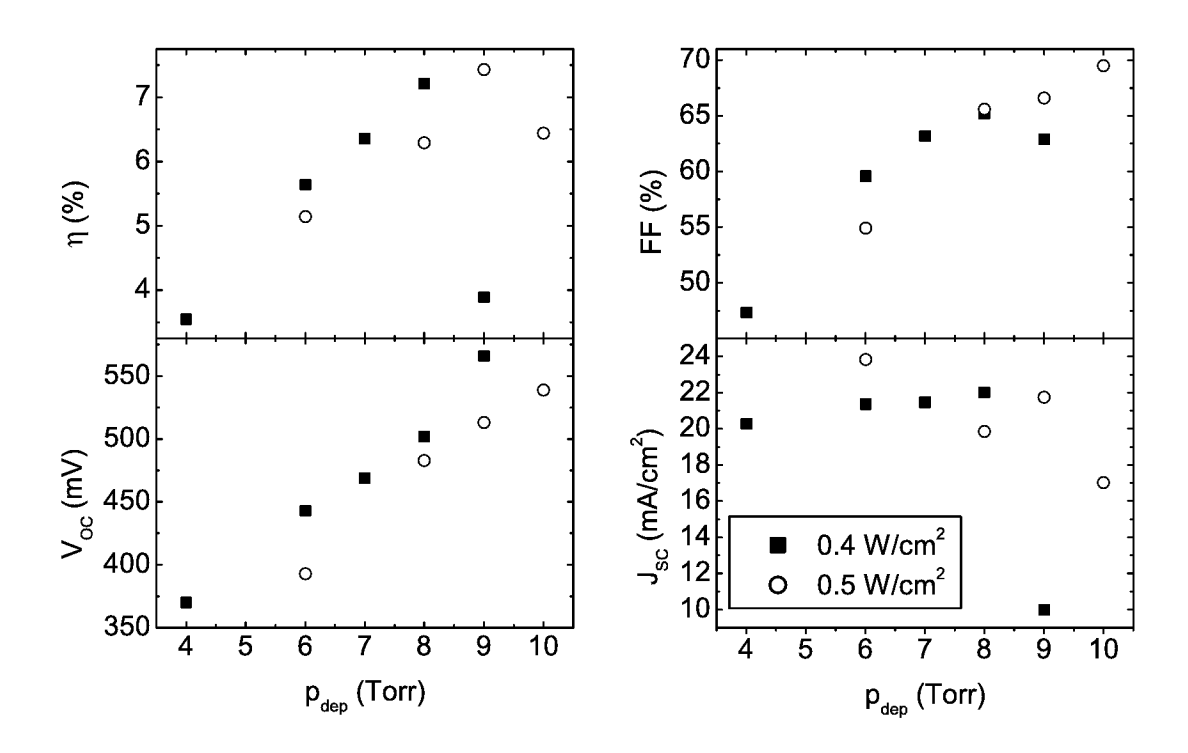


Figure 6.3: Light J-V parameters efficiency η , fill factor FF, open-circuit voltage V_{OC} and short-circuit current density J_{SC} vs. the deposition pressure p_{dep} applied during deposition of the i-layer for two different power densities (1 % silane concentration.)

optical material properties.

6.1.2 Solar Cell Properties at the Transition between Microcrystalline and Amorphous Growth

In the last section we learned in which deposition regime microcrystalline growth can be achieved. In this section the behavior of solar cells is studied if the variation of a single parameter is used to approach the transition regime. For this purpose, the deposition pressure as well as the silane concentration are varied in these experiments.

The variation of the deposition pressure during i-layer growth was performed at two different plasma powers. Figure 6.3 displays the J-V parameters for P_{RF} =0.4 W/cm² and 0.5 W/cm², respectively, as a function of deposition pressure. All solar cells in this series were deposited with $[SiH_4]/[H_2]=1$ %. Both efficiency data show a similar behavior. The

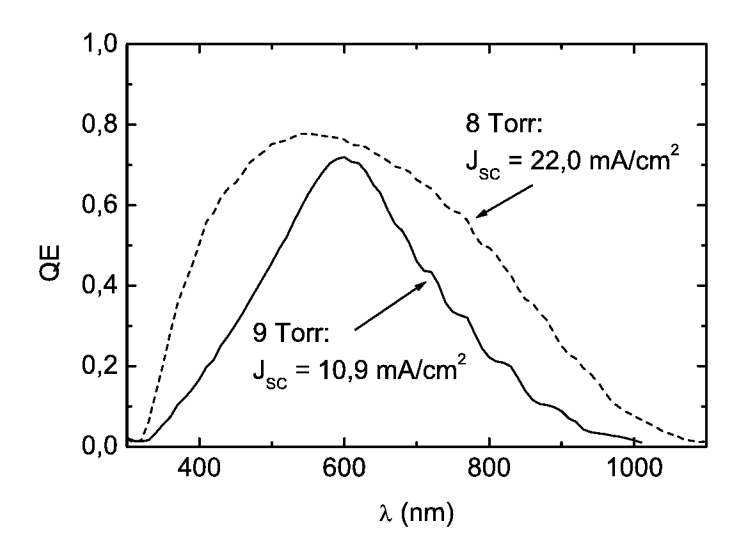


Figure 6.4: Quantum efficiencies QE of solar cells prepared at deposition pressures of 8 and 9 Torr (0.4 W/cm², 1 % silane concentration, 1.4 μ m i-layer thickness.)

efficiency increases linearly until maximum values of 7.2% at 8 Torr and 7.4% at 9 Torr, respectively, are reached. With further increasing pressure the efficiency drops down to a significantly lower value.

The increase in efficiency is due to an increase of V_{OC} and FF with increasing p_{dep} while J_{SC} stays almost constant. The efficiency loss for the highest pressures is caused by a sudden drop in J_{SC} . This J_{SC} drop is illustrated in more detail by quantum efficiency curves. Figure 6.4 shows the QE for the solar cells prepared at 0.4 W/cm² at 8 and 9 Torr, respectively. The cell prepared at 8 Torr shows a typical spectral response for μ c-Si:H cells with a high fraction of crystalline Si in the i-layer [20] in spite of being close to the transition to amorphous growth. The cell prepared at 9 Torr exhibits a reduced quantum efficiency both in the short and long wavelength regime. The losses in the long wavelength region (above 600 nm) indicate a reduced crystalline volume fraction. The i-layer is already partly amorphous. The losses below 600 nm must be related to carrier extraction problems, in spite of the still quite high fill factor (\sim 63 %). This behavior of the J-V parameters and QE at the transition to amorphous growth is generally observed for cells prepared in the transition regime between amorphous and microcrystalline growth.

The transition between microcrystalline and amorphous growth is nicely illustrated by the Raman spectra shown in figure 6.5. This figure shows the Raman spectra of the solar cells prepared at 4, 8 and 9 Torr at 0.4 W/cm². The solar cells which exhibit a high J_{SC} (4 and 8 Torr) show a strong peak at 520 cm⁻¹ indicating crystalline phase. The shoulder at 480 cm⁻¹ is low indicating only a very small amount of amorphous phase.

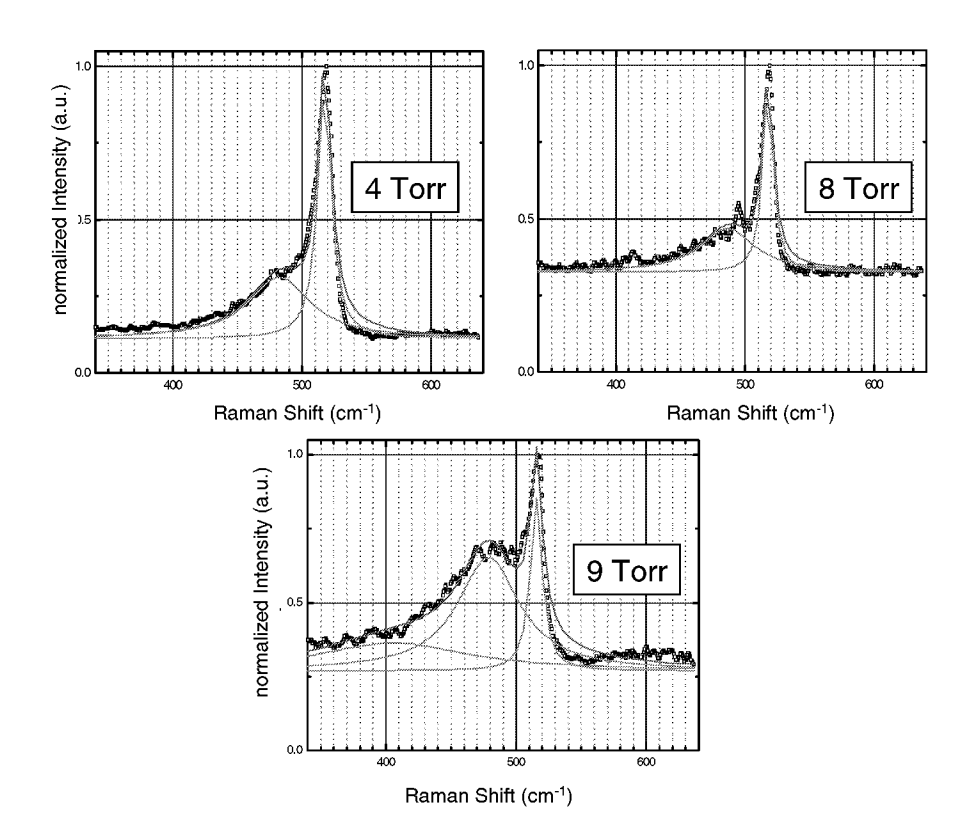


Figure 6.5: Raman spectra of solar cells prepared at deposition pressures of 4, 8 and 9 Torr $(0.4 \text{ W/cm}^2, 1 \% \text{ silane concentration}, 1.4 \,\mu\text{m}$ i–layer thickness). These measurements were performed in a joint German-Israeli research project (project number 01647 E01073) with the Technion Haifa

Note that the measurements were performed from the back side of the cell so that a part of this amorphous signal must be attributed to the a-Si:H n-layer. At 9 Torr the peak near 480 cm⁻¹ is much more pronounced indicating partly amorphous growth.

Figure 6.6 shows the J–V parameters for a variation of the silane concentration prepared in a 30×30 cm² reactor [96]. A comparison with figure 6.3 demonstrates that the trends upon an increase of $[SiH_4]/[H_2]$ are quite similar to an increase of p_{dep} . Similar effects were observed before by Vetterl et al. [20, 24] for a variation of the silane concentration in a VHF regime and is also observed by Klein et al. for hot-wire CVD [17, 114]. This trend in the J–V parameters is generally observed if any of the parameters with an influence on the transition between μ c-Si:H and a-Si:H is varied.

Figure 6.7 shows the deposition rate upon a variation of P_{RF} , p_{dep} and $[SiH_4]/[H_2]$, respectively, with the other parameters fixed. For both an increase in P_{RF} and $[SiH_4]/[H_2]$ there is a strong increase of the deposition rate, while for changes in p_{dep} it stays almost

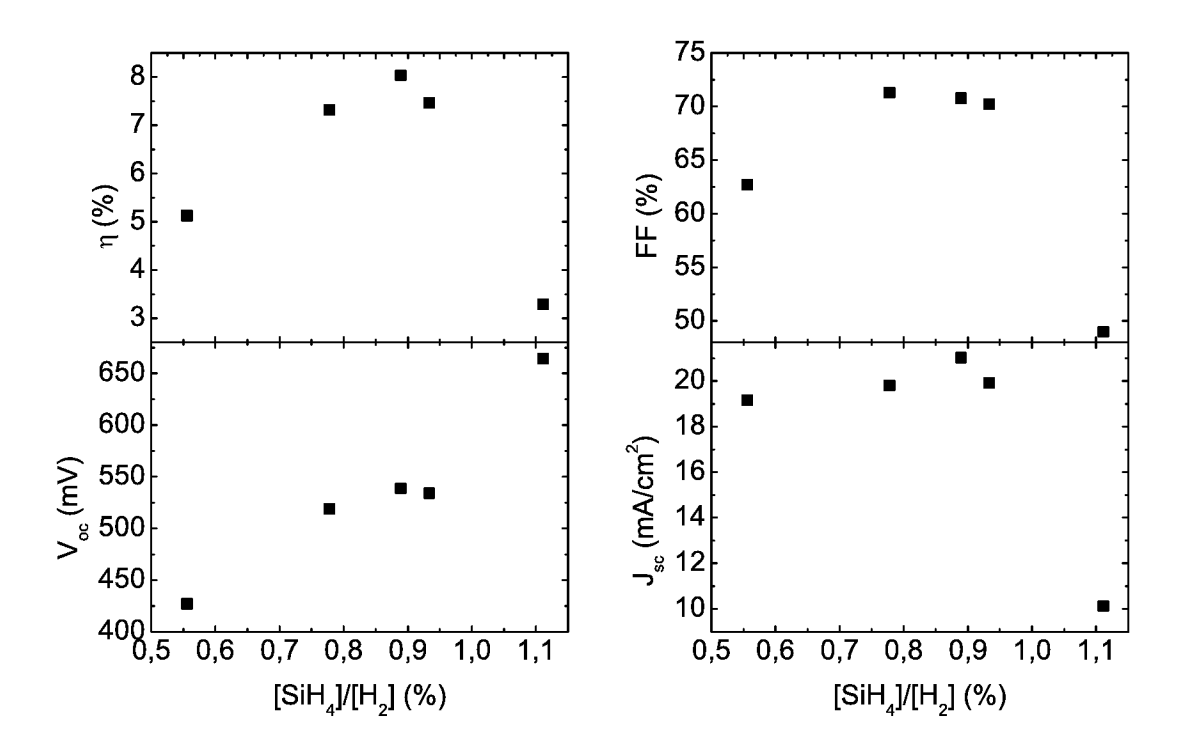


Figure 6.6: Light J-V parameters vs. the silane concentration $[SiH_4]/[H_2]$ applied during deposition of the i-layer (prepared in a 30 × 30 cm² reactor [96]). The i-layer was prepared at 8 Torr and 0.3 W/cm².

constant. That means that the growth rate of optimized solar cells can be enhanced by increasing $[SiH_4]/[H_2]$ and P_{RF} at the same time. The solar cells stay close to the transition regime since $[SiH_4]/[H_2]$ and P_{RF} have an opposite influence on the crystallinity (see figure 6.1).

6.1.3 Solar Cells Prepared under Optimized Conditions

The last section showed, that a significant increase of the efficiency of μ c-Si:H solar cells is observed when the transition to amorphous growth is approached by a variation of p_{dep} or $[SiH_4]/[H_2]$. To separate the role of the deposition pressure from the shift between the amorphous and microcrystalline growth regime, in a further experiment the $[SiH_4]/[H_2]$ was optimized at each p_{dep} to achieve the maximum efficiency for this p_{dep} . Additionally, the plasma power was adapted to maintain similar growth rates $(5 \pm 1 \text{ Å/s})$ over the whole p_{dep} -region. Only the μ c-Si:H solar cells with the highest FF and V_{OC} at a given

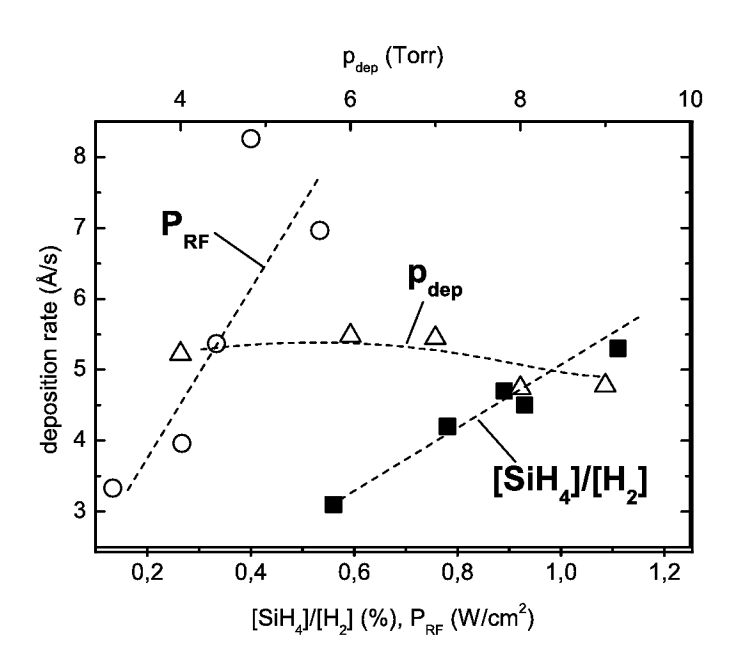


Figure 6.7: Deposition rate vs. P_{RF} (open circles, 7 Torr, 0.8 % $[SiH_4]/[H_2]$), p_{dep} (open triangles, 0.4 W/cm², 1 % $[SiH_4]/[H_2]$ see figure 6.3) and $[SiH_4]/[H_2]$ (closed squares, prepared in a 30 × 30 cm² reactor [96], 8 Torr, 0.3 W/cm², see figure 6.6).

 p_{dep} are used for the following discussion. As explained before FF and V_{OC} served as a measure for the μc -Si:H material quality and are much less influenced by variations of the light trapping properties of the ZnO substrates than J_{SC} . The results are plotted in figure 6.8. For both FF and V_{OC} there is an increase with rising deposition pressure from $\sim 50~\%$ FF and $V_{OC} < 400~\text{mV}$ at 1.5 Torr to $\sim 70~\%$ and 520 mV at 10 Torr, respectively. A further increase of deposition pressure showed only slightly improved cell performance in this series. Only at deposition pressures above 8 Torr we achieved both high efficiencies of above 8 % and high growth rates of 5 – 6 Å/s. At V_{OC} -values above 500 mV these cells exhibit FFs above 70 % indicating good interface quality and electrical transport properties of the corresponding μ c-Si:H i-layer material. From these results we conclude empirically that for the conventional 13.56 MHz excitation frequency the deposition pressure is the key parameter to achieve both high deposition rate and high solar cell efficiencies.

Raman and TEM measurements were performed on three characteristic solar cells to study the structural properties of the μ c-Si:H i-layers. These solar cells deposited near the transition to amorphous growth at 1.5, 4 and 7 Torr (marked with A, B and C in table 6.1) showed efficiencies of 2.9, 4.5 and 6.1 %, respectively. The high quality of the i-layer material in cell C is proven by a solar cell deposited with almost identical

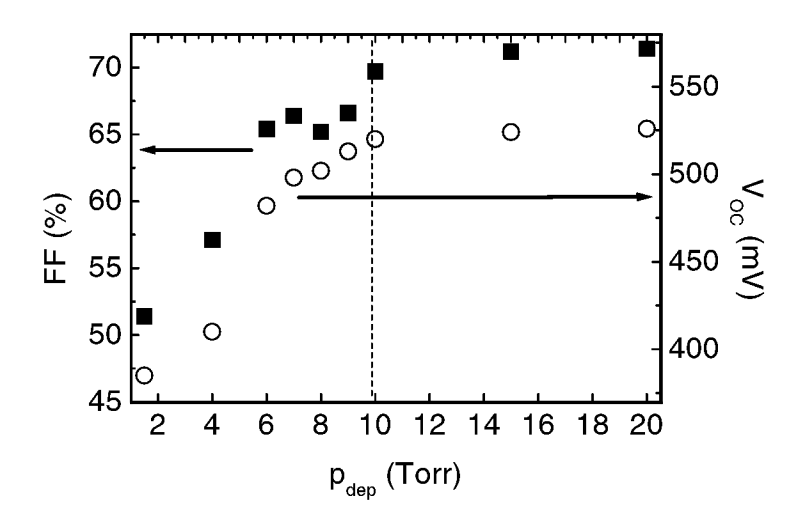


Figure 6.8: Fill factor FF and open-circuit voltage V_{OC} of the best μ c-Si:H solar cells achieved at various deposition pressures p_{dep} (i-layer deposition rate $5\pm 1~\text{Å/s}$).)

	$[\mathrm{SiH_4}]/[\mathrm{H_2}]$	p_{dep}	P_{RF}	rate	${ m thickness}$	η	FF	V_{OC}	$ m J_{SC}$
	(%)	(Torr)	(W)	(Å/s)	$(\mu \mathrm{m})$	(%)	(%)	mV	$ m mA/cm^2$
A	2.8	1.5	40	6	1.0	2.9	51.4	385	14.5*
В	1.4	4	40	6	1.8	4.5	57.1	410	19.2
C	1.0	7	60	6	1.1	6.1	70.4	517	16.7

Table 6.1: Deposition and light J-V parameters of solar cells with i-layers prepared in different depositions regimes. All solar cells are optimized via $[SiH_4]/[H_2]$ for maximum efficiency in their regime. *The low J_{SC} of cell A can be attributed to poor carrier extraction indicating poor i-layer material quality.

deposition parameters as solar cell C reaching an efficiency of 7.7 %. This high value was achieved by a larger i-layer thickness and an improved light trapping due to a ZnO/Ag back contact. Figure 6.9 shows the Raman spectra of samples A, B and C. All spectra exhibit a strong peak at 520 cm⁻¹ indicating crystalline phase. For solar cells A and B a pronounced structure near 480 cm⁻¹ is seen which can be attributed to a relatively high amorphous volume fraction. This finding is quite surprising, considering the results from solar cell characterization. Cells A and B both exhibit a high infrared spectral response as expected for highly crystalline material and, moreover, do not show a high V_{OC} as typically observed for cells with a high amount of amorphous phase. On the other hand, the low FFs would be in agreement with the Raman spectra. The Raman spectrum of cell C is very similar to spectra reported for high efficiency μ c-Si:H solar cells prepared with VHF [20]. Note that the measurements are performed from the back side of the solar cell so that a part of the amorphous signal must be attributed to the

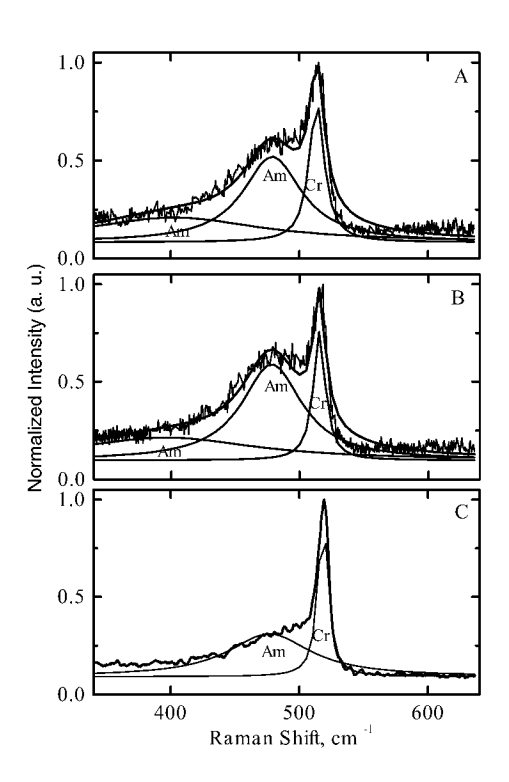


Figure 6.9: Raman spectra of solar cells A, B and C from table 6.1 ("Am" means contribution from amorphous, "Cr" from crystalline volume fractions). These measurements were performed in a joint German-Israeli research project (project number 01647 E01073) with the Technion Haifa [115].

amorphous n-layer. However, the n-layer is identically prepared for all cells, and thus should not be responsible for the differences in the Raman spectra. Figure 6.10 shows TEM cross-sectional views of solar cells A, B and C, respectively. It can be seen that for all the cells the nominal structure is almost identical. Differences between the cells are in the same range as variations between different places on the same cell. All the cells show columnar growth with a high crystalline volume fraction. The μ c-Si:H i–layers appear very similar to the i-layers prepared by VHF-PECVD [20, 45, 116]. The difference in amorphous phase as it was derived from Raman can not be seen in the TEM pictures. It must be concluded that TEM was not sensitive to the differences between these solar cells at the used magnification. On the other hand, the higher amorphous contribution derived from the Raman spectra for the low efficiency cells might be an indication for a deteriorated structure due to high ion bombardment, as expected at low deposition pressures.

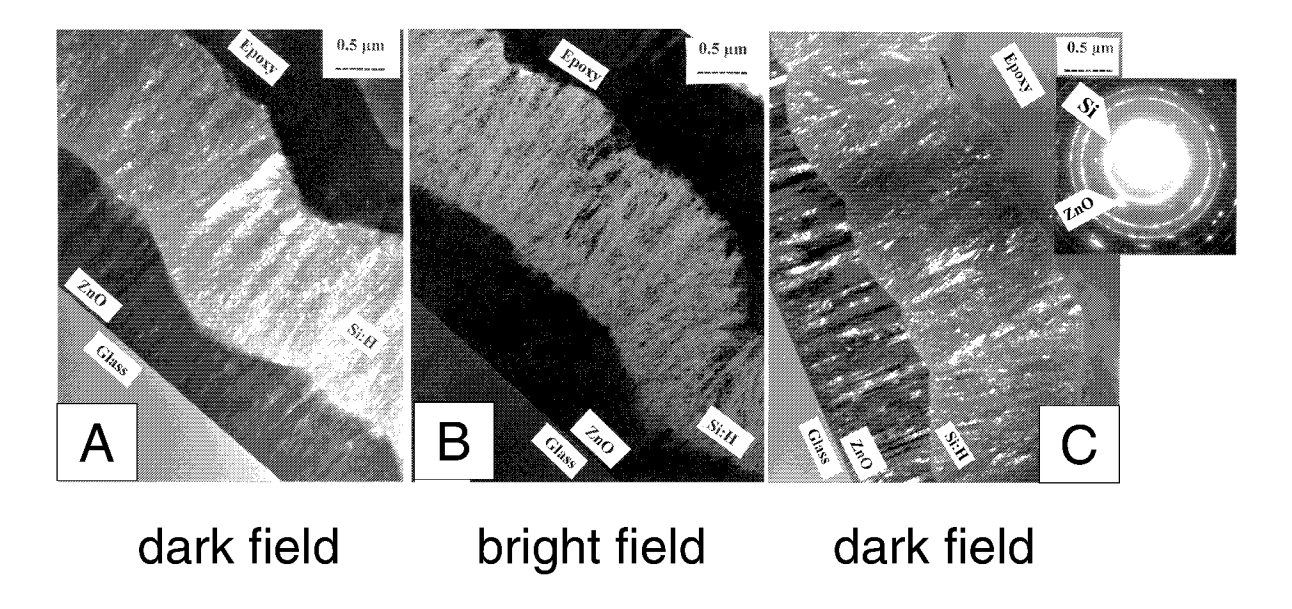


Figure 6.10: Cross sectional TEM images of solar cells A, B and C from table 6.1. For cell C the inset on the right shows the corresponding X-ray diffraction pattern of the Si and ZnO. These measurements were performed in a joint German-Israeli research project (project number 01647 E01073) with the Technion Haifa [115].

6.1.4 Solar Cell Performance versus Deposition Rate

In the high pressure deposition regime at 20 Torr microcrystalline solar cells with good optoelectronical properties can be prepared over a wide range of deposition rates by optimization at different RF powers. Microcrystalline growth could be achieved at deposition rates up to 10 Å/s. At this pressure even higher rates could not be achieved due to limitations of the power coupling (compare figure 7.7). Figure 6.11 shows FF and V_{OC} of μ c-Si:H solar cells prepared at 20 Torr under otherwise varying deposition conditions as a function of deposition rate. The i-layer thickness varied between 1 and 2.5 μ m. The best FF- and V_{OC} -values achieved show only a slight decrease towards higher rates. Even at 10 Å/s a FF of 70 % and V_{OC} above 510 mV was achieved (resulting in 7.7 % efficiency). Other highlights in terms of efficiency were 9.1 % at 1 Å/s, 8.9 % at 4 Å/s and 7.9 % at 9 Å/s.

6.2 Role of the Substrate Temperature

Experiments on microcrystalline n-i-p-type cells prepared using VHF PECVD showed a significantly increased performance after an optimization of the deposition temperature of

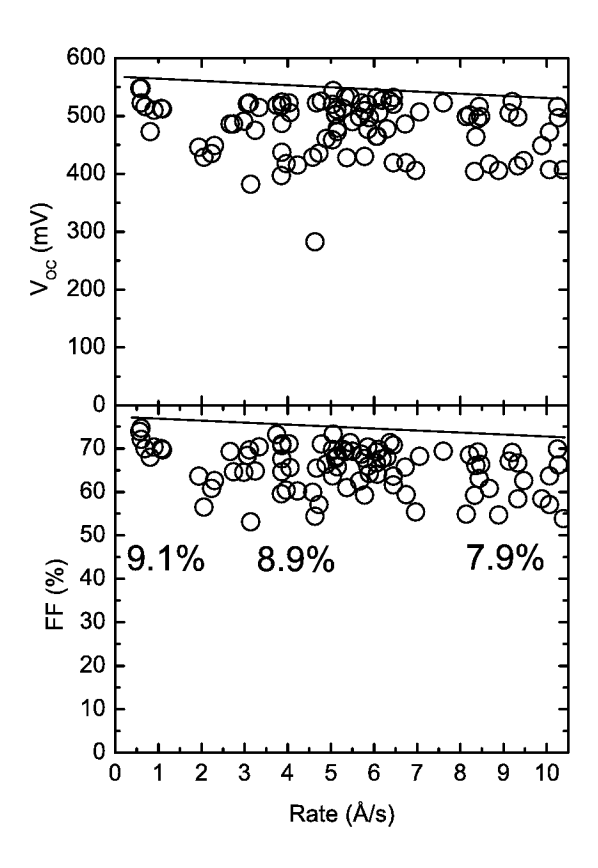


Figure 6.11: Open-circuit voltage V_{OC} and fill factor FF of μ c-Si:H solar cells prepared at 20 Torr vs. the deposition rate. Efficiencies of the best solar cells at a given deposition rate are indicated. The solid lines for the upper limit serve as guides to the eye.

the i-layer [20]. For a-Si:H solar cells a different behavior for the p-i-n and n-i-p deposition sequence was reported when the substrate temperature T_s during i-layer deposition is increased. For p-i-n cells a deterioration of the cell performance is generally observed for $T_s > 200\,^{\circ}\mathrm{C}$ (see e. g. Takahama et al. [117]). The following experiments were performed to optimize T_s : The variation of the i-layer deposition temperature was carried out for p-i-n cells in two deposition regimes. One series was prepared at a deposition pressure of 7 Torr, a plasma power of 0.4 W/cm² and a silane concentration of 1 %, the other one at 10.5 Torr, 0.5 W/cm² and 0.8 %, respectively. Figure 6.12 shows the J-V parameters of microcrystalline cells prepared in the two regimes as a function of heater temperature (not substrate temperature, see section 4.3) applied during i-layer deposition. All trends are similar for both regimes. The efficiency shows a maximum at about 200 °C reaching 7.7 % and 7.8 % for 7 and 10.5 Torr, respectively. For T_H above $\sim 240-280\,^{\circ}\mathrm{C}$ a strong decrease in all J-V parameters is observed. The J_{SC} drop at high T_H is unlikely to be due to a shift to a more amorphous growth regime, because of the low V_{OC} and particularly

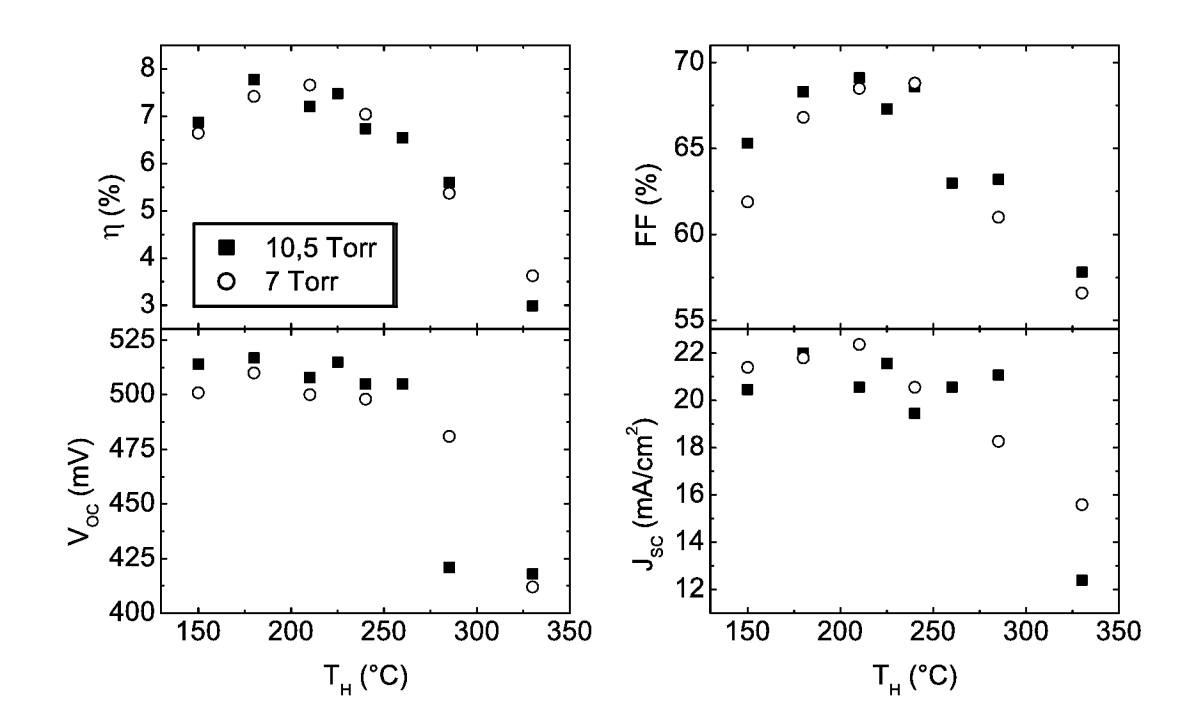


Figure 6.12: Light J-V-parameters as a function of heater temperature T_H during deposition of the i-layer for two different deposition regimes (7 Torr, 0.4 W/cm², 1 % silane concentration and 10.5 Torr, 0.5 W/cm², 0.8 %).

the still quite high J_{SC} of 10 mA/cm² measured under red light illumination (Schott OG590 cut-on filter). The losses in J–V parameters for high deposition temperatures can probably be attributed to an overheating of the p/i-interface as described in ref. [117] for a-Si:H p-i-n-type cells. Since for these a-Si:H cells the deterioration appears for substrate temperatures above 190 °C, that would mean that there is in fact a heating up of the substrate due to the high RF power input. We estimate the substrate temperature to be ~200 °C at the optimal heater temperature of 210–240 °C. Note that a deterioration of the solar cell performance is also observed if the cell is annealed at temperatures >200 °C after the deposition process.

The theory that the deterioration at high temperatures ($T_s\sim200-270~^{\circ}$ C) can mainly be attributed to an interface effect and not to changes in the bulk properties of the material is partly supported by material characterization. Figure 6.13 shows the Raman spectra of solar cells prepared at 7 Torr, 0.4 W/cm², heater temperatures in the 200–400 $^{\circ}$ C range and silane concentrations of 0.8 % and 1 %. Only for the solar cells prepared at the lowest temperatures high performance was observed, all other cells showed reduced

$[SiH_4]/[H_2]$ (%) \ T_H (°C)	210 (200*)	285	400
0.8	6.0 % *	4.5~%	1.8 %
1.0	6.1 %	5.4~%	_

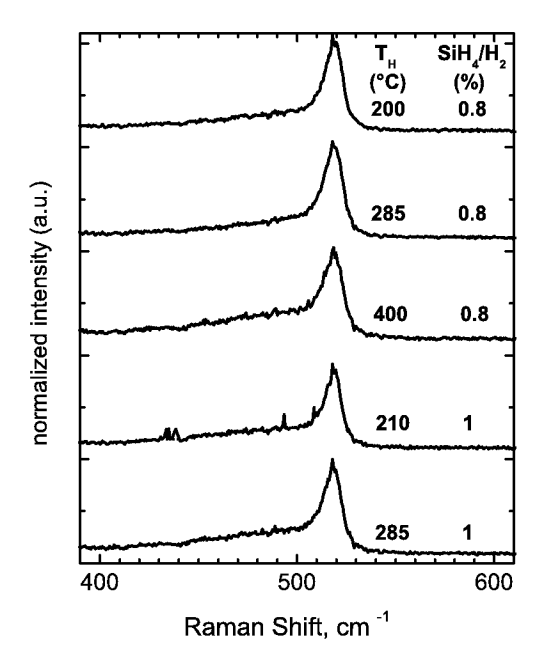
Table 6.2: Efficiencies as a function of silane concentration $[SiH_4]/[H_2]$ and heater temperature T_H applied during growth of i-layers in μc -Si:H solar cells. Deposition pressure and plasma power were fixed at 7 Torr and 60 W, respectively. (*The cell with 6.0 % efficiency was deposited at 200 °C)

efficiencies (see table 6.2). All Raman spectra, however, show a pronounced peak at 520 cm^{-1} indicating a large amount of crystalline phase.

In figure 6.14 the Raman crystallinity calculated from the spectra according to equation 3.7 is shown as a function of T_H for 0.8 %, 1 % and 1.5 % $[SiH_4]/[H_2]$ both on SiO_2/Si and inside the solar cell structure. For 0.8 % the crystallinity is ~ 85 % for 210 and 285 °C, and ~ 75 % at 400 °C on SiO_2/Si . In the solar cell structure these values are reduced by ~ 5 % but show the same trend. For 1.0 % there is a larger difference: On SiO_2/Si the crystallinity decreases from 45 % at 210 °C to 0 % at 400 °C. In the solar cell, however, the crystallinity stays above 70 % for 210 and 285 °C. The i-layers prepared at 1.5 % $[SiH_4]/[H_2]$ on SiO_2/Si were completely amorphous even at 210 °C. While the results on SiO_2/Si show that there is in fact a trend to amorphization towards high temperatures, in the solar cells this effect is not large enough to explain the strong deterioration of solar cell performance at high temperature.

The temperature dependence of hydrogen effusion of several films is shown in figure 6.15. Three different regions a, b, c can be distinguished. According to [118], the low temperature peak $(a, \text{ at } T{\sim}400~\text{°C})$ corresponds to hydrogen desorption from internal surfaces followed by H_2 motion through interconnected voids in the Si:H matrix. Peak b is assigned to atomic H diffusion out of the bulk and peak c is associated with effusion of H_2 trapped in small isolated voids in crystallized material. The three upper curves refer to a variation of the deposition temperature at 0.8~% [SiH₄]/[H₂]. They all show peak a. However peak b is less distinguished for the middle temperature of 285 °C than for the other two. To show that these variations are rather small a fourth curve is included in the figure. At the only slightly increased [SiH₄]/[H₂] of 1.0~% and 210~°C we see a totally different spectrum: Peak a is strongly reduced, we see a distinct peak b and a shoulder at peak c.

Although the hydrogen effusion curves obtained from samples prepared at different heater temperatures are not significantly different, the observed presence of interconnected voids offers an explanation for the difference in solar cell performance. These voids will lead to H surface desorption at elevated deposition temperature and therefore to the formation of dangling bonds. An increased dangling bond concentration may explain the lower efficiencies. However, a direct correlation between these hydrogen effusion measurements and the solar cell performance is difficult because the measurements were performed on μ c-Si:H i-layers deposited on SiO₂/Si substrates and not in a solar cell



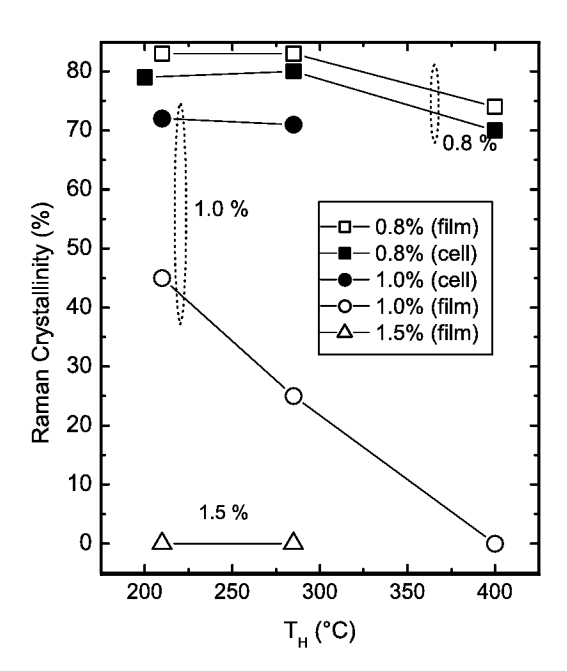


Figure 6.13: Raman spectra of solar cells prepared at heater temperatures T_H of 200 (or 210), 285 and 400 °C and silane concentrations [SiH₄]/[H₂] of 0.8 %, 1 % and 1.5 % (7 Torr, 0.4 W/cm²). These measurements were performed in a joint German-Israeli research project (project number 01647 E01073) with the Technion Haifa [113].

Figure 6.14: Raman crystallinity vs. heater temperature T_H for silane concentrations of 0.8 %, 1 % and 1.5 % on SiO_2/Si substrate and in solar cells.

structure. Therefore it is not clear that the material is identical to the one applied in the solar cells.

Results from Vetterl et al. [119] support the theory of an interface effect. They observed a deterioration of solar cell performance in this temperature range for p-i-n cells but not for n-i-p cells where the p/i-interface is not affected by the deposition temperature of the i-layer. A recent publication by Nasuno et al. [120] describes the same difference between the behavior of p-i-n and n-i-p cells. This was explained by an enhanced diffusion of boron from the p-layer into the i-layer at high temperatures. Note that even at heater temperatures up to 400 °C the corresponding substrate temperatures are still below 300 °C.

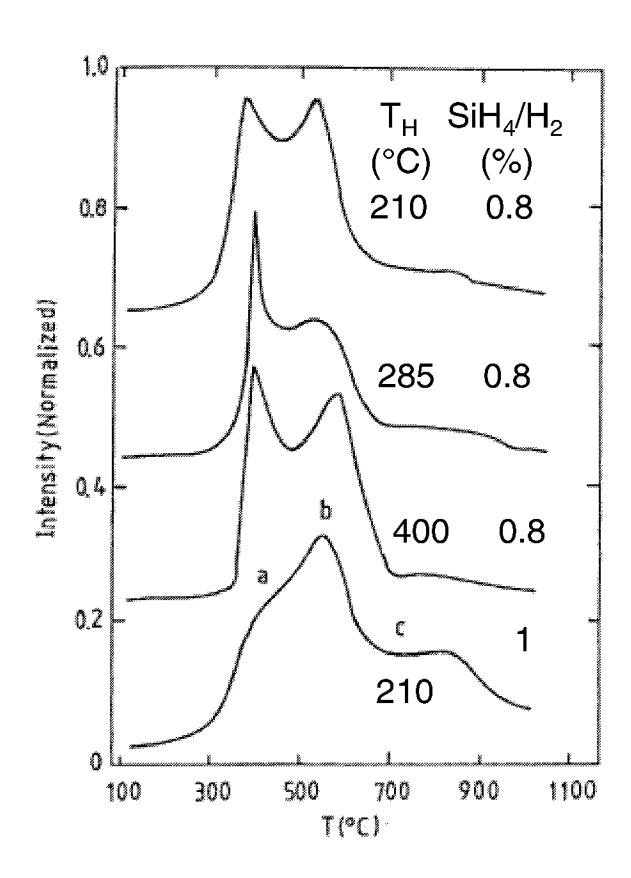


Figure 6.15: Hydrogen effusion curves of Si:H films grown on SiO_2/Si substrates as a function of temperature for samples deposited with different T_H and $[SiH_4]/[H_2]$ (see table 6.2).

6.3 Summary

We prepared microcrystalline p-i-n solar cells in a wide range of deposition parameters for the i-layer. All layers were deposited using solely 13.56 MHz excitation frequency. The transition between amorphous and microcrystalline growth can be achieved either by a decrease of silane concentration or deposition pressure or by an increase of the plasma power. For each variation of deposition parameters the highest μ c-Si:H solar cell efficiencies were achieved in the μ c-Si:H growth regime close to the transition to amorphous Si growth.

The deposition pressure turned out to play a key role for device performance. Only at high deposition pressure we achieved both high efficiencies of > 8 % and high growth rates of 5–6 Å/s. These cells exhibit FF- and V_{OC}-values above 70 % and 500 mV, respectively, indicating good electrical transport properties of the corresponding μ c-Si:H i-layer material. TEM and Raman measurements were performed for solar cells prepared at different deposition pressures. The corresponding efficiencies ranged from 2.9 % at

1.5 Torr to 6.1 % at 7 Torr. No characteristic structural difference could be observed in the TEM pictures. However, the Raman spectra showed an increased amorphous signal for the low pressure, low efficiency cells. Tentatively we attribute this to the high ion bombardment in the low pressure regime presumably causing a deteriorated structure of the μ c-Si:H i-layer.

The heater temperature had a major impact on solar cell performance. Above a heater temperature of $\sim\!240$ °C FF, V_{OC} and J_{SC} decreased significantly. We characterized material deposited at different T_H by Raman spectroscopy and hydrogen effusion. Neither hydrogen effusion nor Raman spectra showed significant changes in dependence of the heater temperature. However, the hydrogen effusion curves indicated the presence of interconnected voids (on SiO₂/Si) which could lead to hydrogen desorption during film growth at elevated temperatures. Takahama et al. [117] described a negative effect from an overheating of the p/i-interface for amorphous solar cells. Indications for a similar effect for μ c-Si:H solar cells are described in literature [119, 120]. Therefore both changes in the bulk material and interface effects are possible explanations for the loss in efficiency in our case.

7 μ c-Si:H Solar Cells: Role of Electrode Distance, Gas Flow and Pulsed Plasma Excitation

In the last chapter we learned how [SiH₄]/[H₂], P_{RF}, p_{dep} and T_H can be used to optimize solar cells for the 13.56 MHz continuous wave excitation at fixed electrode distance. In this chapter we will apply this knowledge to compare solar cells which are optimized at varying electrode distance and total gas flow, as well as cells prepared using a pulse modulation of the RF signal. The reason for this approach is that the variation of a single parameter leads to a couple of problems. Firstly, the variation of most parameters induces a transition between amorphous and microcrystalline growth. Since we usually start from an optimized solar cell, a changed parameter usually leads to a deterioration of cell performance. This means that upon a variation of a single parameter we have to adjust a second parameter to shift the regime back close to the transition region. In this work we usually use the silane concentration for this task. Having optimized the solar cell this way a second problem occurs: Usually the deposition rate will have changed. So you might get a cell with a higher efficiency but a lower deposition rate. Is this better or worse? To avoid this problem, in this chapter we perform [SiH₄]/[H₂] optimization at various P_{RF} . Since $[SiH_4]/[H_2]$ and P_{RF} have the same impact on the deposition rate but opposite effects on the crystallinity, this is an ideal tool to achieve optimized solar cells over a range of deposition rates. So we do not need to compare solar cells at different rates but can compare the trends in different regimes as a function of the deposition rate.

7.1 Electrode Distance

In plasma physics electrode distance and deposition pressure are strongly correlated. Since we observed a strong dependence of solar cell performance on deposition pressure, it is likely for the electrode distance to have a similar impact.

The first step was to study the effect of the variation of the electrode distance at otherwise identically parameters. Figure 7.1 shows the deposition rates of i-layers of solar cells prepared at electrode distances of 5 and 10 mm vs. silane concentration. For

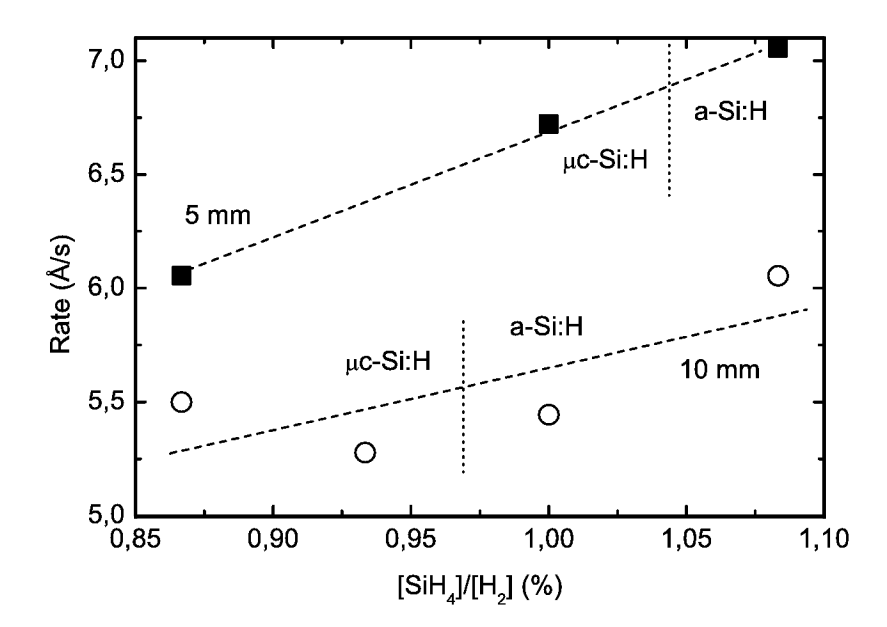


Figure 7.1: Deposition rate as a function of silane concentration [SiH₄]/[H₂] during deposition of the i-layer for electrode distances of 5 and 10 mm (20 Torr, 1 W/cm², 360 sccm H₂) The dashed lines are a guide for the eye. The dotted lines indicate the transition region between μ c-Si:H and a-Si:H growth for each electrode distance.

5 mm the deposition rate increases from 6 to 7 Å/s between 0.85 and 1.1 %. For 10 mm we cannot see such a clear trend in the deposition rate but on average the deposition rate is lower by about 1 Å/s. So a reduction in electrode distance increases the deposition rate. The same behavior was shown in [121,122]. In the figure the onset of a transition to amorphous growth as derived from solar cell characterization and the visual appearance of the cell (see section 4.4) is indicated by dotted lines. For 5 mm this occurs between 1.0 and 1.1 %, for 10 mm between 0.95 and 1.0 %. So a reduction of electrode distance shifts the deposition to a more crystalline growth allowing an increase in silane concentration for an optimized solar cell, which yields an even higher deposition rate. From this experiment a lower electrode distance seems to be better suited for the deposition of high deposition rate solar cells.

To get a deeper insight into the relationship between electrode distance and solar cell performance we prepared a large number of solar cells for each electrode distance. To achieve different deposition rates various plasma powers were applied and the silane concentration was used to approach the transition regime and therefore to achieve the highest efficiency. The deposition pressure was 20 Torr in most cases. However, at 20 mm electrode distance the deposition pressure had to be reduced to 4 Torr as otherwise no plasma

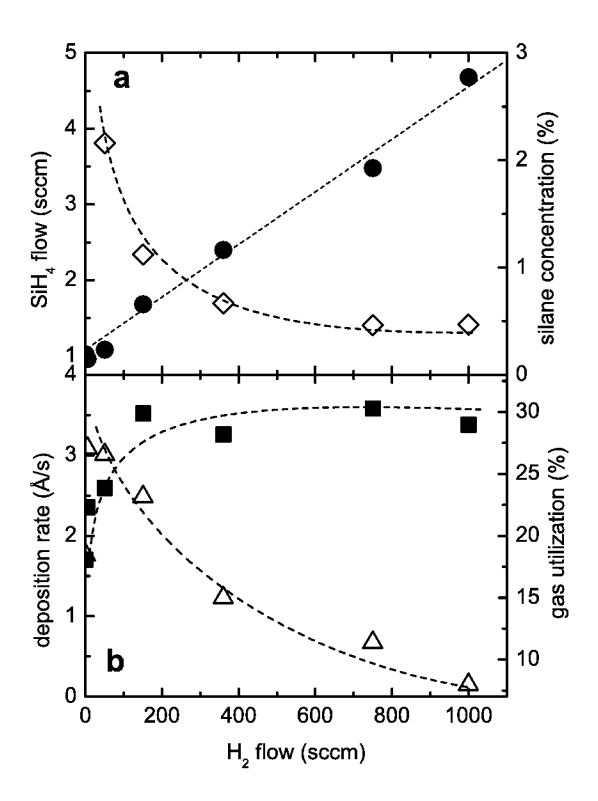


Figure 7.3: (a) Silane flow (closed circles) and silane concentration (open diamonds) for optimized cells vs. hydrogen flow. (b) Deposition rate (closed squares) and gas utilization (open triangles) for optimized cells vs. hydrogen flow. All solar cells were prepared at 20 Torr and 100 W. The dashed lines are a guide for the eye.

7.2 Total Gas Flow

A study of the influence of the total gas flow has a high technological relevance. In an industrial production low gas flows are wanted because the gas consumption is a significant cost factor. However, a certain gas flow is necessary to achieve high deposition rates because the deposition rate is limited by the silane supply. The total gas flow furthermore determines to a major part the residence time t_{res} of gas particles in the plasma space, which is estimated by

$$t_{res} = \frac{V \ p_{dep}}{f_{total} \ p_0} = \frac{A \ d_{el} \ p_{dep}}{f_{total} \ p_0} \approx 8 \ s \times \frac{d_{el}[in \ cm] \ p_{dep}[in \ Torr]}{f_{total}[in \ sccm]} \ [59]$$
 (7.1)

ignoring the heating up of the gas in the chamber because we can not determine it. Since the gas temperature in the chamber is between room temperature (then the formula

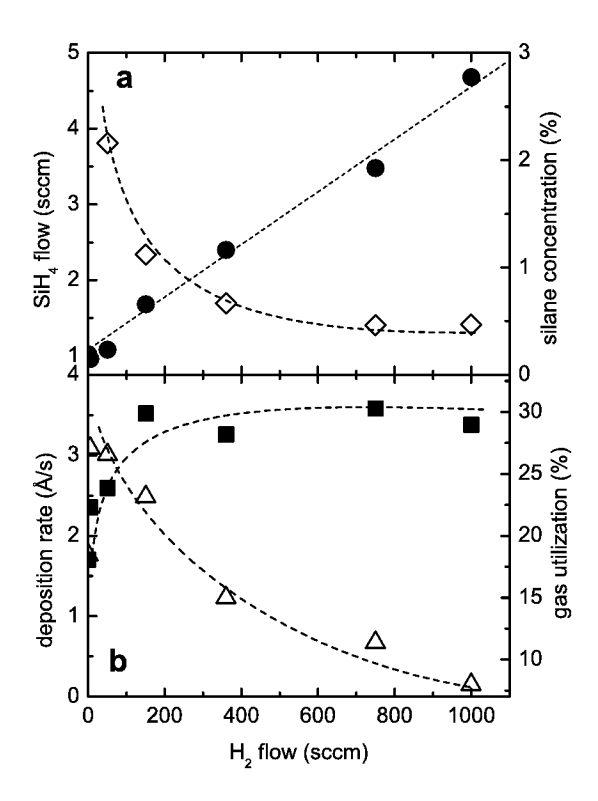


Figure 7.3: (a) Silane flow (closed circles) and silane concentration (open diamonds) for optimized cells vs. hydrogen flow. (b) Deposition rate (closed squares) and gas utilization (open triangles) for optimized cells vs. hydrogen flow. All solar cells were prepared at 20 Torr and 100 W. The dashed lines are a guide for the eye.

7.2 Total Gas Flow

A study of the influence of the total gas flow has a high technological relevance. In an industrial production low gas flows are wanted because the gas consumption is a significant cost factor. However, a certain gas flow is necessary to achieve high deposition rates because the deposition rate is limited by the silane supply. The total gas flow furthermore determines to a major part the residence time t_{res} of gas particles in the plasma space, which is estimated by

$$t_{res} = \frac{V \ p_{dep}}{f_{total} \ p_0} = \frac{A \ d_{el} \ p_{dep}}{f_{total} \ p_0} \approx 8 \ s \times \frac{d_{el}[in \ cm] \ p_{dep}[in \ Torr]}{f_{total}[in \ sccm]} \ [59]$$
 (7.1)

ignoring the heating up of the gas in the chamber because we can not determine it. Since the gas temperature in the chamber is between room temperature (then the formula is correct) and heater temperature (210 °C) the correction factor is $\frac{T_H[K]}{T_0[K]} \approx 1.6$ at maximum. Since the residence time varies by a factor of ~ 1000 in our experiments this accuracy is good enough. In the formula, V is the plasma volume (under the substrate), A the substrate area, d_{el} the electrode distance and p_0 the standard pressure (1013 hPa).

In this section it is examined how strongly the deposition rate is related to the total gas flow. Furthermore, it is studied how the solar cell properties are affected by the gas flow. All solar cells in this section are optimized via the SiH₄ flow at various H₂ flows at otherwise identical deposition parameters (20 Torr, 100 W). Even without H₂ supply during deposition a working μ c-Si:H solar cell could be deposited. The necessary H₂ for μ c-Si:H growth is produced during the deposition of silicon from silane (SiH₄(gas) \rightarrow $Si(solid) + 2H_2(gas)$). Deposition of μ c-Si:H without H₂-dilution was described in [123], called the static closed-chamber vhf glow discharge. In this work the deposition was started with a pure silane plasma resulting in an amorphous incubation layer. Because of this incubation layer solar cells prepared by this method achieved only an efficiency of 2.5 %. We propose a different approach where before the deposition the chamber is flooded by hydrogen-silane mixture (like it is used for standard deposition). With the plasma start the hydrogen flow is switched off and only a low silane flow is applied. That way the hydrogen dilution is high right from the start and an amorphous incubation layer is avoided. Using this approach we realized an efficiency of 7.3 % after an optimization of the silane flow. In spite of the different starting procedure for the deposition of this cell it is included in the following graphs, where the systematic influence of the total gas flow is studied.

In figure 7.3a the necessary SiH₄ flow for an optimized cell and the resulting [SiH₄]/[H₂] are shown in dependence of the used H₂ flow. The SiH₄ flow increases linearly with the H₂ flow from \sim 1 sccm SiH₄ at 0 sccm H₂ to 4.7 sccm at 1000 sccm. However, this linear trend does not begin in the origin (otherwise we could not do H₂ "free" deposition). The reason for that is that the necessary silane concentration is higher at low H₂ flows. It decreases from 20 % at 5 sccm H₂ to 0.5 % at 1000 sccm. That means that an increase in total gas flow (without optimization of silane concentration) leads to a more crystalline growth regime and that at lower total flows we still have a reasonable amount of silane (necessary for high deposition rate). For 0 sccm H₂ a silane concentration is estimated by the gas quantity necessary to build up p_{dep} and the gas flown during the process. This concentration was \sim 130 % but of course this ratio depends strongly on the deposition time and therefore can only be used to estimate the influence of the hydrogen that was in the chamber from the start.

Figure 7.3b shows the corresponding deposition rates and gas utilizations. The deposition rate shows a strong increase from 1.7 Å/s at 0 sccm to ~ 3.5 Å/s at 150 sccm. Then surprisingly, over a wide range of gas flows no influence of the total gas flow can be observed. All deposition rates are about 3.5 Å/s until 1000 sccm. The gas utilization can be seen in figure 7.3b, as well. At low total gas flows the gas utilization is significantly higher (27 % at 5 and 50 sccm H_2) than at high gas flows (<10 % at 1000 sccm H_2). At

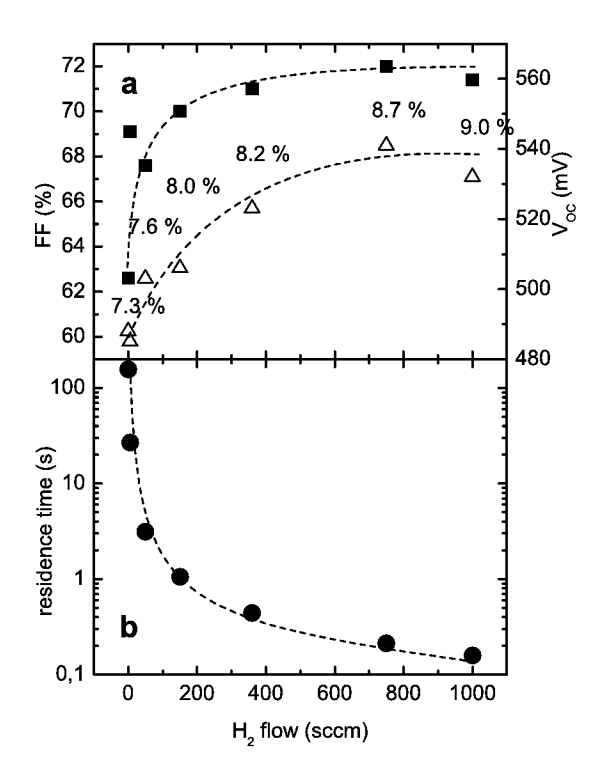


Figure 7.4: (a) Fill factor FF (closed squares) and open-circuit voltage V_{OC} (open triangles) for optimized cells vs. hydrogen flow. Efficiencies of the solar cells are indicated, as well. (b) Gas residence time t_{res} (closed circles) during deposition of optimized cells vs. hydrogen flow. All solar cells were deposited at 20 Torr and 100 W. The dashed lines are a guide for the eye.

0 sccm the gas utilization is only 18 % and therefore significantly reduced compared to the other cells deposited at low gas flows.

Figure 7.4a shows how the solar cell parameters behave upon changes of the gas flows. The FF increases from below 63 % at 0 sccm to 71--72 % at 750 and 1000 sccm. At the same time, the $V_{\rm OC}$ rises from 490 to 530–540 mV. The corresponding efficiencies increase from 7.3 % to 9 %. A possible explanation for this could be the reduced gas residence time at high gas flows (figure 7.4b). At 0 sccm H_2 the residence time is above 100 s, for 1000 sccm it is below 0.2 s. A long gas residence time can lead to gas phase polymerization [103], which can lead to a more porous structure of the material.

High deposition rates were possible over a wide range of gas flows, as the lower silane flows were counterbalanced by an increase in gas utilization and the silane concentration at the transition. At gas flows below 150 sccm the deposition rate decreased. That was because the gas utilization did not increase very strongly anymore. A possible explanation for that is that the gas utilization approaches a natural limit where all gas is either

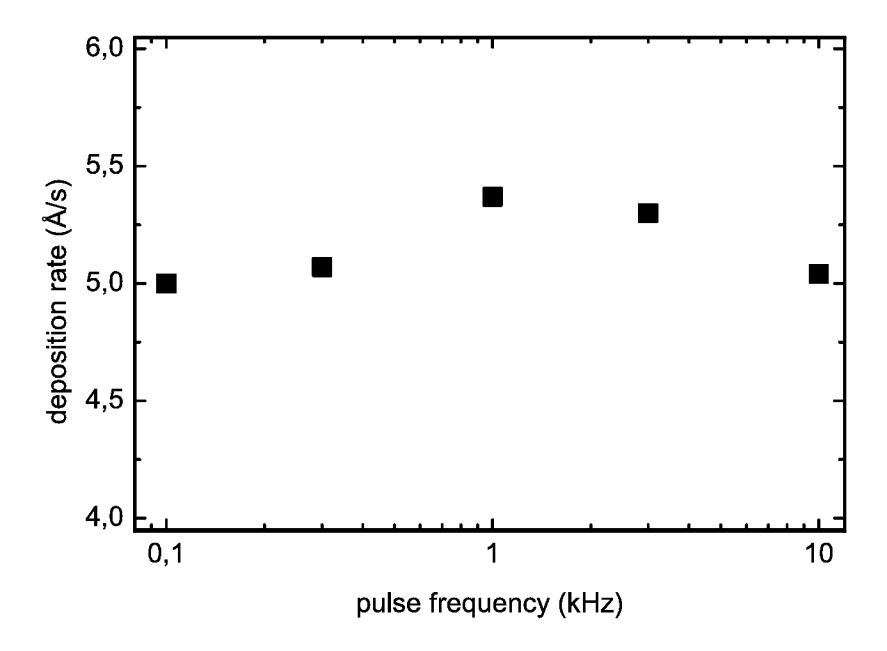


Figure 7.5: Deposition rate as a function of pulse frequency $\nu_{\rm P}$ during deposition of the i-layer (20 Torr, 1.3 W/cm², 60 % duty cycle, 2.4 sccm SiH₄, 360 sccm H₂).

deposited on the substrate, the substrate holder or the powered electrode. This cannot explain the low gas utilization for the deposition without H_2 supply. While one should be careful with fitting this cell into the series (because of the different $[SiH_4]/[H_2]$ at the plasma start) a reason for this drop in gas utilization could be an onset or increase of powder formation, so that this way silicon is lost for deposition. Unfortunately, during this experiments we did not have the possibility to observe the powder formation directly (see section 4.6).

7.3 Pulsed Plasma Excitation

An alternative way of depositing silicon is the pulsed PECVD. A lot of beneficial effects have been reported for the deposition of amorphous silicon by this method: Most interesting for this work is an observed increase in deposition rate without deterioration of the material quality [124–135]. Furthermore, an improved homogeneity [128, 129] and a reduction of powder formation in the deposition chamber [103, 130, 136–141] were reported. Microcrystalline silicon has been prepared by this method as well [129, 136, 142]. Here, the focus is on the questions if pulsed plasma excitation is helpful for the deposition of

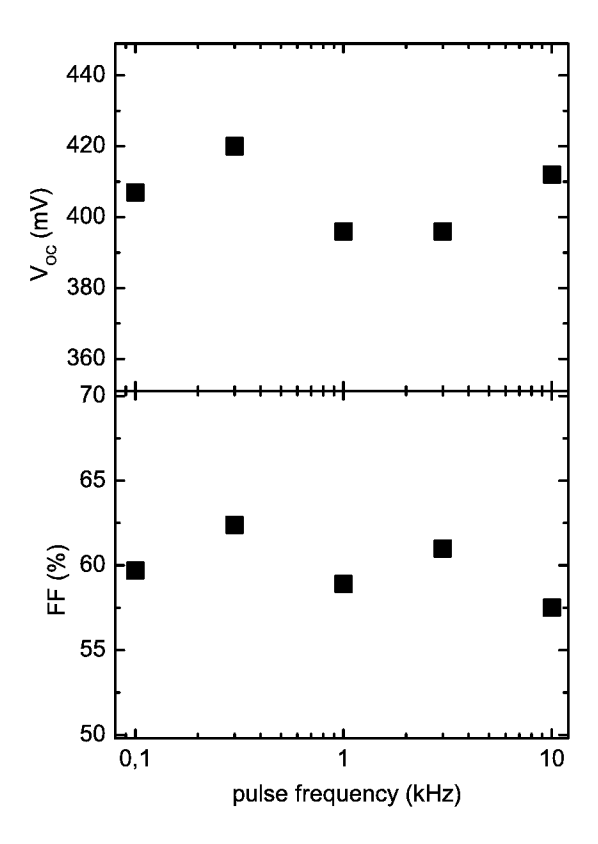


Figure 7.6: V_{OC} and FF of μ c-Si:H solar cells as a function of pulse frequency ν_P during deposition of the i-layer (20 Torr, 1.3 W/cm², 60 % duty cycle, 2.4 sccm SiH₄ 360 sccm H₂).

microcrystalline solar cells at high deposition rates.

The first approach to pulsed plasma deposition was a variation of the pulse frequency $\nu_{\rm P}$ between 100 Hz and 10 kHz at 20 Torr. In figure 7.5 the deposition rates of these cells vs. $\nu_{\rm P}$ are shown. There is a flat maximum around 1 kHz. However, the total variation is below 10 % (5.0–5.4 Å/s) leading to the conclusion that there is no significant influence of $\nu_{\rm P}$ on the deposition rate.

Figure 7.6 shows FF and V_{OC} of the corresponding cells as a function of ν_P . In both parameters no clear trend can be observed. V_{OC} scatters between 395 and 420 mV, FF between 57 and 63 %. These solar cells were all prepared at not optimized μ c-Si:H growth conditions. For optimizing the deposition conditions close to the transition to amorphous growth two ν_p (300 Hz and 10 kHz) were selected for the following experiments, since clear effects were neither observed in the deposition rate nor in the I–V parameters of the solar cells.

In figure 7.7a the deposition rates of optimized solar cells (by adjusting [SiH₄]/[H₂])

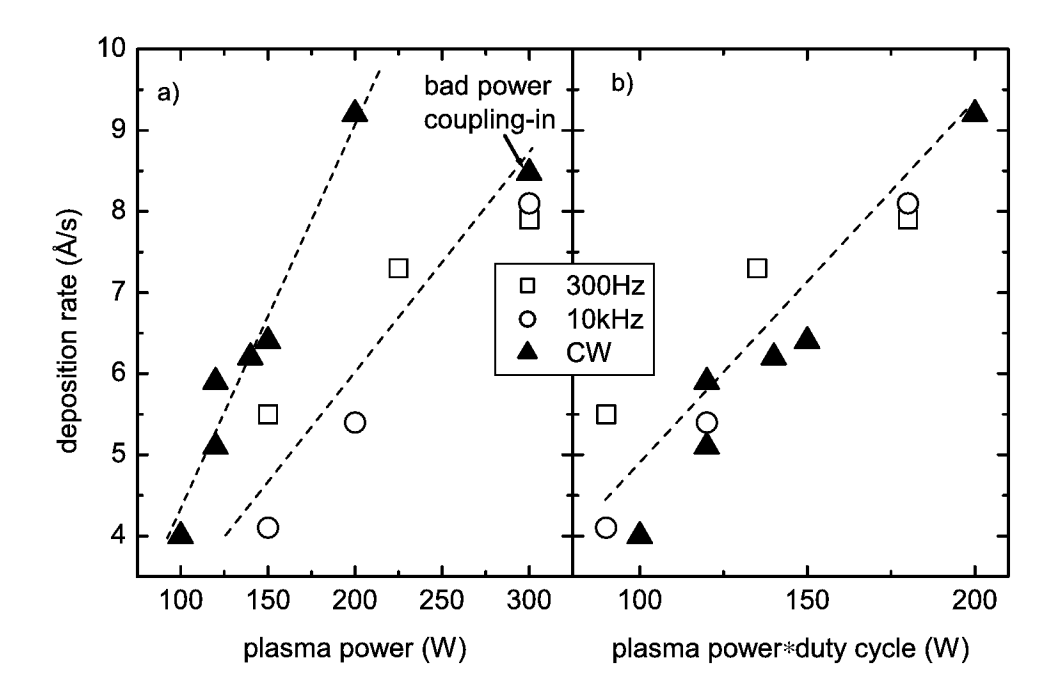


Figure 7.7: a) Deposition rate of μ c-Si:H i-layers of optimized solar cells for CW and pulsed (300 Hz and 10 kHz, duty cycle DC=60 %) excitation vs. plasma power. The dashed lines are guides for the eye. b) Deposition rate of μ c-Si:H i-layers of optimized solar cells for CW and pulsed (300 Hz and 10 kHz) excitation vs. the average plasma power ($P_{RF} \times DC$).

with continuous wave CW as well as 300 Hz and 10 kHz pulsed excitation are shown as a function of the applied plasma power. In all cases there is an increase with plasma power. For CW excitation the rate rises from 4 Å/s at 100 W to 9 Å/s at 200 W. At 300 W there is no further increase in deposition rate which might be due to a limitation of the coupling-in of power into the plasma. In case of the pulsed plasma the deposition rate is significantly lower. For 300 Hz and 10 kHz it increases from 5.5 Å/s and 4 Å/s, respectively, to 8 Å/s at 300 W.

In figure 7.7b the same picture is shown for the average plasma power, which means in case of the pulsed plasma the power is multiplied by the duty cycle (60 %). In this plot the deposition rate linearly increases with the average deposition power. Just the first two values of the 300 Hz case are slightly higher. This shows that for the realization of similar rates with pulsed and CW excitation an identical average power has to be adapted.

To judge the suitability of a pulsed plasma for high rate deposition of solar cells, we optimized μ c-Si:H solar cells at various deposition rates. Figure 7.8 shows V_{OC} and FF of cells prepared with CW as well as 300 Hz and 10 kHz pulsed excitation vs. the deposition

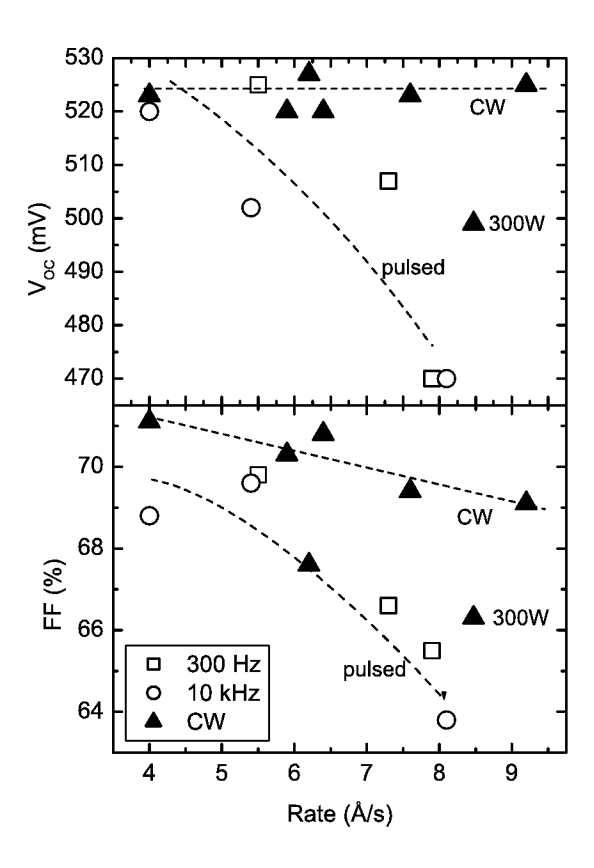


Figure 7.8: V_{OC} and FF of optimized solar cells vs. deposition rate for CW and pulsed (300 Hz and 10 kHz) excitation. The dashed lines are guides for the eye.

rate. In the CW case V_{OC} stays between 520 and 530 mV except for the highest applied power of 300 W where the voltage is only 500 mV. The FF decreases steadily from 71 % at 4 Å/s to 69 % at 9 Å/s. Again there is a drop for the 300 W case. For the pulsed plasma cells there is a continuous decrease for both V_{OC} and FF. V_{OC} decreases from around 520 mV to 470 mV, the FF declines from 70 % to 66 % for rates between 6 and 8 Å/s, respectively. The highest efficiency for a solar cell prepared by pulsed plasma was 8.4 % at 5.5 Å/s (300 Hz). This cell could be further optimized by applying our current state-of-the-art ZnO coated glass substrates. Efficiencies up to 9 % are feasible. This means that at deposition rates up to 5–6 Å/s pulsed and continuous wave excitation lead to similar material quality and solar cell performance.

However at deposition rates above 5–6 Å/s pulsed excitation leads to a stronger deterioration of material quality and the resulting solar cell performance with increasing deposition rate than compared to the CW case. We attribute the stronger decrease in the case of pulsed plasma deposition mainly to the higher plasma power necessary to obtain

a similar rate, since in the CW case for 300 W quite a strong decrease was observed, as well. This means the growth rate is mainly controlled by the average power while the material property is strongly influenced by the applied peak power. In summary, pulsed plasma deposition did not allow to increase the deposition rate as compared to CW excitation. However, good solar cells were obtained with the pulsed plasma at reasonable rates (5 Å/s). While we did not have the possibility to quantify the powder formation, a reduction is often described in literature. If powder reduction turns out to be a necessary prerequisite for the transfer of this technology into industrial production, it could still become a powerful tool. Furthermore, since the solar cell properties did not show a strong dependence on the pulse frequency, whereas the powder formation is expected to do [103, 137, 138], the pulse frequency can be adjusted freely to minimize powder formation.

7.4 Summary

The influence of electrode distance, total gas flow and pulsed excitation on i-layer deposition rate and performance of μ c-Si:H p-i-n solar cells prepared by 13.56 MHz PECVD was studied. As highly efficient solar cells are achieved at electrode distances between 5 and 20 mm, this parameter can still be adapted according to possible technological constraints when up-scaling to large area. For small electrode distances (5 and 10 mm) solar cell quality is maintained up to deposition rates of 9 Å/s due to applicable high deposition pressures, while for 20 mm cell properties worsen for rates above 3 Å/s.

Microcrystalline i-layers could be prepared over a wide range of total gas flows without influence on the deposition rate. Only at gas flows below 150 sccm the deposition rate was significantly reduced. However, microcrystalline i-layers could even be prepared at a silane gas flow of 1 sccm without addition of hydrogen during the deposition at a deposition rate of 1.5 Å/s. At low gas flows the solar cell performance decreased. This is attributed to gas phase polymerization due to the much longer gas residence time at low gas flows.

We observed virtually no influence of the pulse frequency on deposition rate or solar cell performance. For deposition rates comparable to CW excitation, P_{RF} had to be adjusted, so that the average applied power was identical. Pulsed plasma deposition yielded good results with efficiencies up to 8.4 % for deposition rates up to \sim 5 Å/s, for higher rates a strong decrease of efficiency was observed. This is explained by the higher necessary peak power. From comparison of deposition by pulsed and CW excitation we conclude that the growth rate is mainly controlled by the average power while the material property is strongly influenced by the applied peak power.

8 Discussion

This chapter is divided in two parts. In the first part we try to relate the effects we found empirically for solar cell deposition to properties of the deposition plasma. We know from literature which effects a variation of process parameters has on plasma properties. We compare these effects with effects we observed on the solar cell upon a variation of deposition parameters. The second part is a proposal of general guidelines for development and optimization of μc -Si:H solar cells grown by PECVD.

8.1 Correlation with Plasma Properties

The transition between microcrystalline and amorphous growth was observed for variation of almost every deposition parameter ([SiH₄]/[H₂], p_{dep}, P_{RF}, total gas flow and electrode distance). In literature different models for microcrystalline growth are proposed (surface diffusion model [143–145], etching model [146–149] and chemical annealing model [150– 153). All these models have in common that microcrystalline growth is induced by atomic hydrogen. A high atomic hydrogen density can be most easily achieved by a low silane concentration (i. e. high hydrogen dilution). However, also the other parameters can have the same effect. For an increase of p_{dep} the silane acts as a scavenger for atomic hydrogen and the annihilation reaction $H+SiH_4 \rightarrow H_2+SiH_3$ occurs more frequently. At high P_{RF} silane depletion occurs due to the high deposition rate and the annihilation reaction is suppressed. That way microcrystalline growth can be achieved by a reduction of $p_{\rm dep}$ or an increase of P_{RF} [154–156]. Upon a decrease of the electrode distance the deposition rate is increased. That is explained by a higher electron temperature [121, 122, 157]. Due to the higher deposition rate silane depletion occurs and, like in the case of increased power, the annihilation reaction is suppressed. At a reduction of the total gas flow depletion occurs because of the lower silane supply. Howling et al. [158] explain the transition between amorphous and microcrystalline growth at fixed silane concentration independently of plasma parameters by an increase of the ratio of dissociation rate to pumping rate. Since at low gas flows the pumping rate is also low to keep p_{dep} constant, the gas stays in the chamber long enough so that almost all SiH₄ is deposited. Because the deposition of Si from a SiH₄ molecule produces 2 H₂ the hydrogen concentration in the plasma is high even at high silane concentrations.

The influence of the shift between amorphous and microcrystalline growth on the solar cell performance has been discussed in detail in [44] for a silane concentration series using VHF excitation frequency. Two possible explanations are given for the high efficiency close to the transition to amorphous growth: One is a lower defect density due to a better passivation by amorphous silicon at the grain boundaries. In numerical simulation the behavior of FF and $V_{\rm OC}$ could be described by a decrease of the equilibrium charge carrier concentration with increasing silane concentration [159].

In our experiments we observed an increase of deposition rate with plasma power and silane concentration. No significant effect was observed at a variation of the deposition pressure. The approach for the following discussion is that the deposition rate r is proportional to the generation rate of silicon precursors d[X]/dt:

$$r \propto d[X]/dt = \sigma v_{th} N_{SiH_A} N_e [35, 160]$$
 (8.1)

 σ is the dissociation cross section of silane for collisions with electrons higher than the threshold value, v_{th} the thermal velocity of the electrons, N_{SiH_4} the number density of silane molecules, and N_e the number density of electrons responsible for the precursor generation, i. e. the density of electrons with an energy higher than the energy necessary for the production of the precursor from SiH₄. This formula is independent of the precursor assumed to be responsible for μ c-Si:H growth. At an increase of the silane concentration N_{SiH_4} increases. A high plasma power leads to a high plasma (electron) density n_e and therefore increases N_e [161,162]. In the case of p_{dep} three opposing effects occur. N_{SiH_4} as well as n_e [161] increase with increasing p_{dep} which should lead to an increase in growth rate. However, at the same time the electron temperature and therefore the share of electrons above the threshold energy decreases [35, 161, 163]. In the examined regime these effects neutralize each other. In other regimes often an increase of r with p_{dep} is observed (e. g. the regime for our p-layers, see figure 5.1).

The efficiency maximum close to the transition was generally observed for all deposition regimes we applied. However, at high deposition pressures and high plasma powers the efficiency maximum is on a much higher level. We achieved the best results for solar cell deposition at 13.56 MHz in a deposition regime of high $p_{\rm dep}$ (>10 Torr) and high $P_{\rm RF}$ (>0.5 W/cm²). What does this high pressure deposition regime distinguish from conventional RF regimes and what does it have in common with VHF regimes where good cells are also prepared? High deposition pressures in RF discharges reduce the energy of the ions impinging on the growing silicon surface [155, 164, 165]. This way it is possible to increase the plasma power (and therefore the deposition rate) without much deterioration of the film quality. In the experiments of Lihui et al. [156] it was found that at low deposition pressure an increase of plasma power did lead to a decrease in crystallinity in spite of a sufficient atomic hydrogen supply. This was explained by amorphization due to high energy ion bombardment. This is in accordance with our Raman results (see section 6.1.3) where even optimized solar cells at low deposition pressure showed an

increased amorphous content. Reduced crystallinity induced by ion bombardment was described in [154, 155, 166], as well. As explanation for a reduced material quality in a-Si:H at higher ion energy Hamers et al. [164] propose processes like bond breaking induced by the energy released at the neutralization of an ion. Another explanation is the implantation of atoms below the surface due to high ion energy. The same explanations could hold for an amorphization of our material.

In VHF plasmas good materials for solar cells can be prepared at low p_{dep} since an increase in frequency leads to a low sheath voltage and therefore a reduced ion energy, too [167–169]. At the same time the plasma power can be lower since a high frequency leads to high plasma (electron) densities and an enhancement of the high energy electron population [162, 168, 169]. Using hot-wire CVD good material properties can be achieved, because by this method no ionization of the source gas takes place and therefore ion bombardment is avoided.

8.2 Guidelines for the Development of μ c-Si:H Solar Cells

In this section we propose guidelines for the development of microcrystalline silicon solar cells prepared by PECVD.

Choose your regime

As described in the last section for the deposition of high quality solar cells at high growth rates two conditions of the plasma are essential: A low ion energy and a high density of electrons with energy above a certain level. One must choose a regime which generally fulfills both conditions. Examples are the VHF regime or the 13.56 MHz high pressure regime applied during this work. Also a combined approach is promising [170]. But even totally different approaches are imaginable as long as they fulfill these constraints. Furthermore, the total gas flow has to be chosen high enough to keep the residence time low enough to prevent gas phase polymerization.

Adapt your reactor

The choice of the optimal reactor design is strongly correlated to the deposition regime one wants to use. In case of the high pressure—high power regime we used in this work a showerhead electrode proved to be crucial for homogeneous deposition. Furthermore, a reasonably low electrode distance was necessary to facilitate a plasma ignition at these high deposition pressures. At 20 mm electrode distance a plasma start was possible only at strongly reduced deposition pressure. Other deposition regimes will need different adaptations of the reactor.

Find your temperature

In case of the superstrate configuration (p-i-n) the substrate temperature has to be below ~ 200 °C to prevent problems with the p/i interface. Since it will usually be difficult to determine the substrate temperature during deposition this can be done by an optimization of solar cells where the heater temperature at which the cell properties start to deteriorate can be determined.

Optimization

For optimum efficiency, the process parameters have to be adjusted so that the regime approaches the transition to amorphous growth. This is most easily done by a variation of the silane concentration since this has almost no impact on the plasma properties. If the $[SiH_4]/[H_2]$ optimization is performed at varying plasma power a deposition rate of choice can be adjusted which is determined by the $[SiH_4]/[H_2]$ and the applied P_{RF} . In this work deposition rates from 1–10 Å/s were accessible. Up to 6 Å/s high efficiencies were achieved, rates up to 10 Å/s had the drawback of a slightly decreased efficiency.

9 Summary and Conclusions

Topic of this thesis was the development of microcrystalline silicon thin film solar cells using plasma enhanced chemical vapor deposition (PECVD). To ensure later scalability of laboratory processes to an industrial production environment, we restricted ourselves to the standard excitation frequency of 13.56 MHz. The objective was to establish a broad knowledge base to understand the influence of various factors and deposition parameters of the i-layer on the performance of μ c-Si:H solar cells. By comprehensive solar cell studies accompanied by material studies we succeeded in identifying the most important parameters and developed a road map on how to achieve high quality μ c-Si:H solar cells at growth rates >5 Å/s for the i-layer.

First, a microcrystalline p-layer was developed. It is of high importance for the solar cell process since it has to fulfil many requirements: It has to build up the electric field, show a low absorbance, provide a low-ohmic contact to the ZnO and since it acts as a substrate for the i-layer it influences the i-layer structure. The p-layer was deposited in a regime of high deposition pressure and plasma power, similar to the regime later on used for i-layer deposition. It was optimized for high conductivity via dopant gas flows and deposition pressure. Conductivities above 1 S/cm were achieved for both B_2H_6 and TMB as dopant gas indicating highly doped material with high crystallinity. These p-layers proved to be well suited for the use in μ c-Si:H solar cells without further optimization.

We worked out the necessary prerequisites for depositing microcrystalline i-layers with high material quality at high deposition rate. That was mainly done by studying the influence of various deposition parameters directly in the solar cell. These prerequisites were:

- The best μc-Si:H solar cells were always prepared close to the transition to a-Si:H growth. This transition between microcrystalline and amorphous growth could be achieved by variation of almost every deposition parameter ([SiH₄]/[H₂], p_{dep}, P_{RF}, ...). By comparing the experimental data with literature references for all these parameters the transition could be correlated with a decrease of the atomic hydrogen density in the plasma.
- A high deposition pressure turned out to be essential for high quality material at high growth rates. This high deposition pressure could only be achieved at reasonably low electrode distances, otherwise no plasma could be ignited. The increase of

p_{dep} was necessary to reduce the energy of the impinging ions on the growing surface. Material characterization showed an increased amorphous volume content for the cells prepared at lower deposition pressures indicating an increased amorphous volume content of the i-layer material due to high energy ion bombardment.

- High deposition rates could be achieved by an increase of silane concentration and plasma power due to an increased precursor generation rate. For [SiH₄]/[H₂] this was induced by an increased silane partial pressure, for P_{RF} by an increased number of high energy electrons which are responsible for the generation. In our regime the deposition pressure had almost no effect on the deposition rate since a high partial pressure of SiH₄ and a reduced electron temperature have opposite effects.
- A high total gas flow was helpful for good solar cell performance at high growth rates. Surprisingly, that was not so much due to a strong impact on the deposition rate, which turned out to be constant over a wide range of flows for optimized solar cells. The reason was that at low gas flows a strong decrease of solar cell efficiencies was observed. A possible explanation could be a onset of gas phase polymerization due to the higher gas residence time and therefore a more porous material.
- The substrate temperature showed an upper limit beyond which the solar cell performance significantly decreased. There are two possible explanations. One is hydrogen surface desorption during film growth at elevated temperature, the other is an interface effect, namely an overheating of the p/i interface which is a specific problem of the superstrate configuration.

As an additional approach we used the deposition by pulsed plasma. While we succeeded in preparing good μ c-Si:H solar cells at growth rates up to 5 Å/s, at higher rates the performance was significantly reduced. Compared to conventional PECVD no practical advantages could be observed. In literature reduced powder formation is described for pulsed plasmas. While our solar cells were not affected by powder (see section 4.6) powder deposits in the chamber can make laborious cleaning necessary in production. If this problem turns out to be severe pulsed plasmas could become an important tool.

In summary we succeeded in developing high quality solar cells at high deposition rates. Highlights were solar cells with 9.1, 9.0 and 8.9 % efficiency for deposition rates of 1, 3 and 4 Å/s, respectively. At 9 Å/s still 7.9 % was achieved. Besides these technological successes we worked out an understanding which are the prerequisites from the plasma side to achieve high growth rates and high quality material. This comprehensive study of μ c-Si:H solar cells should make it possible to establish a similar process on other deposition systems. The up-scaling of this process is possible and was shown in an accompanying PhD thesis [96] (A short overview is given in appendix B).

Outlook

In this work the deposition of microcrystalline silicon solar cells at 13.56 MHz on small area (10×10 cm²) was shown. In the work of T. Repmann [96] the up-scaling of these results to a $30\times30~\mathrm{cm^2}$ reactor was demonstrated and a-Si:H/ μ c-Si:H tandem solar cells with high stable efficiencies were prepared. Next steps are the up-scaling of the ZnO substrates to the same area and realizing a series connected module by laser-scribing. Both tasks are undertaken in the newly established process technology at the IPV. While the results of this work and the up-scaling to $30\times30~\mathrm{cm}^2$ are quite promising, still a lot of work has to be done to establish this technology in the industrial production. One step is the up-scaling of these results to production size substrates ($\sim 1 \text{ m}^2$). At the same time a further increase of the deposition rate is necessary. To achieve this in our deposition regime an improved power-coupling into the reactor is necessary. A way to increase the growth rates without an increase in the applied power could be the use of alternative source gases (e. g. Si_2H_6) which require lower energies for precursor generation. Apart from our 13.56 MHz PECVD technique several methods, like high pressure VHF PECVD [136, 170], gas jet deposition [27] or microwave plasmas [26], are promising for high rate deposition of μ c-Si:H for solar cells.

From a scientific point of view it would be interesting to correlate the effects in plasma properties and solar cell characteristics quantitatively. If the plasma conditions for production of high efficiency solar cells were determined, this would not only lead to a further understanding of the process, but based on this knowledge fast in-situ techniques for process control could be developed. Possibilities for an in-situ process control based on material characterization are ellipsometry [171] or Raman spectroscopy. Such methods are probably required for stable large quantity industrial productions. Moreover, if one found a method to derive the transition point between microcrystalline and amorphous growth directly from in-situ plasma or material spectroscopy the development of μ c-Si:H solar cells could be much faster and simpler.

A Degradation

The light-induced degradation (increase of bulk defect density under illumination) of amorphous silicon [8] is a well known effect. In case of microcrystalline silicon the few available literature reports do not yield a conclusive picture. Keppner et al. do not report any degradation effect of their solar cells [172]. Kondo et al. [173] examined the defect formation after light exposure in μc -Si:H layers. They observed an increase in defect density which they could correlate with surface oxidation. This is a different effect compared to the degradation of a-Si:H since it is not related to changes in the bulk material and is not an effect of the material alone but induced by its interaction with the atmospheric oxygen. To check the effect of light-induced degradation on our solar cells, a limited number of μ c-Si:H solar cells of this work was exposed to light-soaking. Figure A.1 shows the degradation during 1000 h for three μ c-Si:H solar cells. These cells are taken from the series at $0.5~\mathrm{W/cm^2}$ from figure 6.3. The cell prepared at 9 Torr is the solar cell with the highest efficiency in this series (8 Torr is too crystalline, 10 Torr too amorphous). The efficiency of the cell prepared at 9 Torr decreases from 7.4 % to 7 % after 1000 h of light-soaking. This is mainly due to a decrease of V_{OC} and FF. The 8 Torr cell shows a similar behavior and decreases from 6.2% to 5.5%. The 10 Torr cell decreases from 6.2%to 4.2 %, this is mainly because of a decrease in FF and J_{SC} . This cell already contains an increased amorphous volume content, as can be seen by the reduced J_{SC} . This amorphous phase is possibly responsible for the observed stronger degradation. Additionally in this figure a solar cell prepared in the large area system in a similar deposition regime (high pressure, 13.46 MHz, 5 Å/s) [96] is included. This cell shows almost no light induced degradation (9.2 \rightarrow 8.9 %). In this system also a large number of a-Si:H/ μ c-Si:H tandem cells was prepared whose degradation could be almost fully related to a degradation of the amorphous top cell.

To summarize our results:

- Our best solar cells, close to the transition to amorphous growth but still highly crystalline, show only small degradation effects. Moreover, applied in tandem cells [96] high stable efficiencies were achieved.
- We observed a strong degradation effect for cells with an i-layer which is already partly amorphous.

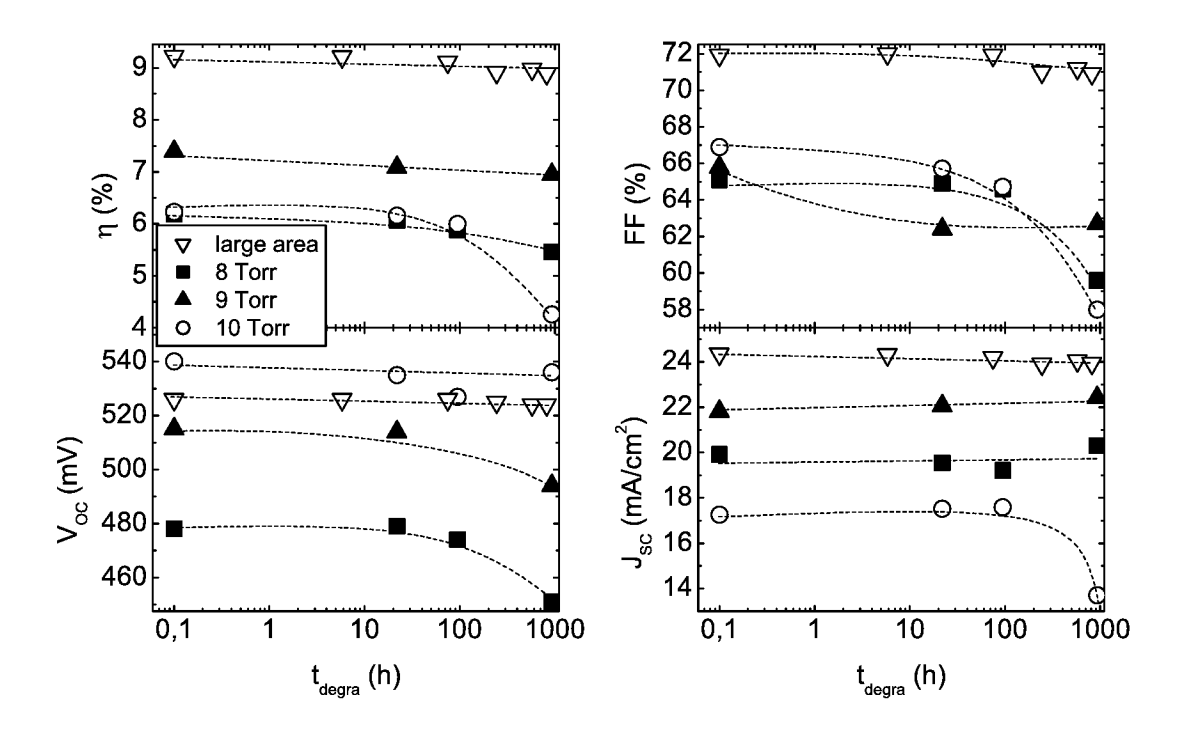


Figure A.1: Degradation of light J-V parameters of μ c-Si:H solar cells as a function of light-soaking time t_{degra} . The solar cells correspond to the cells of the pressure series at 0.5 W/cm² (figure 6.3) which are close to the transition regime between μ c-Si:H and a-Si:H growth. A high efficiency μ c-Si:H solar cell prepared in the 30 × 30 cm² deposition system is added for comparison (from [96]).

• However, we also observed aging effects for some cells, even if we stored them in the dark.

On the basis of the data available up to now, a clear decision on the light-soaking behavior of μ c-Si:H solar cells cannot be made. Here further investigation is required.

B Up-Scaling

On the basis of the process established during this work, a similar process was developed in a $30\times30~\text{cm}^2$ PECVD reactor. This was done in an accompanying PhD thesis [96]. Because of the strong relation of both works the achieved solar cell results from this thesis are summarized in the following.

Like in this work, for all silicon layers 13.56 MHz PECVD was used. Using a newly developed optimized electrode homogeneous deposition of μ c-Si:H was possible on a substrate size of $30\times30~{\rm cm^2}$. The material quality proved to be similarly good as in the small area system resulting in efficiencies of 1 cm² test cells up to 9.4 % at 5 Å/s (The J-V curve of this solar cell is shown in figure B.1). In combination with amorphous top cells these μ c-Si:H solar cells resulted in a-Si:H/ μ c-Si:H tandem cells with stabilized efficiencies up to 11.3 % (the J-V curve of this solar cell is shown in figure B.1, as well). These efficiencies are among the highest published for this type of solar cell.

In cooperation with RWE Solar GmbH, first a-Si:H/ μ c-Si:H modules were realized on Asahi U substrates. The deposition of the silicon layers was performed at the IPV. The best module had an aperture efficiency of 9.7 % before and 8.3 % after light soaking. The J-V curve of this cell is shown in figure B.2. Recently (summer 2002) a complete process technology for the production and development of thin film solar modules on substrate sizes up to 30×30 cm² was established at the IPV including, in addition to 30×30 cm² PECVD, large area magnetron sputtering, laser scribing as well as large area substrate cleaning and etching. With this technology it is possible to prepare modules on wetchemically textured ZnO with substrate sizes up to 30×30 cm² completely at the IPV. So far aperture efficiencies before degradation of 10.7 % (aperture area 64 cm²) and 9.2 % (aperture area 676 cm²) were achieved.

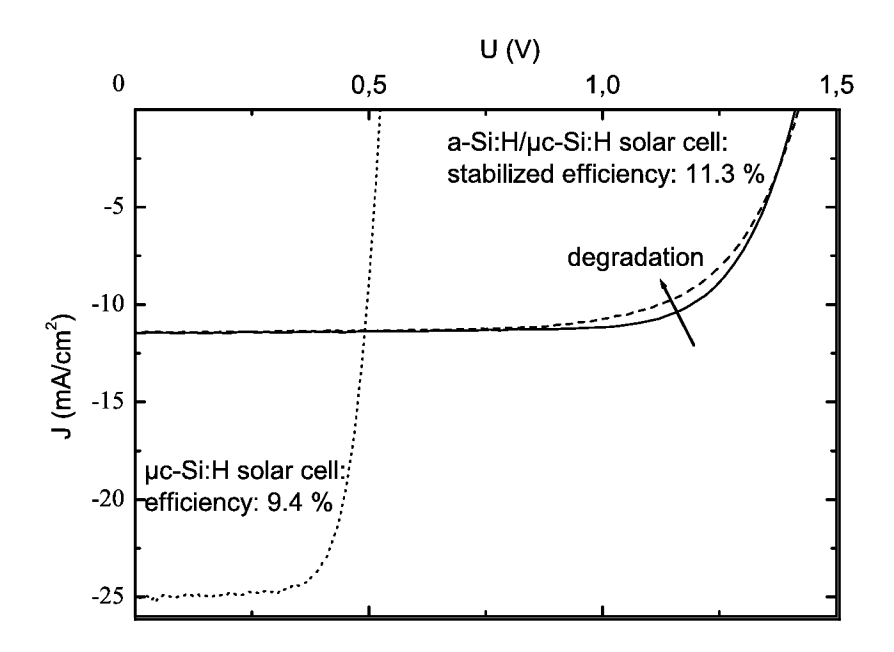


Figure B.1: Light J-V curves of a μ c-Si:H solar cell with 9.4 % efficiency and an a-Si:H/ μ c-Si:H solar cell with 11.3 % stabilized efficiency (degradation behavior is indicated by an arrow for this cell) prepared in the 30×30 cm² PECVD reactor.

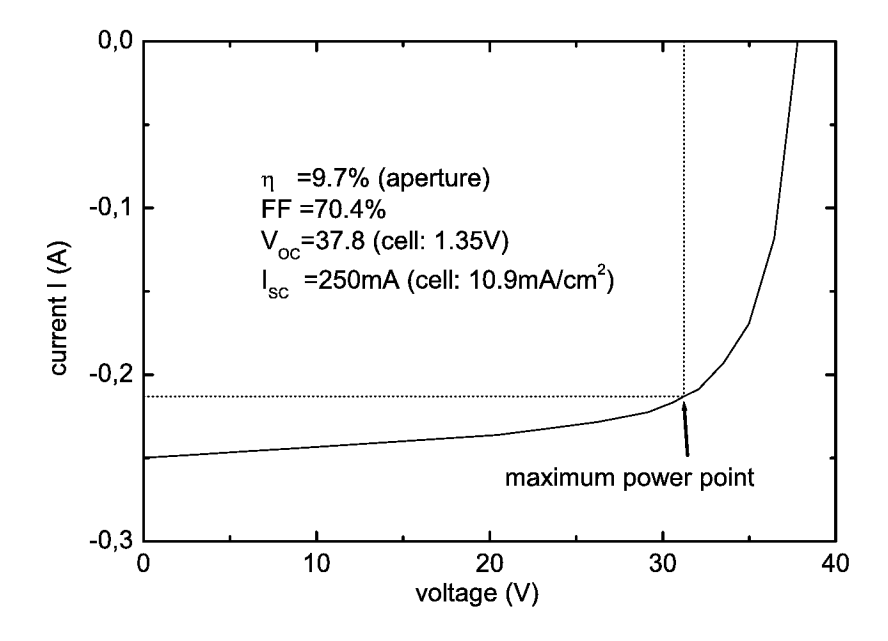


Figure B.2: Light I-V curve of an a-Si:H/ μ c-Si:H 30×30 cm² module on Asahi U TCO with 9.7 % initial aperture efficiency (aperture area: 689 cm²). The stabilized aperture efficiency is 8.3 %. The laser scribing steps were done at RWE Solar GmbH.

Bibliography

- [1] J. M. WOODCOCK, H. SCHADE, H. MAURUS, B. DIMMLER, J. SPRINGER and A. RICAUD. A study of the upscaling of thin film solar cell manufacture towards 500 MWp per annum. In Proc. of the 14th EC PVSEC, p. 857–860 (1997).
- [2] G. HAGEDORN. Hidden Energy in Solar Cells and Photovoltaic Power Stations. In Proc. of the 9th EC PVSEC, p. 542 (1989).
- [3] D. E. CARLSON, R. R. ARYA, M. BENNETT, L.-F. CHEN, K. JANSEN, Y.-M. LI, J. NEWTON, K. RAJAN, R. ROMERO, D. TALENTI, E. TWESME, F. WILLING and L. YANG. Commercialization of multijunction amorphous silicon modules. In Proc. of the 25th IEEE Photovoltaic Specialists Conference, p. 1023 (1996).
- [4] S. Guha. Amorphous silicon alloy solar cells and modules opportunities and challenges. In Proc. of the 25th IEEE Photovoltaic Specialists Conference, p. 1017 (1996).
- [5] S. Fujikake, K. Tabuchi, A. Takano, T. Wada, S. Saito, H. Sato, T. Yoshida, Y. Ichikawa and H. Sakai. Film substrate a-Si solar cells and their novel process technologies. In Proc. of the 25th IEEE Photovoltaic Specialists Conference, p. 1045 (1996).
- [6] B. A. Andersson, C. Azar, J. Holmberg and S. Karlsson. *Material constraints for thin-film solar cells*. Energy **23**(5) 407–411 (1998).
- [7] M. SCHMELA. Beyond expectations. Photon International 3 38–43 (2002).
- [8] D.L. Staebler and C.R. Wronski. Reversible conductivity changes in discharge-produced amorphous Si. Applied Physics Letters **31**(4) 292–294 (1977).
- [9] S. Vepřek and V. Mareček. The preparation of thin layers of Ge and Si by chemical hydrogen plasma transport. Solid-State Electronics 11 683–684 (1968).
- [10] S. Usui and M. Kikuchi. Properties of heavily doped gd-Si with low resistivity. J. Non-Cryst. Solids **34** 1 (1979).

- [11] C. Wang and G. Lucovsky. Intrinsic Microcrystalline Silicon Deposited by Remote PECVD: A New Thin-Film Photovoltaic Material. In Proceedings of the 21st IEEE Photovoltaic Specialists Conference, p. 1614 (1990).
- [12] M. Faraji, S. Gokhale, S. M. Choudari, M. G. Takwale and S. V. Ghaisas. *High mobility hydrogenated and oxygenated microcrystalline silicon as a photosensitive material in photovoltaic applications*. Applied Physics Letters **60** 3289 (1992).
- [13] R. Flückiger, J. Meier, H. Keppner, U. Kroll A. S. O. Greim, M. Morris, J. Pohl, P. Hapke and R. Carius. *Microcrystalline silicon prepared with the very high frequency glow discharge technique for p-i-n solar cell applications*. In *Proc. of the 11th EC Photovoltaic Solar Energy Conference*, p. 617 (1992).
- [14] J. MEIER, S. DUBAIL, R. FLÜCKIGER, D. FISCHER, H. KEPPNER and A. SHAH. Intrinsic microcrystalline silicon (μc-Si:H) – a promising new thin film solar cell material. In Proceedings of the 24th IEEE Photovoltaic Specialist Conference, p. 409–412 (1994).
- [15] J. MEIER, P. TORRES, R. PLATZ, S. DUBAIL, U. KROLL, J. A. ANNA SELVAN, N. PELLATON VAUCHER, CH. HOF, H. KEPPNER, A. SHAH, K. D. UFERT, P. GIANNOULES and J. KOEHLER. On the way towards high efficiency thin film silicon solar cells by the "micromorph" concept. In Mater. Res. Soc. Symp. Proc., p. 3 (1996).
- [16] D. FISCHER, S. DUBAIL, J. A. ANNA SELVAN, N. PELLATON VAUCHER, R. PLATZ, CH. HOF, U. KROLL, J. MEIER, P. TORRES, H. KEPPNER, N. WYRSCH, M. GOETZ, A. SHAH and K.-D. UFERT. The "micromorph" solar cell: Extending a-Si:H technology towards thin film crystalline silicon. In Proceedings of the 25th IEEE Photovoltaic Specialist Conference, p. 1049–1052 (1996).
- [17] S. KLEIN, F. FINGER, R. CARIUS, O. KLUTH, L. BAIA NETO, H. WAGNER and M. STUTZMANN. Intrinsic microcrystalline silicon by hot-wire chemical vapour deposition for solar cell application. In Proceedings of the 17th European Photovoltaic Solar Energy Conference, p. 2965–2968 (2001).
- [18] Y. NASUNO, M. KONDO and A. MATSUDA. Microcrystalline silicon thin-film solar cells prepared at low temperature using PECVD. Solar Energy Materials and Solar Cells 74 497–503 (2002).
- [19] J. MEIER, S. DUBAIL, S. GOLAY, U. KROLL, S. FAŸ, E. VALLAT-SAUVAIN, L. FEITKNECHT, J. DUBAIL and A. SHAH. Microcrystalline silicon and the impact on micromorph tandem solar cell. Solar Energy Materials and Solar Cells 74 457– 467 (2002).

- [20] O. Vetterl, R. Carius, L. Houben, C. Scholten, M. Luysberg, A. Lambertz, F. Finger and H. Wagner. Effects of structural properties of μc-Si:H absorber layers on solar cell preformance. In Mater. Res. Soc. Symp. Proc., Vol. 609 (2000). A15.2.
- [21] K. Saito, M. Sano, K. Matuda, T. Kondo, M. Higasikawa and T. Kariya. High efficiency microcrystalline silicon solar cells by the low temperature plasma CVD method. In Technical Digest of the PVSEC-11, p. 229 (1999).
- [22] K. Yamamoto, M. Yoshimi, Y. Tawada, Y. Okamoto, A. Nakajima and S. Igari. Thin-film poly-Si solar cells on glass substrate fabricated at low temperature. Applied Physics A 69 179–175 (1999).
- [23] K. Saito, M. Sano, K. Matuda, T. Kondo, T. Nishimoto, K. Ogawa and I. Kajita. High efficiency a-Si/\(\mu c\)-Si stacked solar cells. In Proceedings of the Second World Conference and Exhibition on Photovoltaic Solar Energy Conversion, p. 351, Wien (1998).
- [24] O. VETTERL, F. FINGER, R. CARIUS, P. HAPKE, L. HOUBEN, O. KLUTH, A. LAMBERTZ, A. MÜCK, B. RECH and H. WAGNER. *Intrinsic microcrystalline silicon: A new material for photovoltaics*. Solar Energy Materials and Solar Cells **62** 97 (2000).
- [25] K. Yamamoto, M. Yoshimi, Y. Tawada, Y. Okamoto and A. Nakajima. Cost effective and high-performance thin film Si solar cell towards the 21st century. Solar Energy Materials and Solar Cells 66 117–125 (2001).
- [26] H. Shirai, Y. Sakuma, K. Yoshino and H. Ueyama. Spatial distribution of high-density microwave plasma for fast deposition of microcrystalline silicon film. Solar Energy Materials and Solar Cells 66 137–1458 (2001).
- [27] S. J. Jones, R. Cruzet and M. Izu. Use of gas jet deposition technique to prepare microcrystalline Si solar cells. In Proceedings of the 28th IEEE Photovoltaic Specialists Conference, p. 134–137. IEEE (2000).
- [28] J. Meier, E. Vallat-Sauvain, S. Dubail, U. Kroll, J. Dubail, S. Golar, L. Feitknecht, P. Torres, S. Fay, D. Fischer and A. Shah. *Micro-crystalline/micromorph silicon thin-film solar cells prepared by VHF-GD technique*. Solar Energy Materials and Solar Cells **66** 73–84 (2001).
- [29] J. J. Carr. Geheimnisse des HF-Schaltungsentwurfs. Elektor-Verlag, Aachen (1997).
- [30] U. Kroll, D. Fischer, J. Meier, L. Sansonnens, A. Howling and A. Shah. Fast deposition of a-Si:H layers and solar cells in a large-area (40 × 40 cm²) VHF-GD reactor. In Mater. Res. Soc. Symp. Proc., Vol. 557, p. 121 (1999).

- [31] N. Ito, M. Kondo and A. Matsuda. Large area deposition of hydrogenated amorphous silicon by VHF-PECVD using novel electrodes. In Proceedings of the 28th IEEE Photovoltaic Specialist Conference, p. 900. IEEE (2000).
- [32] Y. KAWAI, M. YOSHIOKA, T. YAMANE, Y. TAKEUCHI and M. MURATA. *Radio-frequency plasma production using a ladder-shaped antenna*. Surf. Coat. Technol. **116–119** 662 (1999).
- [33] H. Mashima, M. Murata, Y. Takeuchi, H. Yamakoshi, T. Horioka, T. Yamane and Y. Kawai. *Characteristics of very high frequency plasma produced using a ladder-shaped electrode.* Jpn. J. Appl. Phys. **38** 4305–4308 (1999).
- [34] L. Sansonnens, A. A. Howling and C. Hollenstein. Large area deposition of amorphous and microcrystalline silicon by very high frequency plasma. In Mater. Res. Soc. Symp. Proc., Vol. 507, p. 541 (1998).
- [35] L. Guo, M. Kondo, M. Fukawa, K. Saitoh and A. Matsuda. High Rate Deposition of Microcrystalline Silicon Using Conventional Plasma-Enhanced Chemical Vapor Deposition. Jpn. J. Appl. Phys. 37 L1116-L1118 (1998).
- [36] B. RECH, T. ROSCHEK, J. MÜLLER, S. WIEDER and H. WAGNER. Amorphous and microcrystalline silicon solar cells prepared at high deposition rates using RF (13.56 MHz) plasma excitation frequencies. In Technical Digest 11th PVSEC, p. 241 (1999).
- [37] B. RECH, T. ROSCHEK, J. MÜLLER, S. WIEDER and H. WAGNER. Amorphous and microcrystalline silicon solar cells prepared at high deposition rates using RF (13.56 MHz) plasma excitation frequencies. Solar Energy Materials and Solar Cells 66 267–273 (2001).
- [38] M. TZOLOV, F. FINGER, R. CARIUS and P. HAPKE. Optical and transport studies on thin microcrystalline silicon films prepared by very high frequency glow discharge for solar cell applications. J. Appl. Phys. 81(11) 7376–7385 (1997).
- [39] Y. NASUNO, M. KONDO and A. MATSUDA. Microcrystalline silicon thin-film solar cells prepared at low temperature using RF-PECVD. In Proceedings of the 28th IEEE Photovoltaic Specialists Conference, p. 142–145. IEEE (2000).
- [40] J. Bailat, E. Vallat-Sauvain, L. Feitknecht, C. Droz and A. Shah. *Influence of substrate on the microstructure of microcrystalline silicon layers and cells*. J. Non-Cryst. Solids **299–302** 1219–1223 (2002).
- [41] T. Matsui, M. Tsukiji, H. Saika, T. Toyama and H. Okamoto. *Influence of substrate texture on microstructure and photovoltaic performances of thin film polycrystalline silicon solar cells.* J. Non-Cryst. Solids **299–302** 1152–1156 (2002).

- [42] M. Luysberg, P. Hapke, R. Carius and F. Finger. Structure and growth of microcrystalline silicon: Investigation by TEM and Raman spectroscopy of films grown at different plasma excitation frequencies. Philosophical Magazine A 75(1) 31–47 (1997).
- [43] L. Houben. Plasmaabscheidung von mikrokristallinem Silizium: Merkmale der Mikrostruktur und deren Deutung im Sinne von Wachstumsvorgängen. Ph. D. thesis, Heinrich-Heine-Universität Düsseldorf (1998).
- [44] O. VETTERL. On the physics of microcrystalline silicon thin film solar cells From the material to devices with high conversion efficiencies. Ph. D. thesis, Heinrich-Heine-Universität Düsseldorf (2001).
- [45] L. HOUBEN, M. LUYSBERG, P. HAPKE, R. CARIUS, F. FINGER and H. WAGNER. Structural Properties of Microcrystalline Silicon in the Transition from Highly Crystalline to Amorphous Growth. Philosophical Magazine A 77(6) 1447–1460 (1998).
- [46] L. Houben. Strukturelle Eigenschaften von mikrokristallinem Silizium im Übergang zwischen mikrokristallinem und amorphem Wachstum. Diploma thesis, Heinrich-Heine-Universität Düsseldorf (1995).
- [47] W. Fuhs. in [55], Chap. Amorphe Materialien für Dünnschichtsolarzellen p. 59–70.
- [48] R.A. Street. Hydrogenated Amorphous Silicon. Cambridge Solid State Science Series. Cambridge University Press (1991).
- [49] P. Würfel. *Physik der Solarzellen*. Spektrum, Akademischer Verlag, Heidelberg, Berlin, Oxford (1995).
- [50] S. M. SZE. Semiconductor Devices Physics and Technology. John Wiley & Sons, New York, Chichester, Brisbane, Toronto, Singapore (1985).
- [51] R. C. Neville. Solar Energy Conversion The Solar Cell. Elsevier, Amsterdam, Lausanne, New York, Oxford, Shannon, Tokyo (1995).
- [52] K. W. BÖER. Survey of Semiconductor Physics, Vol. II: Barriers, Junctions, Surfaces and Devices. Van Nostrand Reinhold, New York (1995).
- [53] A. GOETZBERGER, B. VOSS and J. KNOBLOCH. Sonnenenergie: Photovoltaik. B. G. Teubner, Stuttgart (1997).
- [54] M. D. Archer and R. Hill. Clean electricity from photovoltaics, Vol. 1 of the Series on Photoconversion of Solar Energy. Imperial College Press, London (2001).
- [55] D. MEISSNER. Solarzellen Physikalische Grundlagen und Anwendungen in der Photovoltaik. Vieweg & Sohn Verlagsgesellschaft mbH (1993).

- [56] H. J. LEWERENZ and H. JUNGBLUT. *Photovoltaik*. Springer-Verlag, Berlin, Heidelberg, New York (1995).
- [57] A. Gross. Solarzellen aus mikrokristallinem Silizium: Zum Einfluß der Beleuchtungsrichtung und der Substrattemperatur bei der Deposition der intrinsischen Absorberschicht. Diploma thesis, Universität Bonn (2001).
- [58] G. Bruno, P. Capezzuto and A. Madan. *Plasma Deposition of Amorphous Silicon-Based Materials*. Plasma-Materials Interactions. Academic Press, Boston (1995).
- [59] B. Chapman. Glow Discharge Processes. John Wiley & Sons (1980).
- [60] W. Luft and Y.S. Tsuo. Hydrogenated Amorphous Silicon Alloy Deposition Processes. Applied Physics Series. Marcel Dekker, Inc. (1993).
- [61] R. Shul and S. J. Pearton. *Handbook of Advanced Plasma Processing Techniques*. Springer-Verlag, Berlin, Heidelberg, New York (2000).
- [62] H. Frey and G. Kienel. Dünnschichttechnologie. VDI-Verlag (1987).
- [63] K. Heidler. in [55], Chap. Photovoltaische Messtechnik p. 184.
- [64] P. LECHNER, R. GEYER, H. SCHADE, B. RECH and J. MÜLLER. Detailed accounting for quantum efficiency and optical losses in a-Si:H based solar cells. In Proc. of the 28th IEEE Photovoltaic Specialists Conference, p. 861–864. IEEE (2000).
- [65] T. Brammer and H. Stiebig. Characterization of microcrystalline silicon thinfilm solar cells. In Proc. of the 29th IEEE Photovoltaic Specialists Conference (2002). to be published.
- [66] T. WITTCHEN, H. C. HOLSTENBERG, D. HUNERHOFF, Z. J. MIN and J. METZ-DORF. Solar cell calibration and characterization: Simplified DSR apparatus. In Proceedings of the 20th IEEE Photovoltaic Specialists Conference, p. 1251–1257 (1988).
- [67] J. Metzdorf. Calibration of solar cells. 1: The differential spectral responsivity method. Applied Optics 26(9) 1701–1708 (1987).
- [68] S. WILL, H. MELL, M. POSCHENRIEDER and W. Fuhs. a-Si:H deposited at high rate on the cathode of a rf-PECVD reactor. J. Non-Cryst. Solids 227–230 29–33 (1998).
- [69] L. Reimer. Transmission Electron Microscopy. Springer, Berlin, Heidelberg, New York (1993).
- [70] W. Beyer. Semiconductors and Semimetals, Vol. 61, Chap. Hydrogen Phenomena in Hydrogenated Amorphous Silicon p. 165–239. Academic Press (1999).

- [71] W. Beyer, J. Herion, H. Wagner and U. Zastrow. *Hydrogen stability in amorphous germanium films*. Philosophical Magazine B **63**(1) 269–279 (1991).
- [72] B. D. CULLITY. *Elements of X-Ray Diffraction*. Addison Wesley Series in Metallurgy and Materials. Reading, Mass. (1978).
- [73] D. A. Long. Raman Spectroscopy. McGraw-Hill International Book Company, New York (1977).
- [74] M. CARDONA. Light Scattering in Solids. Springer, Berlin (1982).
- [75] P. Hapke. VHF-Plasmaabscheidung von mikrokristallinem Silizium (μc-Si:H): Einfluß der Plasmaanregungsfrequenz auf die strukturellen und elektrischen Eigenschaften. Ph. D. thesis, RWTH Aachen (1995).
- [76] M. Bendayan. Influence of doping on the Raman scattering of quantum well structures. Ph. D. thesis, Technion Israel Institute of Technology, Haifa (1997).
- [77] M. H. BRODSKY, M. CARDONA and J. J. CUOMO. Infrared and Raman spectra of the silicon-hydrogen bonds in amorphous silicon prepared by glow discharge and sputtering. Physical Review B **16**(8) 3556–3571 (1977).
- [78] M. Kubon. Präparation und Eigenschaften der p-seitigen Grenzflächen in Solarzellen aus amorphem Silizium. Ph. D. thesis, RWTH Aachen (1995).
- [79] E. BOEHMER. Analyse der TCO/p Grenzfläche von Solarzellen aus amorphem Silizium mittels Photoelektronen-Spektroskopie. Diploma thesis, RWTH Aachen (1999).
- [80] O. Kluth. Texturierte Zinkoxidschichten für Silizium-Dünnschichtsolarzellen. Ph. D. thesis, RWTH Aachen (2001).
- [81] A. LÖFFL. Präparation hochleitfähiger transparenter Zinkoxidschichten mit kontrollierter Texturierung für Dünnschichtsolarzellen. Diploma thesis, Fachhochschule München (1997).
- [82] A. LÖFFL, S. WIEDER, B. RECH, O. KLUTH, C. BENEKING and H. WAGNER. Aldoped ZnO films for thin-film solar cells with very low sheet resistance and controlled texture. In Proceedings of the 14th European Photovoltaic Solar Energy Conference, p. 2089–2092 (1997).
- [83] O. Kluth, A. Löffl, S. Wieder, C. Beneking, W. Appenzeller, L. Houben, B. Rech, H. Wagner, S. Hoffmann, R. Waser, J. A. Anna Selvan and H. Keppner. Texture etched Al-doped ZnO: A new material for enhanced light trapping in thin film solar cells. In Proceedings of the 26th IEEE Photovoltaic Specialists Conference, p. 715–718 (1998).
- [84] R. A. Haefer. Oberflächen- und Dünnschicht-Technologie Teil I, Beschichtungen von Oberflächen. Springer-Verlag, Berlin (1987).

- [85] J. Perrin, O. Leroy and M. C. Bordage. Cross-sections, rate constants and transport coefficients in silane plasma. Contrib. Plasma Phys. 36 3–495 (1996).
- [86] U. Kroll, J. Meier, H. Keppner, A. Shah, S. D. Littlewood, I. E. Kelly and P. Giannoulès. Origins of atmospheric contamination in amorphous silicon prepared by very high frequency (70 MHz) glow discharge. J. Vac. Sci. Technol. A 13(6) 2742–2746 (1995).
- [87] P. Torres, J. Meier, R. Flückiger, U. Kroll, J. A. Anna Selvan, H. Keppner, A. Shah, S. D. Littlewood, I. E. Kelly and P. Giannoulès. *Device grade microcrystalline silicon owing to reduced oxygen contamination*. Applied Physics Letters **69**(10) 1373–1375 (1996).
- [88] L. LAYEILLON, P. DUVERNEUIL, J.P. COUDERC and B. DESPAX. Analysis and modelling of plasma enhanced CVD reactors. Part I: two-dimensional treatment of a-Si:H deposition. Plasma Sources Sci. Technol. 3 61–71 (1994).
- [89] L. LAYEILLON, P. DUVERNEUIL, J.P. COUDERC and B. DESPAX. Analysis and modelling of plasma enhanced CVD reactors. Part II: model improvement and systematic use. Plasma Sources Sci. Technol. 3 72–79 (1994).
- [90] L. LAYEILLON A. DOLLET and B. DESPAX. Plasma enhanced deposition of a-Si:H: comparison of two reactor arrangements. Chemical Engineering Journal 58 1–5 (1995).
- [91] H. CAQUINEAU, G. DUPONT, B. DESPAX and J. P. COUDERC. Reactor modeling for radio frequency plasma deposition of SiN_xH_y: Comparison between two reactor designs. J. Vac. Sci. Technol. A 14(4) 2071–2082 (1996).
- [92] H. CAQUINEAU and B. DESPAX. Influence of the reactor design in the case of silicon nitride PECVD. Chemical Engineering Science **52**(17) 2901–2914 (1997).
- [93] G. J. NIENHUIS and W. GOEDHEER. Modelling of a large scale reactor for plasma deposition of silicon. Plasma Sources Sci. Technol. 8(2) 295–298 (1999).
- [94] J. Perrin, J. Schmitt, C. Hollenstein, A. Howling and L. Sansonnens. The physics of plasma-enhanced chemical vapour deposition for large-area coating: industrial application to flat panel displays and solar cells. Plasma Sources Sci. Technol. 42 B353–B363 (2000).
- [95] L. Sansonnens, A. A. Howling and C. Hollenstein. A gas flow uniformity study in large-area showerhead reactors for RF plasma deposition. Plasma Sources Sci. Technol. 9 205–209 (2000).
- [96] T. REPMANN. Stapelsolarzellen aus amorphem und mikrokristallinem Silizium: Prozeß- und Modulentwicklung. Ph. D. thesis, RWTH Aachen (2003).

- [97] A. A. HOWLING, C. HOLLENSTEIN and P. J. Paris. Direct visual observation of powder dynamics in rf plasma-assisted deposition. Applied Physics Letters **59**(12) 1409–1411 (1991).
- [98] J. Perrin. Plasma and surface reactions during a-Si:H film growth. J. Non-Cryst. Solids 137 & 138 639-644 (1991).
- [99] A. BOUCHOULE, A. PLAIN, L. BOUFENDI, J. PH. BLONDEAU and C. LAURE. Particle generation and behaviour in a silane-argon low-pressure discharge under continuous or pulsed radio-frequency excitation. J. Appl. Phys. **70**(4) 1991–2000 (1991).
- [100] R. C. Ross. Plasma polymerization and deposition of amorphous hydrogenated silicon from rf and dc silane plasmas. J. Appl. Phys. **55**(10) 3785–3795 (1984).
- [101] H. KAUSCHE and R. D. PLÄTTNER. Effect of a-Si:H powder formation in silane plasmas on solar cell processing. In Proceedings of the 11th EC Photovoltaic Solar Energy Conference, p. 195–198 (1992).
- [102] M. Hundhausen and L. Ley. The formation and stability of sub-micron clusters in silane and argon plasmas. J. Non-Cryst. Solids 137 & 138 795–798 (1991).
- [103] Ch. Hollenstein. The physics and chemistry of dusty plasmas. Plasma Phys. Control. Fusion 42 R93–R104 (2000).
- [104] R. Flückiger, J. Meier, A. Shah, A. Catana, M. Brunel, H. V. Nguyen, R. W. Collins, R. Carius and H. Wagner. Structural, optical and electrical properties of μc-Si:H very thin films deposited by the VHF-GD technique. In Mater. Res. Soc. Symp. Proc., Vol. 336, p. 511–516 (1994).
- [105] A. DASGUPTA, A. LAMBERTZ, O. VETTERL, F. FINGER, R. CARIUS, U. ZASTROW and H. WAGNER. *P-layers of microcrystalline silicon thin film solar cells.* In *Proceedings of the 16th European Photovoltaic Solar Energy Conference*, p. 557–560 (2000).
- [106] S. Wieder. Amorphous Silicon Solar Cells Comparison of p-i-n and n-i-p Structures with Zinc-Oxide Frontcontact. Ph. D. thesis, RWTH Aachen (1999).
- [107] S. Guha, J. Yang, P. Nath and M. Hack. Enhancement of open circuit voltage in high efficiency amorphous silicon alloy solar cells. Applied Physics Letters 49 218–219 (1986).
- [108] J. V. Sali, V. D. Panaskar, M. G. Takwale, B. R.Marathe and V. G. Bhide. Preparation of highly conductive p-type μc-Si:H window layer using lower concentration of hydrogen in the rf glow discharge plasma. Solar Energy Materials and Solar Cells 45 413–421 (1997).

- [109] J. K. RATH and R. E. I. Schropp. Incorporation of p-type microcrystalline silicon films in amorphous silicon based solar cells in a superstrate structure. Solar Energy Materials and Solar Cells **53** 189–203 (1998).
- [110] K. J. LAIDLER. Chemical Kinetics. McGraw-Hill (1965).
- [111] J. Perrin, Y. Takeda, N. Hirano, Y. Takeuchi and A. Matsuda. Sticking and recombination of the SiH₃ radical on hydrogenated amorphous silicon: the catalytic effect of diborane. Surface Science **210** 114 (1989).
- [112] P. Hapke and F. Finger. High deposition rates for microcrystalline silicon with low temperature plasma enhanced chemical vapor deposition processes. J. Non-Cryst. Solids 227–230 861–865 (1998).
- [113] F. EDELMAN, A. CHACK, R. WEIL, R. BESERMAN, Y. K. KHAIT, P. WERNER, B. RECH, T. ROSCHEK, R. CARIUS, H. WAGNER and W. BEYER. Structure of PECVD Si:H films for solar cell applications. Solar Energy Materials and Solar Cells (2002). to be published.
- [114] S. Klein, J. Wolff, F. Finger, R. Carius, H. Wagner and M. Stutzmann. Microcrystalline silicon prepared by hot-wire chemical vapour deposition for thin film solar cell applications. Jpn. J. Appl. Phys. 41 L10–L12 (2002).
- [115] T. ROSCHEK, B. RECH, W. BEYER, P. WERNER, F. EDELMAN, A. CHACK, R. Weil and R. Beserman. Microcrystalline silicon solar cells prepared by 13.56 MHz PECVD at high growth rates: Solar cell and material properties. In Mater. Res. Soc. Symp. Proc. (2001). A25.5.
- [116] A. Shah, E. Vallat-Sauvain, P. Torres, J. Meier, U. Kroll, C. Hof, C. Droz, M. Goerlitzer, N. Wyrsch and M. Vanecek. Intrinsic microcrystalline silicon (μc-Si:H) deposited by VHF-GD (very high frequency-glow discharge): a new material for photovoltaics and optoelectronics. Materials Science and Engineering B69-70 219-226 (2000).
- [117] T. TAKAHAMA, S. OKOMOTO, K. NINOMIYA, M. NISHIKUNI, N. NAKAMURA, S. TSUDA, M. OHNISHI, S. NAKANO, Y. KISHI and Y. KUWANO. Application of high temperature deposition to a-Si solar cells. In Technical Digest of the 5th International PVSEC, p. 375–378 (1990).
- [118] W. Beyer, P. Hapke and U. Zastrow. Diffusion and Effusion of Hydrogen in Microcrystalline Silicon. In Mater. Res. Soc. Symp. Proc., Vol. 467, p. 343–349 (1997).
- [119] O. VETTERL, A. DASGUPTA, A. LAMBERTZ, H. STIEBIG, F. FINGER and H. WAGNER. Preparation temperature effects in microcrystalline silicon thin film solar cells. In Mater. Res. Soc. Symp. Proc., Vol. 664 (2001). A25.8.

- [120] Y. NASUNO, M. KONDO, A. MATSUDA, H. FUKUHORI and Y. KANEMITSU. Formation of interface defects by enhanced impurity diffusion in microcrystalline silicon solar cells. Solar Energy Materials and Solar Cells 81(17) 3155–3157 (2002).
- [121] Y. MAEMURA, H. FIJIYAMA, T. TAKAGI, R. HAYASHI, W. FUTAKO, M. KONDO and A. MATSUDA. Particle formation and a-Si:H film deposition in narrow-gap RF plasma CVD. Thin Solid Films **345** 80–84 (1999).
- [122] Y. Fukuda, Y. Sakuma, Ch. Fukai, Y. Fujimura, K. Azuma and H. Shirai. Optical emission spectroscopy study towards high rate growth of microcrystalline silicon. Thin Solid Films 386 256–260 (2001).
- [123] L. FEITKNECHT, J. MEIER, P. TORRES, J. ZÜRCHER and A. SHAH. *Plasma deposition of thin film silicon: kinetics monitored by optical emission spectroscopy*. Solar Energy Materials and Solar Cells **74** 539–545 (2002).
- [124] J. K. Rath, A. C. W. Biebericher, R. Jimenez Zambrano, R. E. I. Schropp, W. F. van der Weg and W. J. Goedheer. Hydrogenated amorphous silicon with high growth rate, gas utilization and homogeneous deposition by amplitude modulated VHF-PECVD for solar cell application. In Mater. Res. Soc. Symp. Proc. (2002). A6.6.
- [125] C. Mukherjee, C. Anandan, T. Seth, P. N. Dixit and R. Bhattacharyya. Effect of hydrogen dilution on the deposition rate of hydrogenated amorphous silicon films in a modified pulsed plasma discharge. Applied Physics Letters **68**(6) 835–837 (1996).
- [126] C. Anandan, C. Mukherjee, T. Seth, P. N. Dixit and R. Bhattacharyya. Effect of pulse parameters on the deposition rate of hydrogenated amorphous silicon in a modified pulsed plasma discharge. Applied Physics Letters 66(1) 85–87 (1995).
- [127] C. Mukherjee, C. Anandan, T. Seth, P. N. Dixit and R. Bhattacharyya. Optoelectronic properties of hydrogenated amorphous silicon films grown using a modified pulsed plasma discharge. Applied Physics Letters 68(2) 194–196 (1996).
- [128] T. Nakahigashi, T. Hayashi, Y. Izumi, M. Kobayashi, H. Kuwahara and M. Nakabayashi. Properties of a-Si:H film deposited by amplitude modulated rf plasma chemical vapour deposition for thin film transistor. Jpn. J. Appl. Phys. 36 328–332 (1997).
- [129] U. K. Das, S. Morrison and A. Madan. Amorphous and microcrystalline silicon solar cells grown by pulsed PECVD technique. In Mater. Res. Soc. Symp. Proc. (2002). A26.6.
- [130] H. Kirimura, H. Maeda, H. Murakami, T. Nakahigashi, S. Ohtani, T. Tabata, T. Hayashi, M. Kobayashi, Y. Mitsuda, N. Nakamura,

- H. Kuwahara and A. Doi. Study of deposition process in modulated RF silane plasma. Jpn. J. Appl. Phys. **33** 4389–4394 (1994).
- [131] A. C. W. BIEBERICHER. Deposition techniques of hydrogenated amorphous silicon using modulated radio-frequency plasmas. Ph. D. thesis, Universiteit Utrecht (2002).
- [132] J. L. Andújar, E. Bertran, A. Canillas, J. Campmany, J. Serra, C. Roch and A. Lloret. *Properties of amorphous silicon thin films grown in square wave modulated silane rf discharge.* J. Appl. Phys. **71**(3) 1546–1548 (1992).
- [133] A. MADAN and S. MORRISON. High deposition rate amorphous and polycrystalline silicon materials using the pulsed plasma and "Hot-Wire" CVD techniques. Solar Energy Materials and Solar Cells **55** 127–139 (1998).
- [134] A. C. W. BIEBERICHER, J. BEZEMER, W. F. VAN DER WEG and W. J. GOED-HEER. Deposition rate in modulated radio-frequency silane plasmas. Applied Physics Letters **76**(15) 2002–2004 (2000).
- [135] S. MORRISON and A. MADAN. Deposition of amorphous silicon solar cells via the pulsed PECVD technique. In Proceedings of the 28th IEEE Photovoltaic Specialist Conference, p. 928–931. IEEE (2000).
- [136] M. Fukawa, S. Suzuki, L. Guo, M. Kondo and A. Matsuda. *High rate growth of microcrystalline silicon using a high-pressure depletion method with VHF plasma*. Solar Energy Materials and Solar Cells **66** 217–223 (2001).
- [137] M. SHIRATANI, T. FUKUZAWA and Y. WATANABE. Particle growth kinetics in silane RF discharges. Jpn. J. Appl. Phys. **38** 4542–4549 (1999).
- [138] M. SHIRATANI, S. MAEDA, K. KOGA and Y. WATANABE. Effects of gas temperature gradient, pulse discharge modulation, and hydrogen dilution on particle growth in silane RF discharges. Jpn. J. Appl. Phys. 39 287–293 (2000).
- [139] A. A. HOWLING, L. SANSONNENS, J.-L. DORIER and C. HOLLENSTEIN. Time-resolved measurements of highly polymerized negative ions in radio frequency silane plasma deposition experiments. J. Appl. Phys. **75**(3) 1340–1353 (1994).
- [140] Y. WATANABE, M. SHIRATANI and H. MAKINO. Powder-free plasma chemical vapor deposition of hydrogenated amorphous silicon with high rf power density using modulated rf discharge. Applied Physics Letters 57(16) 1616–1618 (1990).
- [141] J. T. VERDEYEN, J. BEBERMAN and L. OVERZET. Modulated discharges: Effect on plasma parameters and deposition. J. Vac. Sci. Technol. A 8(3) 1851–1856 (1990).
- [142] U. K. DAS, S. MORRISON and A. MADAN. Deposition of microcrystalline silicon via the pulsed PECVD technique. J. Non-Cryst. Solids **299–302** 79–82 (2002).

- [143] K. NOMOTO, Y. URANO, J. L. GUIZOT, G. GANGULY and A. MATSUDA. Role of hydrogen in the formation process of hydrogenated microcrystalline silicon. Jpn. J. Appl. Phys. **29**(8) L1372–L1375 (1990).
- [144] A. Matsuda. Formation kinetics and control of microcrystallite in μc -Si:H from glow discharge plasma. J. Non-Cryst. Solids **59** & **60** 767–774 (1983).
- [145] A. Matsuda. Growth mechanism of microcrystalline silicon obtained from reactive plasmas. Thin Solid Films 337 1–6 (1999).
- [146] N. Blayo and B. Drévillon. Infrared ellipsometry study of the vibrational properties of growing microcrystalline silicon thin films. J. Non-Cryst. Solids 137 & 138 775–778 (1991).
- [147] M. FANG, J. B. CHEVRIER and B. DRÉVILLON. In situ investigations of the growth of microcrystalline silicon obtained by alternating deposition and hydrogen-etching sequences. J. Non-Cryst. Solids 137 & 138 791–794 (1991).
- [148] I. SOLOMON, B. DRÉVILLON, H. SHIRAI and N. LAYADI. *Microcrystalline silicon:* the selective etching model. J. Non-Cryst. Solids **164–166** 985–988 (1993).
- [149] M. Heintze, W. Westlake and P. V. Santos. Surface controlled plasma deposition and etching of silicon near the chemical equilibrium. J. Non-Cryst. Solids 164–166 985–988 (1993).
- [150] D. DAS, H. SHIRAI, J. HANNA and I. SHIMIZU. Narrow band gap a-Si:H with improved minority carrier-transport prepared by chemical annealing. Jpn. J. Appl. Phys. **30**(2B) L239–L242 (1991).
- [151] H. SHIRAI, J. HANNA and I. SHIMUZU. Role of atomic hydrogen during growth of hydrogenated amorphous silicon in the "chemical annealing". Jpn. J. Appl. Phys. 30(4B) L679–L682 (1991).
- [152] H. SHIRAI, D. DAS, J. HANNA and I. SHIMUZU. A novel preparation technique for preparing hydrogenated amorphous silicon with a more stable Si network. Applied Physics Letters **59**(9) 1096–1098 (1991).
- [153] H. SHIRAI, H. SHIRAI, B. DRÉVILLON and I. SHIMUZU. Role of hydrogen plasma during growth of hydrogenated microcrystalline silicon: In situ UV-visible and infrared ellipsometry study. Jpn. J. Appl. Phys. 33 5590–5598 (1994).
- [154] M. KONDO and A. MATSUDA. High rate growth of microcrystalline silicon. In Technical Digest of the 13th "Sunshine Workshop on Thin Film Solar Cells", p. 49–56 (2000).
- [155] M. KONDO, M. FUKAWA, L. GUO and A. MATSUDA. High rate growth of micro-crystalline silicon at low temperatures. J. Non-Cryst. Solids **266–269** 84 (2000).

- [156] G. Lihui and L. Rongming. Studies on the formation of microcrystalline silicon with PECVD under low and high working pressure. Thin Solid Films **376** 249–254 (2000).
- [157] H. MIYAHARA, M. TAKAI, T. NISHIMOTO, M. KONDO and A. MATSUDA. Electrode distance dependence of photo-induced degradation in hydrogenated amorphous silicon. Solar Energy Materials and Solar Cells **74** 351–356 (2002).
- [158] A. A. HOWLING, L. SANSONNENS, J. BALLUTAUD, F. GRANGEON, T. DELACHAUX, CH. HOLLENSTEIN, V. DAUDRIX and U. KROLL. The influence of plasma chemistry on the deposition of microcrystalline silicon for large area photovoltaic solar cells. In Proceedings of the 16th European Photovoltaic Solar Energy Conference, p. 518–521 (2000).
- [159] T. Brammer, H. Stiebig, A. Lambertz, W. Reetz and H. Wagner. Temperature dependent transport in microcrystalline pin diodes. In Mater. Res. Soc. Symp. Proc., Vol. 609 (2000). A32.3.
- [160] M. TAKAI, T. TAKAGI, T. NISHIMOTO, M. KONDO and A. MATSUDA. Excitation frequency dependence of the optical emission intensity vs. deposition rate relationship in silane plasmas. Surf. Coat. Technol. **131** 50–53 (2000).
- [161] S. Oda, J. Noda and M. Matsumura. Diagnostic study of VHF plasma and deposition of hydrogenated amorphous silicon films. Jpn. J. Appl. Phys. 29(10) 1889–1895 (1990).
- [162] M. KLICK, L. EICHHORN, W. REHAK, M. KAMMEYER and H. MISCHKE. Influence of excitation frequency on plasma parameters and etching characteristics of radio-frequency discharges. Surf. Coat. Technol. 116–119 468–471 (1999).
- [163] M. TAKAI, T. NISHIMOTO, M. KONDO and A. MATSUDA. *Chemical-reaction dependence of plasma parameter in reactive silane plasmas*. Science and Technology of Advanced Materials **2** 495–503 (2001).
- [164] E. A. G. Hamers, W. G. J. H. M. Van Sark, J. Bezemer, H. Meiling and W. F. van der Weg. Structural properties of a-Si:H related to ion energy distributions in VHF silane deposition plasmas. J. Non-Cryst. Solids **226** 205–216 (1998).
- [165] M. ZEUNER, H. NEUMANN and J. MEICHSNER. Pressure and electrode distance effects on ion energy distributions in RF discharges. Jpn. J. Appl. Phys. **36** (1)(7B) 4711–4716 (1997).
- [166] M. Kondo and A. Matsuda. Low temperature growth of microcrystalline silicon and its application to solar cells. Thin Solid Films 383 1–6 (2001).

- [167] W. Schwarzenbach, A. A. Howling, M. Fivaz, S. Brunner and Ch. Hollenstein. Sheath impedance effects in very high frequency plasma experiments. J. Vac. Sci. Technol. A 14 132 (1996).
- [168] M. Heintze. Versatile high rate plasma deposition and processing with very high frequency excitation. In Mater. Res. Soc. Symp. Proc., Vol. 467, p. 471–482 (1997).
- [169] M. Heintze. Diagnostics of high-rate a-Si:H deposition in a variable frequency plasma. Solid State Phenomena B: 44–46 181–194 (1995).
- [170] A. LAMBERTZ, O. VETTERL and F. FINGER. High deposition rate for μc-Si:H absorber layers using VHF PECVD at elevated discharge power and deposition pressure. In Proceedings of the 17th European Photovoltaic Solar Energy Conference, p. 541–544 (2001).
- [171] C. Ross, F. Finger and R. Carius. An approach to the in situ control of the crystallinity of hydrogenated silicon layers for thin-film solar cells. In Proceedings of PV in Europe From PV Technology to Energy Solutions (Conference and Exhibition), Rom (2002). in press.
- [172] H. KEPPNER, J. MEIER, P. TORRES, D. FISCHER and A. SHAH. *Microcrystalline silicon and micromorph tandem solar cells*. Appl. Phys. A.: Mater. Sci. Process. **69** 169–177 (1999).
- [173] M. KONDO, T. NISHIMIYA, K. SAITO and A. MATSUDA. Light induced phenomena in microcrystalline silicon. J. Non-Cryst. Solids **227–230** 1031–1035 (1998).

Danksagung

Ich bedanke mich bei:

- Herrn Prof. Dr. H. Wagner für sein Interesse an der vorliegenden Arbeit und die Möglichkeit sie am Institut für Photovoltaik durchführen zu können.
- Herrn Prof. Dr. K. Schierbaum für die spontane Bereitschaft zur Ubernahme des Zweitgutachtens.
- Herrn Dr. B. Rech für die engagierte Betreuung.
- Herrn Dr. J. Müller für das Korrekturlesen der Arbeit, hilfreiche Diskussionen und die gute Zusammenarbeit.
- Herrn Dr. W. Beyer für Wasserstoff-Effusionsmessungen und Diskussion zu Materialeigenschaften und Wachstum von μ c-Si:H.
- Herrn Dr. O. Vetterl für hilfreiche Diskussionen.
- Herrn E. Bunte und Herrn A. Lambertz für das Korrekturlesen der Arbeit.
- Herrn T. Repmann für die gute Zusammenarbeit und den Erfahrungsaustausch bei der Entwicklung mikrokristalliner Solarzellen.
- Herrn Dr. F. Edelman, Herrn Dr. A. Chack, Herrn Dr. W. Beyer, Herrn Dr. P. Werner, Herrn Dr. R. Scholz, Herrn Prof. Dr. R. Weil und Herrn Dr. R. Beserman für die gute Zusammenarbeit und die Messungen im Rahmen des deutschisraelischen Projektes (Project-Nr. 01647 E01073).
- Herrn R. Schmitz für die Unterstützung bei der Deposition und bei technischen Problemen.
- Frau H. Siekmann und Herrn G. Schöpe für die Versorgung mit ZnO-Substraten und ZnO/Ag-Rückkontakten.
- Herrn F. Birmans für die Hilfe bei der Kennlinienmessung und Durchführung von Alterungsmessungen.

- Herrn W. Reetz für die Durchführung von DSR-Messungen.
- Frau A. Mülheims für ihre Hilfe in organisatorischen Angelegenheiten.
- Allen nicht namentlich genannten Mitarbeitern des Instituts für Photovoltaik für ihre freundliche Hilfe und das gute Arbeitsklima.



Jül-4083 August 2003 ISSN 0944-2952